https://doi.org/10.5194/egusphere-2026-484
Preprint. Discussion started: 16 February 2026

Ice-nucleating particles in Greenlandic glacial outwash plains

Nora Bergner[1], Grace Marsh[2], Kevin Barry[3], Larissa Lacher[4], Alexander Böhmländer[4], Joanna Alden[1,a], Carina Ahlqvist[1], Ianina Altshuler[2], Lisa Bröder[5], Daniel Farinotti[6,7], Lionel Favre[1], Coline Guillosson[1], Benjamin Heutte[1], Kristina Höhler[4], Roman Pohorsky[1], Julian Weng[8], Julia Schmale[1]

[1]Extreme Environments Research Laboratory, École Polytechnique Fédérale de Lausanne (EPFL) Valais Wallis, Sion, Switzerland.
[2]Microbiome Adaptation to the Changing Environment Laboratory, École Polytechnique Fédérale de Lausanne (EPFL) Valais Wallis, Sion, Switzerland.
[3]Department of Atmospheric Science, Colorado State University, Fort Collins, USA.
[4]Institute of Meteorology and Climate Research Atmospheric Aerosol Research (IMKAAF), Karlsruhe Institute of Technology (KIT), Karlsruhe, Germany.
[5]Geological institute, ETH Zürich, Zürich, Switzerland.
[6]Laboratory of Hydraulics, Hydrology and Glaciology (VAW), ETH Zürich, Zürich, Switzerland
[7]Swiss Federal Institute for Forest, Snow and Landscape Research WSL, Sion, Switzerland
[8]Laboratory of Atmospheric Chemistry, Paul Scherrer Institute, Villigen, 5232, Switzerland
[a]now at: Université Savoie Mont Blanc, INRAE, CARRTEL, Thonons-Les-Bains, France

Correspondence to: Julia Schmale (julia.schmale@epfl.ch)

Abstract

High-latitude dust (HLD) represents a source of ice-nucleating particles (INPs) with potential impacts on cloud formation and radiative forcing in the Arctic. Previous studies have shown that HLD can exhibit high ice-nucleating activity at high subzero temperatures, likely linked to a biological component. Yet, comprehensive assessments of HLD ice-nucleating characteristics and sources remain limited, especially in Greenland. Here, we show that glacial dust from three outwash plains in southwestern Greenland effectively nucleates ice at temperatures relevant for mixed-phase clouds, but with lower ice-nucleating activity than other HLD regions. Ice-nucleating activity of glacial dust shows high variability and is largely driven by small amounts of organic and biological material, as indicated by sample treatments and positive correlations of ice-active mass site densities with total organic carbon and microbial abundance. Atmospheric INP concentrations above -20 °C were higher at the outwash plain sites compared to a nearby fjord site, indicating localized influence under summertime background conditions. This is further supported by similarities between atmospheric and dust INP spectra, as revealed by principal component analysis. The atmospheric INP population was dominated by organic and biological contributions, with no clear role of local meteorology or long-range transport. Overall, the ice-nucleating activity of glacial dust in southwestern Greenland lies within the lower range of reported HLD INP activity, suggesting that highly active HLD parameterizations may overestimate INP concentrations in this region. This highlights the importance of region-specific dust characterizations for improving representation of cloud processes and climate impacts in the Arctic.

https://doi.org/10.5194/egusphere-2026-484
Preprint. Discussion started: 16 February 2026

1 Introduction

Climate-relevant properties of mid- and high latitude mixed-phase clouds are sensitive to the aerosol population, particularly ice-nucleating particles (INPs) (e.g., Storelvmo, 2017; Tan et al., 2016; Vergara-Temprado et al., 2018). INPs initiate heterogeneous ice-formation within the temperature range from 0 °C to -38 °C (Hoose and Möhler, 2012; Kanji et al., 2017; Murray et al., 2012), influencing the partitioning between cloud liquid and ice water content through both the Wegener-Bergeron-Findeisen mechanism (Korolev, 2007) and secondary ice-production pathways (Field et al., 2016; Korolev and Leisner, 2020). These microphysical processes ultimately impact the radiative properties and lifetime of clouds (Ceppi et al., 2017; Storelvmo et al., 2015). The cloud-phase feedback, where changes in cloud phase under a warming climate alter the Earth's radiation budget, thus strongly depends on the current and future abundance and characteristics of INPs (Murray et al., 2021). However, our understanding and quantification of INP sources, their freezing characteristics, and their variability remain incomplete, particularly in high-latitude environments.

Globally, the dominant source of INPs at relatively low temperatures (approximately < -20 °C) is mineral dust emitted from arid and semi-arid regions (Atkinson et al., 2013; Boose et al., 2016; DeMott et al., 2003; Sassen et al., 2003). In the Arctic, long-range transported mineral dust mainly originates from Asia and North Africa (Huang et al., 2015; Kawai and Matsui, 2025), with the strongest influence occurring during winter and spring and at higher altitudes (Groot Zwaaftink et al., 2016; Kawai et al., 2023; Shi et al., 2022). More recently, increasing attention has been directed toward high-latitude dust (HLD), defined as sources north of 50° N or south of 40° S (Bullard et al., 2016; Meinander et al., 2022), which may act as a regional source of INPs in polar regions (Barr et al., 2023; Kawai et al., 2023; Paramonov et al., 2018; Sanchez-Marroquin et al., 2020; Shi et al., 2022; Tobo et al., 2019; Xi et al., 2022). HLD sources are commonly linked to glacial and periglacial environments, particularly glacial outwash plains, where emissions often peak in autumn due to abundant sediment supply and higher wind speeds (Bullard et al., 2016, 2023; Crusius et al., 2011). In addition to transported and local mineral dust, primary biological aerosol particles (PBAPs), including bacteria, pollen, plant debris, fungal spores, and viruses from both marine and terrestrial environments, have been identified as INPs in Arctic environments, and are particularly active during summer and at relatively high subzero temperatures (Beck et al., 2024; Pereira Freitas et al., 2023; Šantl-Temkiv et al., 2019; Wieber et al., 2025). Beyond PBAPs, organic material such as extracellular polymeric substances, polysaccharides, humic-like substances, proteins, and other biogenic macromolecules can act as INPs (Dreischmeier et al., 2017; O'Sullivan et al., 2015; Pummer et al., 2015). Both intact PBAPS and organic macromolecules can attach to and be transported with mineral dust, thereby enhancing its ice-nucleating activity (Conen et al., 2011; O'Sullivan et al., 2014; Prospero et al., 2005), a mechanism that likely contributes to the ice-nucleating activity of HLD (Barr et al., 2023; Tobo et al., 2019; Xi et al., 2022).

Tobo et al. (2019) reported remarkably high ice-active mass site densities at temperatures between -5 and -25 °C from dust collected in an outwash plain in Svalbard, likely linked to small amounts of organic matter that may be more ice-active in cold

https://doi.org/10.5194/egusphere-2026-484
Preprint. Discussion started: 16 February 2026

compared to temperate or warm climates. Other HLD studies also document high ice-nucleating activity at relatively high temperatures, though with notable variability. For example, Xi et al. (2022) observed dust near the Kaskawulsh Glacier in Yukon, Canada, with ice-nucleating activity about two orders of magnitude lower than that of the Svalbard samples, showing biological contributions above –15 °C but mineral dominance at colder temperatures. Airborne dust from the Copper River Delta in Alaska exhibited higher activity, comparable to Svalbard, with heat-sensitive INPs detected down to -25 °C (Barr et al., 2023). Barr et al. (2023) further suggested that watershed characteristics, including the presence of vegetation and forest as sources of organic and biological INPs, may explain differences among regions. In contrast, ice-nucleating activity reported from Iceland, an active HLD source (Dagsson-Waldhauserova et al., 2013), is more comparable to low latitude dust sources (Paramonov et al., 2018; Sanchez-Marroquin et al., 2020). Modelling studies show that HLD contributes substantially to the dust load and INP population of the lower troposphere in summer and autumn (Groot Zwaaftink et al., 2016; Kawai et al., 2023; Shi et al., 2022), and incorporating a parameterization based on the high ice-nucleating activity of Svalbard HLD yields more than 100 times higher INP concentrations in the Arctic lower troposphere during these seasons and better reproduces observations (Kawai et al., 2023). With climate change, increasing HLD emissions with high ice-nucleating activity may partially offset the reduced INP activation expected at higher temperatures (Matsui et al., 2024). Taken together, these sensitivities in combination with the scarcity and heterogeneity of available observations highlight the need to better understand the ice-nucleating properties of different HLD sources.

Greenlandic glacial outwash plains have been identified as significant dust sources (Bullard et al., 2023; Bullard and Mockford, 2018), but their INP characteristics remain poorly constrained. Regional terrestrial environments in Greenland, including biogenic material, are known to contribute to INPs in summer (Šantl-Temkiv et al., 2019; Sze et al., 2023; Wex et al., 2019), yet the specific extent and properties of Greenlandic dust have yet to be determined. While Greenland accounts for only a small fraction of the total Arctic dust load (~0.1% north of 60° N; Groot Zwaaftink et al., 2016), the dust could exert a notable local to regional influence, as shown by estimates that up to 67 % of deposited dust on the ice sheet originates from Greenlandic sources (Groot Zwaaftink et al., 2016). Greenlandic outwash plains are expected to expand and proglacial areas have undergone pronounced changes in the last decades, including increased availability of fine sediments and expanding vegetation cover (Grimes et al., 2024). Both processes may influence INP emissions, highlighting the variable and evolving nature of Greenlandic INP sources.

To address the uncertainties regarding Greenlandic dust sources as INPs, we use field and laboratory measurements to (i) quantify the ice-nucleating activity and variability of dust in glacial outwash plains in southwestern Greenland, (ii) identify sources contributing to the ice-nucleating activity, and (iii) assess atmospheric INP concentrations in southern Greenland and their possible origins, including HLD.

https://doi.org/10.5194/egusphere-2026-484
Preprint. Discussion started: 16 February 2026

2 Methods

2.1 Measurement overview

Field measurements were conducted in southern and southwestern Greenland during 2023 and 2024 as part of the projects "Greenlandic Fjord Ecosystems in a Changing Climate: Socio-cultural and Environmental Interactions" (GreenFjord) and "Ecological and Climate Impacts of Greenlandic Glacial Outwash Plains" (ECO-Plains). The primary field campaign occurred from 16 June to 5 August 2023 in Narsarsuaq and Narsaq, focusing on atmospheric measurements and dust sampling. Additional dust samples were collected in Igaliku (May 2023) and Kangerlussuaq (July 2023 and July 2024), as well as in Narsarsuaq in July 2024 (Fig. 1).

Narsarsuaq, Narsaq, and Igaliku are situated in the fjords of southern Greenland, with the Narsarsuaq outwash plain stretching in front of the glacier Kiattuut sermiat, while Igaliku is located at the Aniaaq fjord, near the glacier Jespersen Brae. Narsaq lies at the intersection of Tunulliarfik fjord and Ikersuaq fjord. The Kangerlussuaq outwash plain is located on the southwestern coast, spanning from Russell Glacier to the head of Kangerlussuaq fjord. These glacial outwash plains exhibit varying vegetation covers, including unvegetated areas and regions with sparse, low-level vegetation such as grasses, mosses, lichens, and, in some cases, lower shrub vegetation. Shrub vegetation is dominant around Narsaq.

2.1.1 Bulk dust samples

Dust samples were collected following a chronosequence approach (Bradley et al., 2016), where locations farther from the glacier have been exposed longer following glacial retreat, and may show advanced microbial succession or soil development, potentially influencing the dust's ice-nucleating activity. We distinguish between two types of dust samples: *transect* and *microbiology*. *Transect* samples were collected along glacier-to-fjord transects, targeting surface sediments (top ~1 cm) from primarily vegetation-free areas or river deposits, where dust emissions are likely. Samples were air-dried under a laminar flow hood and sieved to < 45 µm to focus on the particle size fraction most relevant for atmospheric transport, following common approaches in similar studies (e.g., sieving to sizes between 32-63 µm in Barr et al., 2023; Boose et al., 2016; Hamzehpour et al., 2022). *Microbiology* samples (top ~5 cm) were collected at two sites each in Narsarsuaq and Kangerlussuaq, with site 1 closer to the glacier than site 2. Each site included multiple subsites from both vegetated and unvegetated surfaces. Since these samples were primarily analyzed for microbiological purposes, they were air-dried but not sieved, allowing for better comparison between microbiological measurements and INP analyses for this sample type. Details and sampling locations are shown in Table 1 and Fig. 1, with photos of some sampling locations in Fig. B1.

Additional bulk dust samples were collected for comparison in three glacial outwash plains in the Swiss Alps, allowing us to assess whether ice-nucleating properties observed in Arctic samples are specific to Arctic conditions or represent a more general feature of glacially derived dust, including at mid-latitudes**.** The sampling sites are shown in Table C1 and Fig. C2.

https://doi.org/10.5194/egusphere-2026-484
Preprint. Discussion started: 16 February 2026

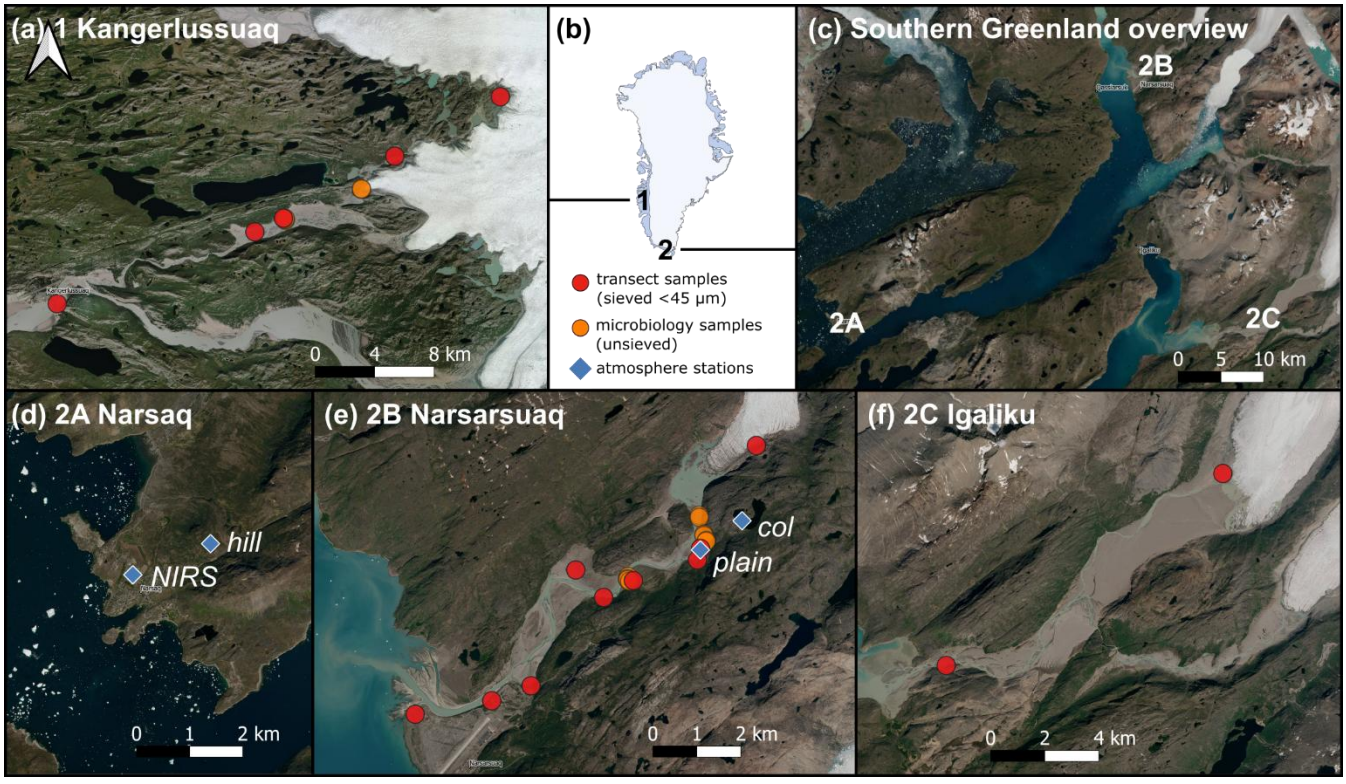

Figure 1. Field work sites overview. (a) Sample locations in Kangerlussuaq, (b) overview of sampling regions in Greenland, (c) main study area in Southern Greenland with zoomed-in views of (d) Narsaq with the atmospheric stations at Narsaq International Research station (*NIRS*) and *hill*, (e) Narsarsuaq including the *plain* and *col* atmospheric stations, and (f) Igaliku. Map background imagery was obtained from the Greenlandic satellite orthophoto mosaic provided by Dataforsyningen and accessed via QGreenland (Moon et al., 2023).

Table 1. Overview of bulk dust samples. INP treatments refer to heat and hydrogen peroxide treatments for compositional information (Sect. 2.2). Additional analyses refer to ancillary measurements (Sect. 2.3) including total organic carbon (TOC), X-ray diffraction (XRD), and microbial abundance based on flow cytometry (FC) and colony forming units (CFU).

Location	Sampling set	ID	Latitude (°)	Longitude (°)	Date (YYYY-MM-DD)	Description	INP treatments	Additional analyses
Narsarsuaq	transect	N1	61.220991	-45.306142	2023-07-17	dust on glacier	heat, H_2O_2	TOC, XRD
		N2	61.200598	-45.328784	2023-06-25	outwash plain	heat	TOC
		N3	61.198341	-45.330013	2023-06-20	dust deposit near river bed	heat	TOC
		N4	61.194188	-45.356143	2023-06-25	small sand dune	heat, H_2O_2	TOC
		N5	61.190831	-45.368287	2023-06-25	dust deposits near river bed	heat, H_2O_2	TOC, XRD
		N6	61.196204	-45.379716	2023-06-25	Outwash plain	heat	TOC
		N7	61.173301	-45.397706	2023-06-23	Dust deposits near river bed	heat	TOC
		N8	61.170274	-45.413717	2023-06-23	Dust deposits near river bed	heat	TOC

https://doi.org/10.5194/egusphere-2026-484
Preprint. Discussion started: 16 February 2026

		N9	61.167508	-45.444936	2023-06-23	Dust at outflow to fjord	heat	TOC
Narsarsuaq	microbiology	N1AT	61.207152	-45.329376	2024-07-05	unvegetated	heat	TOC, FC, CFU
		N1BT	61.206739	-45.329335	2024-07-05	unvegetated		TOC, FC, CFU
		N1ET	61.203417	-45.327393	2024-07-05	sparsely vegetated	heat	TOC, FC, CFU
		N1FT	61.203136	-45.327403	2024-07-05	vegetated		TOC, FC, CFU
		N1GT	61.202204	-45.326349	2024-07-05	vegetated	heat	TOC, FC, CFU
		N1IT	61.202012	-45.326524	2024-07-05	vegetated		TOC, FC, CFU
		N2AT	61.194997	-45.358292	2024-07-08	unvegetated		TOC, FC, CFU
		N2CT	61.194518	-45.3586	2024-07-08	unvegetated	heat	TOC, FC, CFU
		N2ET	61.194349	-45.358387	2024-07-08	sparsely vegetated	heat	TOC, FC, CFU
		N2GT	61.194064	-45.357687	2024-07-08	sparsely vegetated	heat	TOC, FC, CFU
Kangerlussuaq	transect	K1	67.151944	-50.0405	2023-07-07	dust on glacier	heat	TOC, XRD
		K2	67.110861	-50.194083	2023-07-07	river bank	heat, H_2O_2	TOC
		K3	67.067806	-50.355556	2023-07-07	river bank	heat, H_2O_2	TOC
		K4	67.058083	-50.397278	2023-07-07	river bank	heat	TOC, XRD
		K5	67.003917	-50.687833	2023-07-07	river bank	heat	TOC
	microbiology	K1AT	67.089284	-50.240169	2024-07-12	unvegetated	heat	TOC, FC, CFU
		K1ET	67.089631	-50.240629	2024-07-12	sparsely vegetated	heat	TOC, FC, CFU
		K1IT	67.089500	-50.240506	2024-07-12	sparsely vegetated	heat	TOC, FC, CFU
		K2AT	67.066776	-50.352532	2024-07-13	unvegetated	heat	TOC, FC, CFU
		K2ET	67.06729	-50.352299	2024-07-13	sparsely vegetated	heat	TOC, FC, CFU

https://doi.org/10.5194/egusphere-2026-484
Preprint. Discussion started: 16 February 2026

		K2HT	67.067879	-50.353181	2024-07-13	vegetated	heat	TOC, FC, CFU
Igaliku	transect	I1 I2	60.97159 60.90985	-45.052219 -45.234064	2023-05-28 2023-05-31		heat, H_2O_2 heat	TOC, XRD TOC

2.1.2 Atmospheric measurements

Atmospheric measurements were conducted in both Narsarsuaq and Narsaq with two sites per location (Fig. 1), each equipped with small solar- and battery-powered stations. In Narsarsuaq, one station was installed on the outwash plain, hereafter referred to as the *plain* station. A second station was positioned on a small col, located approximately 1.1 km northeast of the *plain* station at an elevation of 300 m a.s.l., hereafter referred to as the *col* station. In Narsaq, measurements were performed at the Narsaq International Research Station (*NIRS*), where a more extensive suite of instruments was deployed, the set-up is described in detail by Alden et al. (2025). The second Narsaq site was situated on Tasigaaq hill, approximately 1.6 km northeast of *NIRS* at an elevation of 372 m a.s.l. Photos of all measurement stations are provided in Fig. B1.

At each site, meteorological variables including atmospheric pressure, temperature, relative humidity, solar radiation, wind/gust speed and precipitation were measured with ATMOS41 GEN 2 weather stations (METER Group, USA). Particle number concentrations and size distributions were obtained with optical particle counters: at *NIRS*, in the size range 0.19-93.06 µm (optical diameter, d_{opt}), using a Fidas Frog (Palas, Germany), and at the *plain*, *col*, and *hill* sites in the size range 186-3370 nm (d_{opt}) using a Portable Optical Particle Sizer (POPS, Handx Scientific, USA). Aerosol filter samples were collected for INP measurements using a custom-built aerosol filter sampler. The system consisted of a stainless-steel inlet, an in-line plastic filter holder (Whatman®, Cytiva, USA), a mass flow controller (Sensirion AG, Switzerland), and a pump (KNF Neuberger GmbH, Germany). Nuclepore™ polycarbonate filters (47 mm diameter, 0.2 µm pore diameter) were prepared according to the protocol described by Barry et al. (2021) and inserted into the holders under clean conditions. Filter samples were operated at a flow between 5 and 10 std L min^{-1} (std denotes volumetric flow referenced to standard temperature and pressure) for a typical duration of 1-3 days, with some filters up to 14 days due to logistical reasons. An overview of all filters analyzed for INPs is provided in Table 2.

Table 2. Overview of filter samples collected for INP measurements.

Location	Latitude (°)	Longitude (°)	Altitude (m a.s.l.)	Sample ID	Filter samples start date	Filter samples end date
Narsarsuaq plain (*plain*)	61.20032	-45.32882	25	NUP2 NUP3 NUP4	2023-06-17 13:32 2023-06-18 13:17 2023-06-19 16:10	2023-06-18 12:01 2023-06-19 12:24 2023-06-20 11:48

https://doi.org/10.5194/egusphere-2026-484
Preprint. Discussion started: 16 February 2026

				NUP6	2023-06-21 15:50	2023-06-22 11:54
				NUP7	2023-06-22 12:30	2023-06-23 13:11
				NUP8	2023-06-23 13:34	2023-06-24 11:48
				NUP9	2023-06-24 12:19	2023-06-25 10:09
				NUP10	2023-06-25 10:16	2023-06-26 06:53
				NUP11	2023-06-26 07:03	2023-06-27 13:47
				NUP12	2023-06-27 14:13	2023-06-28 09:52
				NUP13	2023-06-28 10:28	2023-07-05 17:43
				NUP15	2023-07-17 16:17	2023-08-02 09:08
				NUP16	2023-08-02 09:42	2023-08-09 17:29
Narsarsuaq col (*col*)	61.2061254	-45.3118504	300	NUC1	2023-06-16 17:56	2023-06-19 16:41
				NUC3	2023-06-21 12:53	2023-06-23 14:27
				NUC4	2023-06-23 15:54	2023-06-26 07:34
				NUC5	2023-06-26 07:39	2023-06-28 12:14
				NUC6	2023-06-28 12:15	2023-07-05 19:02
				NUC7	2023-07-05 19:50	2023-07-17 16:57
				NUC8	2023-07-17 17:12	2023-08-02 10:26
				NUC9	2023-08-02 11:52	2023-08-09 18:08
Narsaq International Research Station (*NIRS*)	60.9157503	-46.053326	17	NA3	2023-06-27 17:15	2023-06-29 12:18
				NA4	2023-06-29 12:20	2023-07-02 14:36
				NA5	2023-07-02 14:40	2023-07-06 15:58
				NA7	2023-07-08 10:15	2023-07-10 12:17
				NA8	2023-07-10 12:21	2023-07-12 10:00
				NA9	2023-07-12 10:05	2023-07-14 11:42
				NA10	2023-07-14 11:45	2023-07-16 17:06
				NA11	2023-07-16 17:11	2023-07-19 10:41
				NA13	2023-07-19 10:48	2023-07-21 13:26
				NA14	2023-07-21 13:32	2023-07-23 10:37
Tasigaaq hill near Narsaq (*hill*)	60.9210617	-46.0274668	372	T1	2023-06-23 16:57	2023-06-25 18:57
				T4	2023-06-27 16:03	2023-06-29 12:51
				T7	2023-07-02 10:16	2023-07-04 09:59
				T10	2023-07-08 17:38	2023-07-10 16:23
				T15	2023-07-16 12:09	2023-07-19 11:56

https://doi.org/10.5194/egusphere-2026-484
Preprint. Discussion started: 16 February 2026

				T17	2023-07-21 14:58	2023-07-23 09:21
				T21	2023-07-27 15:13	2023-07-30 11:44

2.2 Ice-nucleation freezing measurements

Bulk dust and filter samples were analyzed for INPs using the Sion Particle Ice Crystallization Experiment (SPICE), an immersion-mode INP measurement set-up described in detail in Appendix A. Suspensions were made in pre-rinsed 50 mL Corning® polypropylene centrifuge tubes (Cat. No. 10788561, Corning Inc., USA) with molecular-biology-free reagent water (Cat. No. W4502, Sigma Aldrich, USA; hereafter referred to as SA water) with 10-fold dilutions for bulk dust samples (0.5 mL sample, 4.5 mL SA water), resulting in a concentration range of approximately 2 to 0.0002 g L^{-1}. Filter samples were suspended in 12 mL of SA water (8 mL for procedural blank filters), and the aerosol was washed off by placing the Corning tube in a tube rotator at 60 rpm for 20 min. Two 15-fold dilutions (0.4 mL sample and 5.6 mL SA water) were prepared for the filter samples. The suspensions and corresponding dilutions were pipetted in 50 µL droplets into the wells of two single use PCR-trays (Cat. No. 781368, Brand, Germany), with blocks of a minimum of 32 wells per suspension, in addition to 32 wells of background SA water for each experiment. Transparent foil (Cat. No. AXYPCR-TS, Axygen, Corning Inc., USA) was placed on top of the PCR trays to prevent contamination. The PCR trays were placed into the two aluminum cooling blocks of SPICE and cooled down with a chiller (RP 245 E, Lauda, Germany) from 2 °C to approx. -35 °C at a cooling rate of -0.33 °C min^{-1}. From the observed freezing events, the ice nucleation active sites per unit volume of water as a function of temperature, $INP_{sus,corr}(T)$, also referred to as cumulative INP spectrum, can be calculated with the frozen fraction of droplets ($FF(T)$) and droplet volume (V_d = 50 µL) following Vali (1971):

$$INP_{\mathrm{sus,corr}}(T) = -\ln\left(\frac{1-FF(T)}{1-FF_{\mathrm{background}}(T)}\right)\frac{d}{V_{\mathrm{d}}} \quad (1)$$

The above assumes a dependence only on temperature (T) but not on time, and includes a correction for the water background ($FF_{background}$). d is the dilution ratio of the suspension relative to the initial suspension.

The ice-active mass site densities for bulk samples are then calculated by

$$n_{\mathrm{m}}(T) = INP_{\mathrm{sus,corr}}(T)\frac{1}{C_{\mathrm{m}}} \quad (2)$$

where C_m denotes the mass concentration of the initial suspension.

Ice-active surface site densities are calculated by

$$n_{\mathrm{s}}(T) = INP_{\mathrm{sus,corr}}(T)\frac{1}{C_{\mathrm{m}}SSA} \quad (3)$$

where *SSA* is the specific surface area measured using the Brunauer-Emmer-Teller (BET) method with a Surface Analyzer Anton Paar Nova 800 (Anton Paar GmbH, Austria). Surface area normalization was only applied to the *transect* samples.

Atmospheric INP concentrations are computed by

https://doi.org/10.5194/egusphere-2026-484
Preprint. Discussion started: 16 February 2026

$$N_{\mathrm{INP}}(T) = INP_{\mathrm{sus,corr}}(T)\frac{V_{\mathrm{wash}}}{V_{\mathrm{air}}} \quad (4)$$

where V_{air} is the total volume of air sampled on the filter, and V_{wash} the volume of the washing water.

95 % confidence intervals for all INP spectra were calculated according to equation 2 in Agresti and Coull (1998) and more detailed data processing and quality checks are described in Sect. A1.3. Procedural filter blanks at each station were taken by inserting the filter holder with a filter but without turning on the air flow. The background filters showed lower frozen fraction curves compared to the filter samples (Fig. B2), but were above the typical background freezing from SA water only, with some blank filters showing non-negligible amounts of INPs. Procedural blanks were not subtracted from sample spectra and contribution is likely minor for most samples and confined to low temperatures. However, background contamination introduces additional uncertainty to the reported INP concentrations, particularly for samples with low INP concentrations.

For compositional information, we performed heat and hydrogen peroxide treatments to a subset of bulk dust and filter samples. Heat treatment denatures proteins, and the difference between untreated and heat-treated spectra indicates the proteinaceous, likely biological INPs (Daily et al., 2022). Hydrogen peroxide treatment oxidizes organic matter, leaving spectra that reflect the inorganic or mineral INPs (McCluskey et al., 2018a). For the heat treatment, a Corning tube containing 3 mL of the sample suspension was placed into a boiling water bath (approximately 98.4 °C) for 20 min. For the hydrogen peroxide treatment, 1 mL of 30 % H_2O_2 (Cat. No. 216763-100ML, Merck Millipore, Germany) was added to 2 mL of the sample suspension and placed into a boiling water bath with UV light for 20 min. Remaining peroxide was neutralized by adding small quantities (90 to 130 µL) of 0.1 µm filtered catalase (Cat. No. MPB-210042910-10ML, MP Biomedicals, USA). Dilution series and freezing experiment for the treated samples were performed as described above. In total, we analyzed 32 bulk dust samples with 28 heat and 5 hydrogen peroxide treatments, as well as 38 filter samples with 5 heat, and 5 peroxide treatments (Table 1). In addition, 14 procedural blank filter samples were analyzed. Additional experiments including SA blanks and validation material for the SPICE characterization are shown in Sect. A2.2 and A2.3.

2.3 Ancillary measurements

To evaluate the role of organic matter for ice-nucleating activity, total organic carbon (TOC) was measured for all dust samples using catalytic high-temperature combustion with CO_2 quantification via non-dispersive infrared detection (Elementar Enviro TOC analyzer, Elementar Analysensysteme GmbH, Germany). The microbial abundance in the *microbiology* dust samples was assessed using two different methods: flow cytometry and plate culturing. For flow cytometry, bacterial cells were extracted from 1 g soil suspended in 9 mL 1x phosphate-buffered saline (PBS) (sterile filtered at 0.2 µm), following a protocol adapted from Górniak et al. (2017). After shaking (120 rpm, 2 h, 10 °C) and fixation with 3.7 % formaldehyde, cells were separated from soil particles via Histodenz (Cat. No. D2158, Sigma-Aldrich, USA) density centrifugation (17,000 × *g* (relative

https://doi.org/10.5194/egusphere-2026-484
Preprint. Discussion started: 16 February 2026

centrifugal force), 90 min, 4 °C) (Frossard et al., 2016). The upper aqueous phase was extracted, stained with SYTO13 (50 µM), and analyzed using a NovaCyte flow cytometer (ACEA, Bioscience, USA) (flow rate 14 µL min^{-1}), with cell counts determined from forward and side scatter signals. For plate culturing, 1 g of soil was suspended in 9 mL 1x sterile PBS, shaken for 2 h at 10 °C, and allowed to settle for 15 min. Serial dilutions were plated (500 µL) onto R2A agar media (Neogen Culture Media, USA) and incubated at 12.5 °C (the average temperature across sites). Colony-forming units (CFUs) were counted after three weeks.

X-ray diffraction (XRD) measurements were performed on a subset of representative samples of each outwash plain to determine the relative abundance of ice-nucleating active minerals. Diffractograms were collected using a D8 Discover Vario (Bruker, USA) with Cu $K\alpha_1$ radiation, and mineral phases were identified using the Rietveld refinement method. Semi-quantitative estimates of relevant mineral abundances are summarized in Table B1.

2.4 Principal component analysis

To examine similarities between bulk dust and aerosol INP spectra, we performed a principal component analysis (PCA) on derived spectral features, following the approach of Barry et al. (2023). INP concentrations between -8 °C and -20 °C were log-transformed (log_{10}) and missing values were interpolated or extrapolated linearly. From these spectra, we derived (i) slopes in 2 °C windows shifted in 1 °C steps, and (ii) logarithmic ratios of mean INP concentrations in each 2 °C window relative to -15 °C. The resulting feature set (22 variables across 70 samples) was standardized (z-scores) prior to PCA, which was applied to the combined dataset of bulk and aerosol samples.

3 Results and discussion

3.1 Ice-nucleating properties of dust in southwestern Greenlandic glacial outwash plains

The following sections present an analysis of the ice-nucleating properties of dust collected from glacial outwash plains in southwestern Greenland. We first characterize the ice-nucleating activity of bulk dust samples across different sites and how they compare to other high-latitude dust sources in Sect. 3.1.1. We then explore the spatial variability within the outwash plains (Sect. 3.1.2) and examine the influence of organic and biological material on the observed ice-nucleating activity through treatments (Sect. 3.1.3). Finally, we assess correlations between total organic carbon (TOC), microbial abundance, and ice-nucleating activity (Sect. 3.1.4.) to better understand the drivers of variability across samples.

3.1.1 Overview of the ice-nucleating activity of glacial dust

To characterize the bulk dust in glacial outwash plains in Greenland as a potential INP source, we present the ice-active mass site densities (n_m) and ice-active surface site densities (n_s) in Fig. 2. The ice-nucleating activity of the glacial dust is quite variable for a given site, but similar across the three outwash plains in southwestern (Kangerlussuaq) and southern Greenland

https://doi.org/10.5194/egusphere-2026-484
Preprint. Discussion started: 16 February 2026

(Narsarsuaq, Igaliku), with n_m values (Fig. 2a) from all sites falling within a comparable range and showing no systematic differences between locations. A subset of samples with higher ice-nucleating activity (e.g., some *microbiology* samples) likely indicates an influence of vegetation cover (Fig. B3). The n_s values (Fig. 2c, *transect* samples only) are likewise similar across sites and, for most samples, cluster more tightly than the n_m values, which partly reflects the effect of differences in grain-size distributions (samples sieved to < 45 µm).

The Greenlandic dust's n_m values are substantially lower (sample average ~2-3 orders of magnitude) compared to glacial dust collected in Svalbard (Tobo et al., 2019, < 5 µm) and midlatitude soils (Hill et al., 2016), particularly for the relatively warm temperatures (Fig. 2b). In contrast, the n_m values are more comparable to airborne dust from a glacial outwash plain in Yukon, Canada (Xi et al., 2022), and sediments (not a glacial outwash plain) collected near Utqiaġvik, Alaska (Barry et al., 2023). The n_s values mostly fall within the lower range of other HLD observations (Fig. 2d), including airborne dust from the Copper River Delta in Alaska (Barr et al., 2023), Icelandic dust plumes (Sanchez-Marroquin et al., 2020), and airborne dust from Yukon, Canada (Xi et al., 2020, same samples as n_m). However, it should be noted that differences in sampling and normalization methods (e.g., bulk dust vs. aerosol sampling, n_s based on geometric vs. BET surface area) may influence the direct comparability of these datasets.

Low latitude desert dust parameterizations (Niemand et al., 2012; Ullrich et al., 2017) fall at the upper end of the ice-nucleating activity observed in our samples but are only applicable at lower temperatures (<-12 °C). Ice-nucleating-active minerals typically control the ice-nucleating activity of desert dust samples, and we include parameterizations for potassium (K-Feldspar), albite, and quartz (Harrison et al., 2019), scaled to their average relative abundances determined by XRD analysis of the sieved (< 45 µm) bulk samples (Sect. 2.3, Table B1). While the quartz- and albite-based parameterizations predict lower n_s values than observed, the K-Feldspar parameterization is in a similar range, albeit with a steeper slope, suggesting a potential contribution of this mineral to the measured ice-nucleating activity.

Overall, the Greenland dust samples exhibit freezing onsets at relatively high temperatures (-6 °C to -10 °C) relevant for mixed-phase clouds, and show partly comparable (Xi et al., 2022), but generally lower ice-nucleating activity than other HLD sites (Tobo et al., 2019; Barr et al., 2023). These findings suggest that HLD could represent a rather heterogeneous source of INPs, with variable ice-nucleation efficiencies depending on location. The variability could stem from differences in mineralogy as well as from biological and organic compounds, which have been identified as important contributors to the HLD ice-nucleating activity (Barr et al., 2023; Sanchez-Marroquin et al., 2020; Tobo et al., 2019; Xi et al., 2022). In the following sections, we investigate potential sources of ice-nucleating activity and discuss possible reasons for these differences.

https://doi.org/10.5194/egusphere-2026-484
Preprint. Discussion started: 16 February 2026

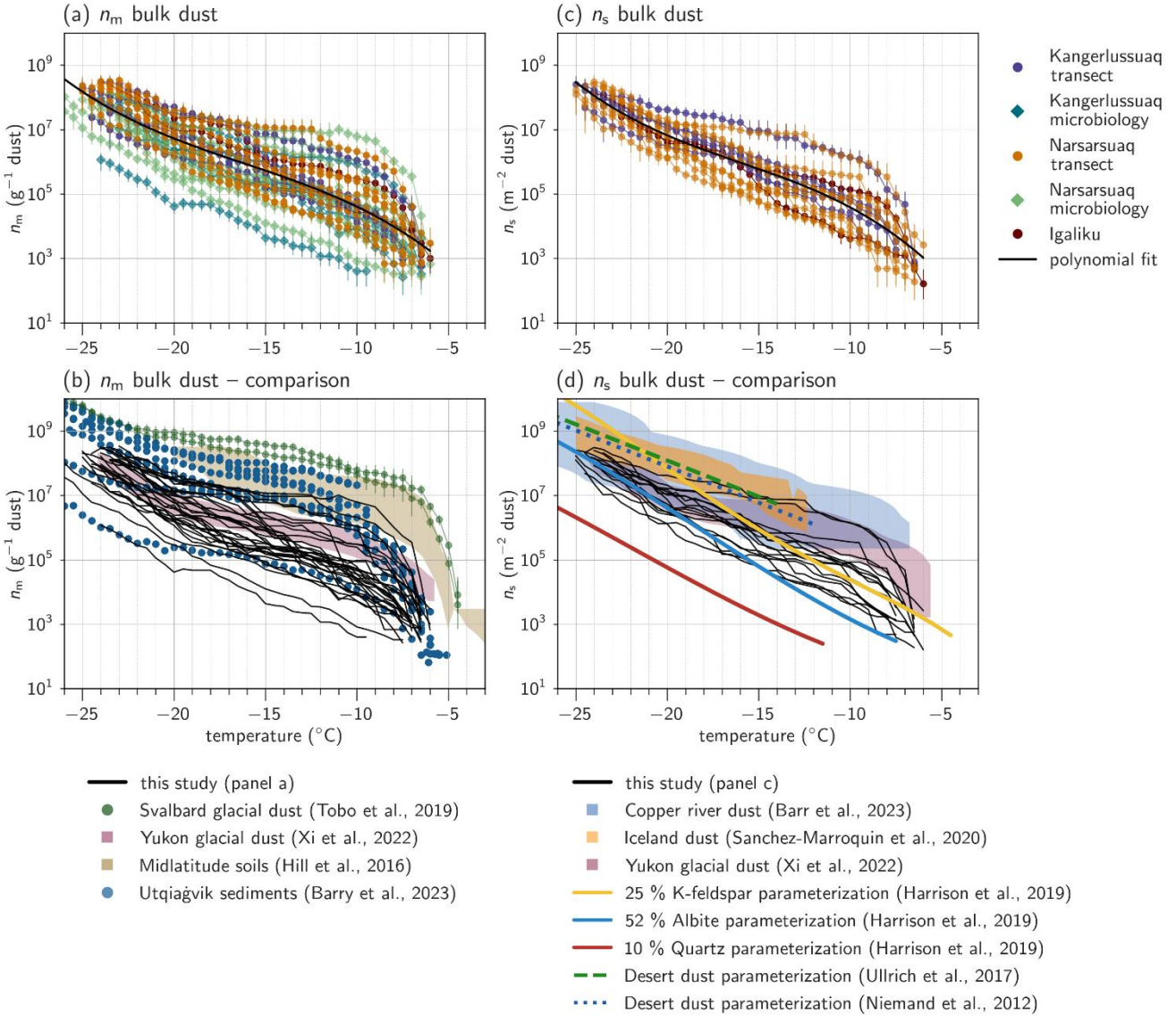

Figure 2. Bulk dust ice-nucleating activity and comparison. (a) Ice-active mass site densities (n_m) in Narsarsuaq, Kangerlussuaq and Igaliku with the polynomial fit for all data combined ($n_m(T)$ = exp(-0.702 - 1.804T - 0.085T^2 - 0.00176T^3) and (b) comparison with literature data by Tobo et al., (2019, bulk dust sieved to <5 µm), Xi et al. (2022, dust aerosol samples with n_m determined gravimetrically), Hill et al. (2016, unsieved bulk soil samples), and Barry et al. (2020, unsieved bulk sediment samples). (c) Ice-active surface site densities (n_s) of dust samples based on BET surface area measurements with a polynomial fit ($n_s(T)$ = exp(-2.887 – 2.221T - 0.111 T^2 - 0.00231 T^3) and (d) comparison with literature data by Barr et al. (2023, dust aerosol samples converted to $n_{s,\,geo}$), Sanchez-Marroquin et al. (2020, dust aerosol samples converted to $n_{s,\,geo}$), Xi et al. (2022, dust aerosol samples converted to $n_{s,\,geo}$), K-Feldspar, albite, and quartz parameterizations (Harrison et al., 2019, based on $n_{s,\,BET}$), scaled to the average abundance of the respective mineral in the sample based on XRD measurements (Table B1), Ullrich et al. (2017, parameterization based on $n_{s,\,geo}$), Niemand et al. (2012, parameterization based on $n_{s,\,geo}$).

https://doi.org/10.5194/egusphere-2026-484
Preprint. Discussion started: 16 February 2026

3.1.2 Spatial variability

To investigate potential sources of ice-nucleating activity, we first assess the spatial variability of the Greenland dust samples, depicted in Fig. 3 for n_m at -15 °C, which is chosen due its relevance for mixed-phase clouds (Morrison et al., 2012) and comparison to other Arctic studies (e.g., Barry et al., 2023). The ice-nucleating activity shows high spatial variability, which is largest in the Narsarsuaq glacial outwash plain. Notably, this variability does not show clear trends across the transects, suggesting that distance from the glacier, or overall position within the outwash plain does not exert a dominant influence on n_m. Based on the chronosequence concept, more developed soils farther from the glacier, exposed for longer after glacial retreat, would be expected to host greater microbial abundance and biogenic material, and thus potentially higher ice-nucleating activity. However, this pattern is not observed in our samples, suggesting that local environmental factors are more likely to influence the dust's ice-nucleating activity. Moreover, the chronosequence represents a theoretical space for time substitution that is not fully applicable to glacial outwash plains, which are highly dynamic environments characterized by strong seasonal changes and episodic flooding (e.g., glacial lake outburst floods from Lake Hullet occur regularly in Narsarsuaq; Carlson et al., 2020; Carrivick and Tweed, 2019). These processes can strongly affect the presence of vegetation, organic matter, sediment deposition, and therefore also the ice-nucleating ability.

https://doi.org/10.5194/egusphere-2026-484
Preprint. Discussion started: 16 February 2026

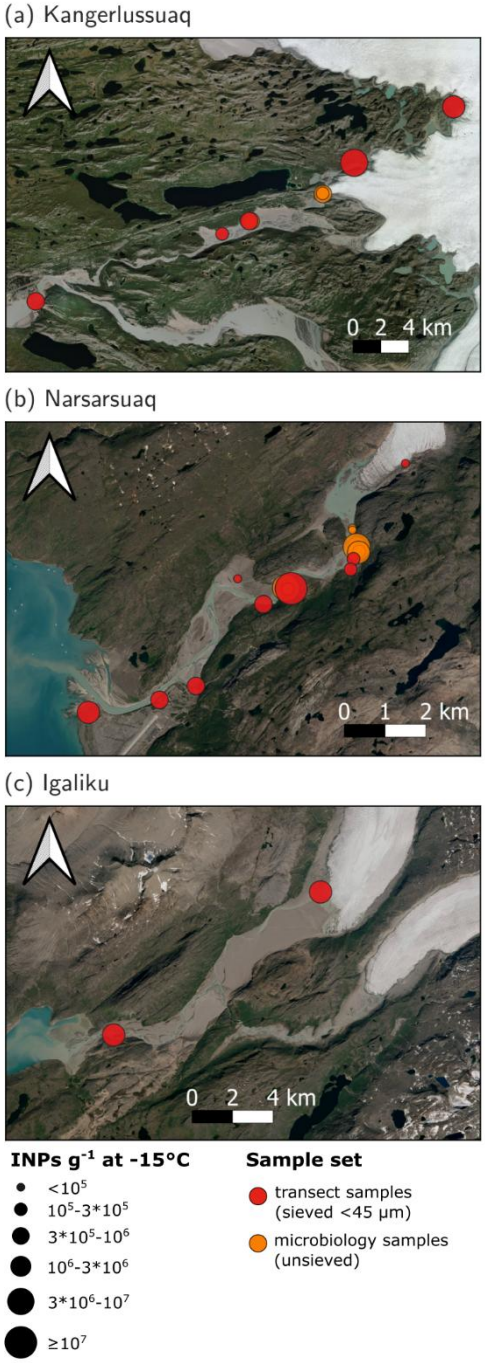

Figure 3. Spatial variability of ice-nucleating activity. INP concentration per gram of bulk dust at -15 °C in (a) Kangerlussuaq, (b) Narsarsuaq, and (c) Igaliku. The red markers correspond to the *transect* samples that were sieved to < 45 µm. *Microbiology* samples refer to unsieved samples (Sect. 2.1.1). The size of the markers corresponds to the INP concentration. Map background imagery was obtained from the Greenlandic satellite orthophoto mosaic provided by Dataforsyningen and accessed via QGreenland (Moon et al., 2023).

https://doi.org/10.5194/egusphere-2026-484
Preprint. Discussion started: 16 February 2026

3.1.3 Sources of ice-nucleating activity

To better understand the sources of the dust's ice-nucleating activity and potential biogenic contributions, we performed heat and hydrogen peroxide treatments to the bulk dust samples, as shown in Fig. 4. The treated samples exhibit INP spectra similar to the example shown in Fig. 4a and are summarized for -10 °C, -15 °C, and -20 °C in Fig. 4b-d. Heat treatment reduces the ice-nucleating activity mainly at temperatures above -13.5 °C (average heat-labile fraction >75 % for temperatures >-13 °C, n = 28) but still shows substantial contributions at -20 °C (Fig. B4). After peroxide treatment, ice-nucleating activity decreases substantially, with the remaining n_m making up only a few percent (2.5 %, average across temperatures and samples, n=5) of the n_m of the untreated sample (Fig. B5). These results suggest that organic compounds are primarily responsible for the ice-nucleating activity of the dust samples, despite the presence of ice-active minerals. This is overall consistent with the literature, where all samples show substantially lower ice-nucleating activity following heat and hydrogen peroxide treatment (Fig. B6; Barry et al., 2025; Tobo et al., 2019; Xi et al., 2022). No clear relationship is observed between heat-labile fraction and n_m values among the Greenlandic samples, even a negative correlation for some temperatures (-8.5 °C to -9.5 °C, Fig. B7). A relationship is also not evident when comparing with the literature: the Greenlandic samples show higher organic fractions than Tobo et al. (2019) (Fig. B5), and the change in median freezing temperature ΔT_{50} (Fig. B8) from untreated to heat-treated samples is similar as in Barr et al. (2023, Fig. 4), although both studies show higher overall ice-nucleating activity (Fig. 2c, d). This may indicate that differences in the type or composition of organic matter play a key role in determining the magnitude of ice-nucleating activity.

3.1.4 Positive correlation of TOC, microbial abundance and INPs

Given the important contribution of organic material on the ice-nucleating activity of the dust samples, we assess the correlation between TOC and n_m, as well as microbial abundance and n_m (Fig. 5). The TOC of the samples is generally low (<0.02-0.74 wt%, average of 0.18 wt%, 10 samples below detection limit of 0.24 mg C g^{-1}), and therefore all samples are lower than the 0.9 wt% measured by Tobo et al. (2019). Samples in the vicinity of vegetation show higher TOC content, but even samples with low TOC content (or just above detection limit) show important organic contributions to the dust's ice-nucleating activity (e.g., Fig. B5d). TOC significantly correlates with n_m at different temperatures. The correlation coefficient shows a slight increase at lower temperatures, possibly due to reduced noise in the data, but also subsets of the data (e.g., only Kangerlussuaq or Narsarsuaq, heat treated samples) show significantly positive correlations (Fig. B9). While comparison of TOC and ice-nucleating activity of soils in different climate zones from Tobo et al. (2019) shows no simple correlation of organic content and ice-nucleating activity, the positive correlation in our samples within the same climate zone could indicate that TOC amount may contribute to the differences across HLD sites. Samples from glacial outwash plains in the Alps in Switzerland have similar or lower n_m values compared to the Greenland samples (Fig. C2). They also show a significant positive correlation with TOC (Fig. C3), but generally have higher TOC values (Fig. C4). Changes in ice-nucleating activity following heat and hydrogen peroxide treatment (Fig. C5, C6) are comparable to the Greenland samples, although the Alp samples show higher

https://doi.org/10.5194/egusphere-2026-484
Preprint. Discussion started: 16 February 2026

inorganic fractions at temperatures < -20 °C. This supports that the ice-nucleating efficiency of TOC may differ across climatic regions, suggesting the importance of TOC composition rather than abundance alone. However, limited information of TOC and HLD INPs are available in the literature to further investigate this relationship.

Tobo et al. (2019) hypothesized that the ice-nucleating activity in the unvegetated glacial outwash plain in Svalbard could primarily stem from microbial sources. We find a significant correlation of microbial abundance with n_m, which is consistent across temperatures when microbial abundance is assessed via colony-forming units (CFU, culturing method, Fig. 5b) and flow cytometry (FC) based cell counts (Fig 5c). Some bacterial species are highly efficient ice nucleators due to ice-binding proteins on their cell membranes, and genera known to include such species (*Pseudomonas* and *Pseudoxanthomonas*, Failor et al., 2017; Joly et al., 2013) were detected in samples from the same outwash plain (Marsh et al., in preparation). Ice-nucleating active species have been identified in precipitation samples at different locations including Greenland (Šantl-Temkiv et al., 2015, 2019; Stopelli et al., 2017). Notably, Šantl-Temkiv et al. (2019) found a positive correlation of airborne bacterial cell concentrations and INPs at -10 °C at Villum Research station in northern Greenland, although they did not detect the ice-nucleation active *ina* genes in their isolates. The positive correlation of microbial abundance and n_m in our samples could directly reflect the presence of ice-nucleating bacterial species. However, TOC also correlates positively with microbial abundance, making it challenging to disentangle their relative contributions to the ice-nucleating activity. Microbiota fix carbon and nitrogen, allowing the development of more complex microbial communities and possibly soil development and plant succession. Therefore, higher microbial abundance may primarily enhance ice-nucleating activity over time and rather indirectly, by contributing to the accumulation of ice-nucleating organic compounds (Bradley et al., 2016; Donhauser and Frey, 2018). This is also reflected in the higher microbial abundance, TOC, and n_m values for vegetated sites compared to unvegetated sites (Fig. B10, *microbiology* samples). In addition, other organisms can contribute to ice-nucleating compounds, e.g., various fungal species have been shown to be ice-nucleating active (Fröhlich-Nowoisky et al., 2015; Huffman et al., 2013; Morris et al., 2013; Pouleur et al., 1992), and likely have an important contribution to the INP population in different Arctic environments (Barry et al., 2025; Gratzl et al., 2025; Jensen et al., 2025).

Overall, the ice-nucleating activity of dust in southwestern Greenlandic glacial outwash plains is lower compared to other high-latitude dust sources. The ice-nucleating activity appears to be primarily influenced by the presence of small quantities of organic and biological matter within the dust samples. Variability in n_m values is closely linked to local environmental factors, including TOC content, microbial cell abundance, and presence of vegetation. Given the lower ice-nucleating efficiency compared to some other sites (Tobo et al., 2019; Barr et al., 2023), applying highly ice-efficient parameterization schemes to all HLD dust sources may overestimate atmospheric INP concentrations (Kawai et al., 2023). Moreover, while increasing Arctic vegetation (Grimes et al., 2024) may enhance ice-nucleating activity by contributing to more biogenic material, it could simultaneously reduce aeolian dust emissions, adding complexity to future projections of Arctic dust and INP dynamics.

https://doi.org/10.5194/egusphere-2026-484
Preprint. Discussion started: 16 February 2026

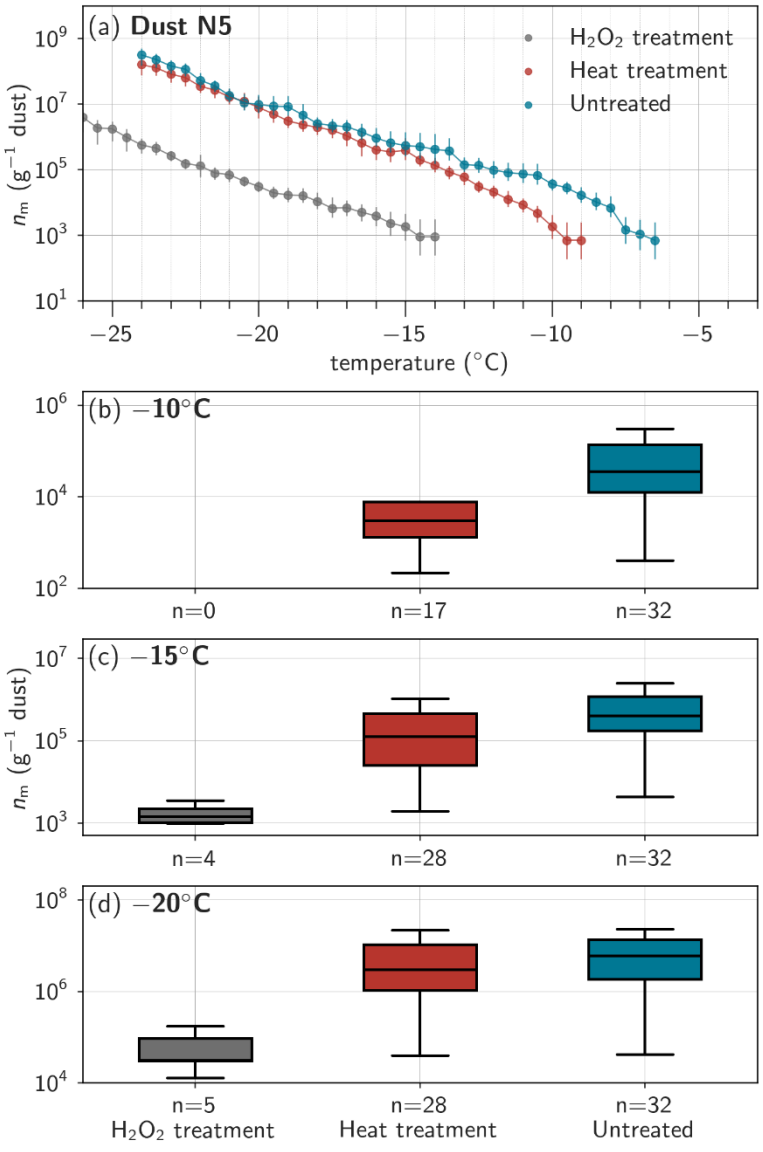

375

Figure 4. INP composition of dust samples. (a) n_m spectra of N5, a bulk dust sample from Narsarsuaq, including heat and hydrogen peroxide treatment. Boxplots of INP concentrations at (b) -10 °C, (c) -15 °C, and (d) -20 °C of bulk dust samples without treatment (n=32), heat treatment (n=28), and hydrogen peroxide treatment (n=5). Note the different y-axis in b-d.

380

https://doi.org/10.5194/egusphere-2026-484
Preprint. Discussion started: 16 February 2026

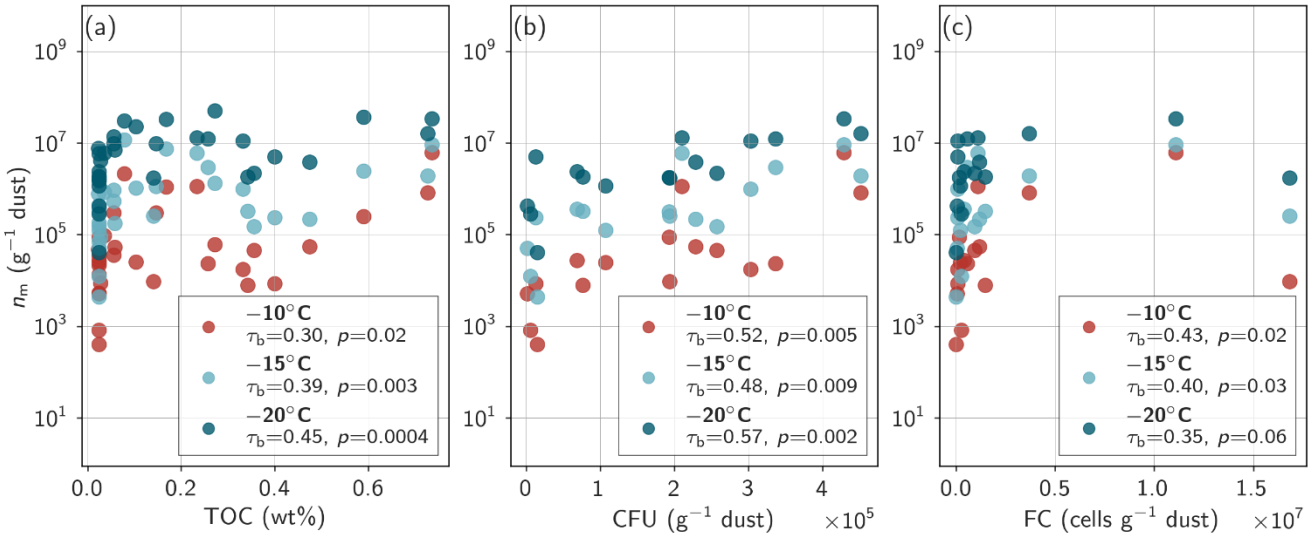

Figure 5. INPs, TOC and microbial cell count. Scatterplot of (a) total organic carbon (TOC) content, microbial abundance determined by (b) colony forming units (CFU), and (c) flow cytometry (FC) vs INP concentration per gram of bulk dust for the temperatures -10 °C, -15 °C, and -20 °C. For each temperature, Kendall's tau correlation coefficient (τ_b) and p-value are annotated.

https://doi.org/10.5194/egusphere-2026-484
Preprint. Discussion started: 16 February 2026

3.2 Atmospheric INP concentrations

Following the dust characterization as a potential INP source in the glacial outwash plains in southwestern Greenland, we assess the atmospheric INP concentrations during summer (June-August 2023) at two sites in Narsaq (*NIRS* and *hill*, fjord environment), and two sites in Narsarsuaq (*plain* and *col*, glacial outwash plain), as described in Sect. 2.1.2. First, we show the general overview of INP concentrations focusing on spatial variability and comparison to literature data, followed by identifying the temporal variability and possible meteorological drivers. Finally, we discuss the potential contribution of the bulk dust ice-nucleating activity on the atmospheric INP population based on a PCA to explore glacial outwash plains as a source of INPs.

3.2.1 Overview of atmospheric INPs in southern Greenland

Fig. 6a depicts the INP spectra colored by location. Overall, the INP concentrations at the Narsarsuaq *plain* and *col* site tend to be higher at relatively warmer temperatures (approximately -20 °C to -8 °C), whereas the *NIRS* site shows elevated INP concentrations at colder temperatures (< -20 °C). INP concentrations at the hill site display the greatest variability, with some periods characterized by very low INP concentrations and others showing higher concentrations in the higher temperature range. The differences in INP concentrations at the different sites likely reflect the influence of very local INP sources, superimposed on a common regional background INP population. The similar, and in part higher, INP concentrations at the Narsarsuaq *plain* and *col* sites suggest a local influence of a more active INP source, such as could be the glacial outwash plain. Although no visible (by eye) dust emissions were observed during the predominantly calm summertime conditions, scanning electron microscopy images of aerosol filter samples (Fig. B11) confirmed the presence of airborne dust at the Narsarsuaq *plain* site. At the more fjord-dominated *NIRS* site, the lower abundance of high-temperature INPs could reflect less biological or other highly active INP sources, whereas the higher INP concentrations at colder temperatures could reflect inputs from road dust, anthropogenic activities, or marine aerosol such as sea salt aerosol. The variable INP concentrations at the *hill* site may reflect a lower background INP level due to stronger marine influence, intermixed with occasional increases in high-temperature INPs, possibly originating from nearby vegetation. Notably, several samples from the *hill* and *col* sites exhibit a sharp increase in INP concentrations between -18 °C and -20 °C, potentially indicating sporadic emissions such as pollen, which are known to become ice-active within this temperature range (Duan et al., 2023).

The observed INP spectra fall within the range reported for other mid- and high-latitude regions (Figure 6b). Compared to other high-latitude dust regions, the INP concentrations in southern Greenland are lower (~1 order of magnitude at -20 °C), likely reflecting the absence of major dust emission events during our campaign, whereas some previous observations (Sanchez-Marroquin et al., 2020; Xi et al., 2022; Barr et al, 2023) were made during periods of elevated atmospheric dust loading and in different seasons (spring and fall). Nevertheless, background INP concentrations in southern Greenland are comparable to summertime observations in Svalbard (Tobo et al., 2019) and Utqiaġvik (Barry et al., 2023), and lie at the higher end of values reported for mid- and high-latitude marine environments and Arctic stations (Mason et al., 2015;

https://doi.org/10.5194/egusphere-2026-484
Preprint. Discussion started: 16 February 2026

Welti et al., 2020; Wex et al., 2019), underlining the likely predominance of local terrestrial INP sources during this period. This interpretation is further supported by the INP spectra normalized to surface area (Fig. B12), where concentrations consistently lie above the parameterization by McCluskey et al. (2018b), which represents clean marine environmental conditions.

To evaluate whether commonly used parameterizations adequately represent the observed INP spectra, we compare our data to the global aerosol parameterization of DeMott et al. (2010, *D10*, Fig. 6c) and the global desert dust parameterization of DeMott et al. (2015, *D15*, Fig. 6d), which are both based on aerosol number concentrations > 0.5 µm. The *D10* parameterization substantially overestimates high-temperature INPs by several orders of magnitude, though it reasonably captures INP concentrations at colder temperatures. In contrast, the *D15* desert dust parameterization aligns more closely with our observations across the full temperature range.

Applying heat and hydrogen peroxide treatment to a subset of filter samples (Fig. 7) leads to strong reductions in INP concentrations at each location, suggesting a large contribution of heat-labile, likely proteinaceous, and organic INP sources. This is generally consistent with other Arctic sites, that also show the predominance of biogenic and heat-labile INPs during summer (Barry et al., 2023; Pereira Freitas et al., 2023; Sze et al., 2023). In comparison to the bulk dust samples (Fig. B5), the heat labile fractions of the atmospheric filter samples are overall larger (Fig. B13, B14), as well as the magnitude of ΔT_{50} (Fig. B8), highlighting the larger contribution of heat-labile, likely biogenic, material in the atmosphere, possibly from vegetated sources. Notably, there is an increased organic and inorganic fraction (and decreased heat labile fraction) in the temperature range around -18 °C (Fig. B13, B14), which points to a non-proteinaceous, possibly polysaccharide source of INPs, such as from pollen (Dreischmeier et al., 2017; Duan et al., 2023). Interestingly, the *D15* dust parameterization still reasonably captures the INP concentrations despite different ice-nucleation mechanisms based on the treatment results.

https://doi.org/10.5194/egusphere-2026-484
Preprint. Discussion started: 16 February 2026

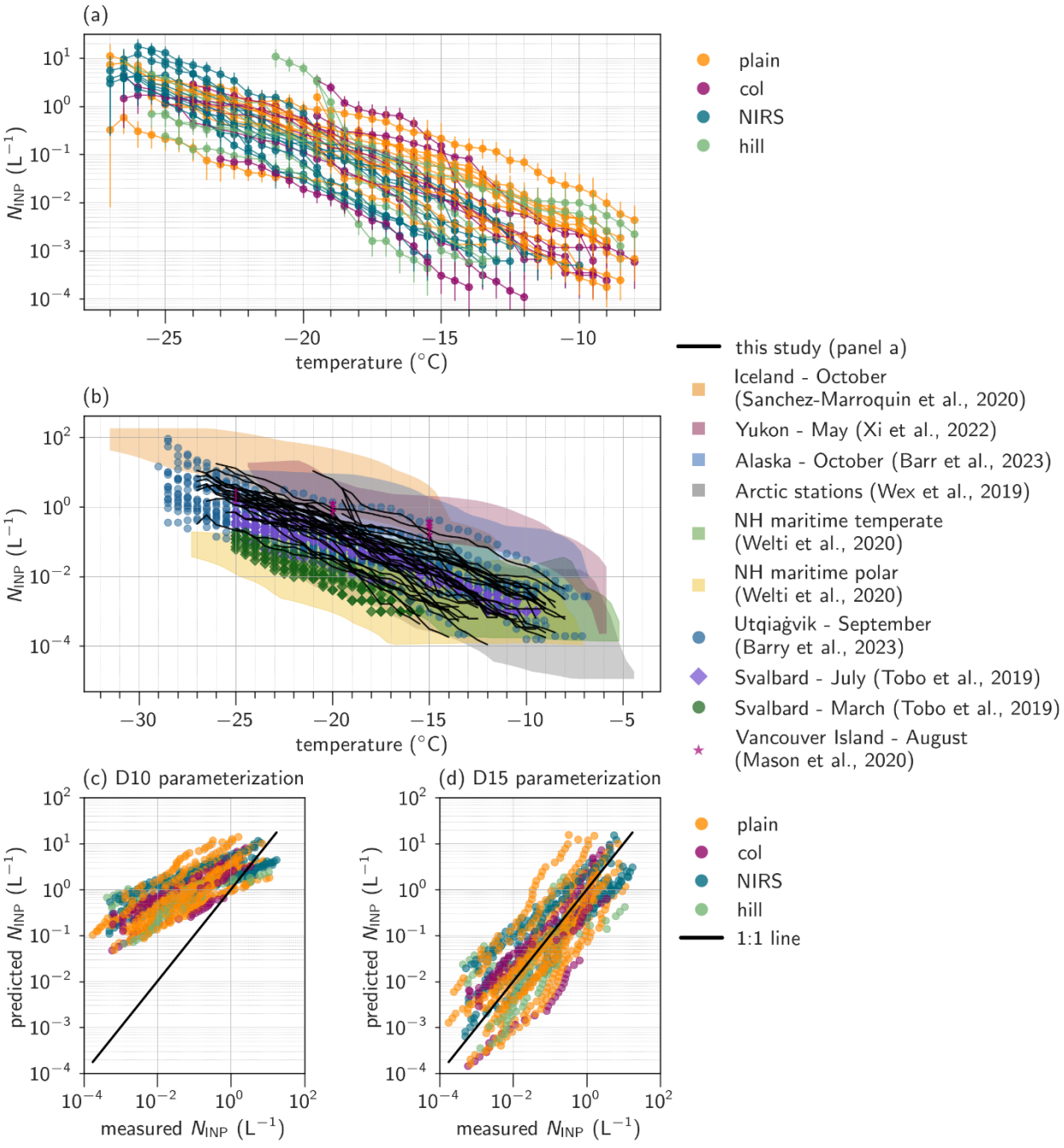

Figure 6. Atmospheric INP concentrations. (a) INP spectra at the different locations including Narsarsuaq plain (*plain*), Narsarsuaq col (*col*), Narsaq International Research station (*NIRS*), and Tasigaaq hill (*hill*) near Narsaq. (b) INP spectra including comparisons from different high- and mid-latitude sites, including Sanchez-Marroquin et al. (2020), Xi et al. (2022), Wex et al. (2019), Welti et al. (2020), Barry et al. (2023), Tobo et al. (2019), Mason et al. (2020). (c) Scatterplot of measured INPs and predicted INP concentrations based on a global aerosol parameterization (DeMott et al. 2010, *D10*), and the global desert dust parameterization (DeMott et al., 2015, *D15*) between -27 °C and -8 °C.

https://doi.org/10.5194/egusphere-2026-484
Preprint. Discussion started: 16 February 2026

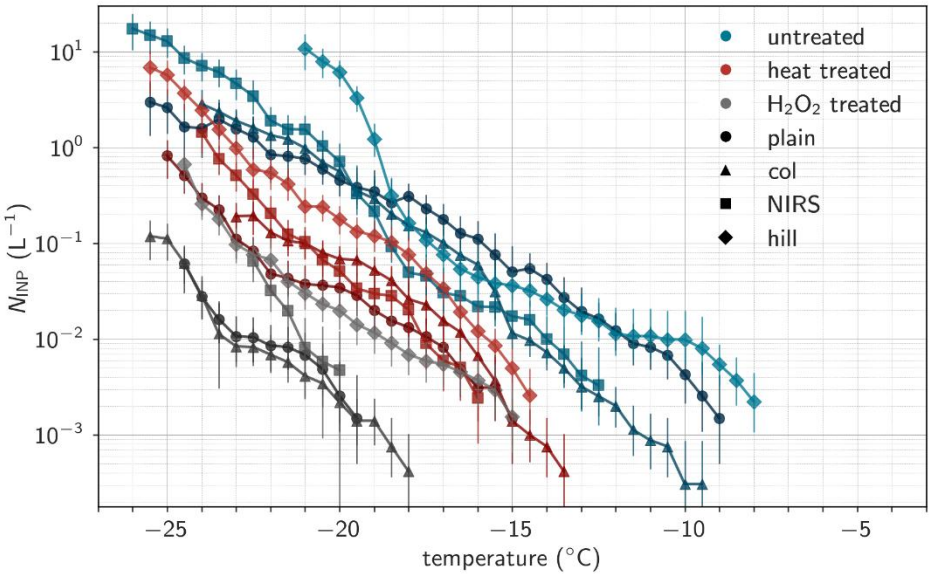

450

Figure 7. INP composition from filter samples. (a) INP spectra of filter samples including heat and hydrogen peroxide treatment at the four different sites: *plain* and *col* in Narsarsuaq, and *NIRS* and *hill* in Narsaq. Marker shape and color shading indicate the different sampling locations.

https://doi.org/10.5194/egusphere-2026-484
Preprint. Discussion started: 16 February 2026

3.2.2 Temporal INP variability

To identify potential sources of atmospheric INPs, we assess the temporal variability in combination with coarse-mode aerosol and meteorological variables in Fig. 8. The highest coarse-mode aerosol concentrations (> 0.5 µm d_{opt}) at the different sites coincided with the transport of biomass-burning plumes from Canadian wildfires (Fig. 8d,e) (Alden et al., 2025). However, despite high aerosol concentrations, the INP concentrations during these periods were typically not higher than during other times (Fig. 8a,b,c, Fig. B15, with exception at the hill site for plume 3), suggesting that the transported plumes had low ice-nucleating efficiency. Although biomass burning aerosols can contribute to INPs (Petters et al., 2009; Pratt et al., 2011; Twohy et al., 2010), they are generally of minor importance in the immersion-mode (Adams et al., 2020) and rather activate at colder temperatures (approximately < -30°C, Kanji et al., 2017).

No clear relationship emerged between meteorological variables, air mass trajectories, and the ambient INP concentrations (though such links may have been obscured by the long and/or variable sampling durations). For most of the campaign, weather conditions were sunny, dry and calm, and air masses came predominantly from the southwestern direction (Fig. B16). The only high-wind speed Foehn event (28-20 July 2023, wind speeds up to 12.5 m s^{-1} at *plain* and 14.8 m s^{-1} at *col*) did not lead to increased coarse-mode aerosol number concentrations, nor INP concentrations (Fig. 8, Fig. B17). Possibly, dust emissions where limited by elevated soil moisture, even though estimates based on Fécan et al. (1999) would suggest that the threshold velocity was exceeded (Fig. B18).

Bioaerosols and INPs have previously been observed to increase during and after precipitation (Conen et al., 2017; Huffman et al., 2013), and observations from northern Finland reported a positive correlation between the abundance of fluorescent particles indicative of fungal spores and relative humidity during summer and autumn, suggesting humidity-driven fungal spore release mechanisms that could contribute to INPs (Gratzl et al., 2025). In our dataset, some spectra with elevated high-temperature INP concentrations occurred during precipitation events (Fig. B19), and the negative correlation between high-temperature INPs and air temperature (Fig. B20) may hint at enhanced biological emissions under the cooler conditions surrounding precipitation events. However, meteorological variables, including precipitation and humidity, do not show a consistent pattern with INP variability across the campaign.

https://doi.org/10.5194/egusphere-2026-484
Preprint. Discussion started: 16 February 2026

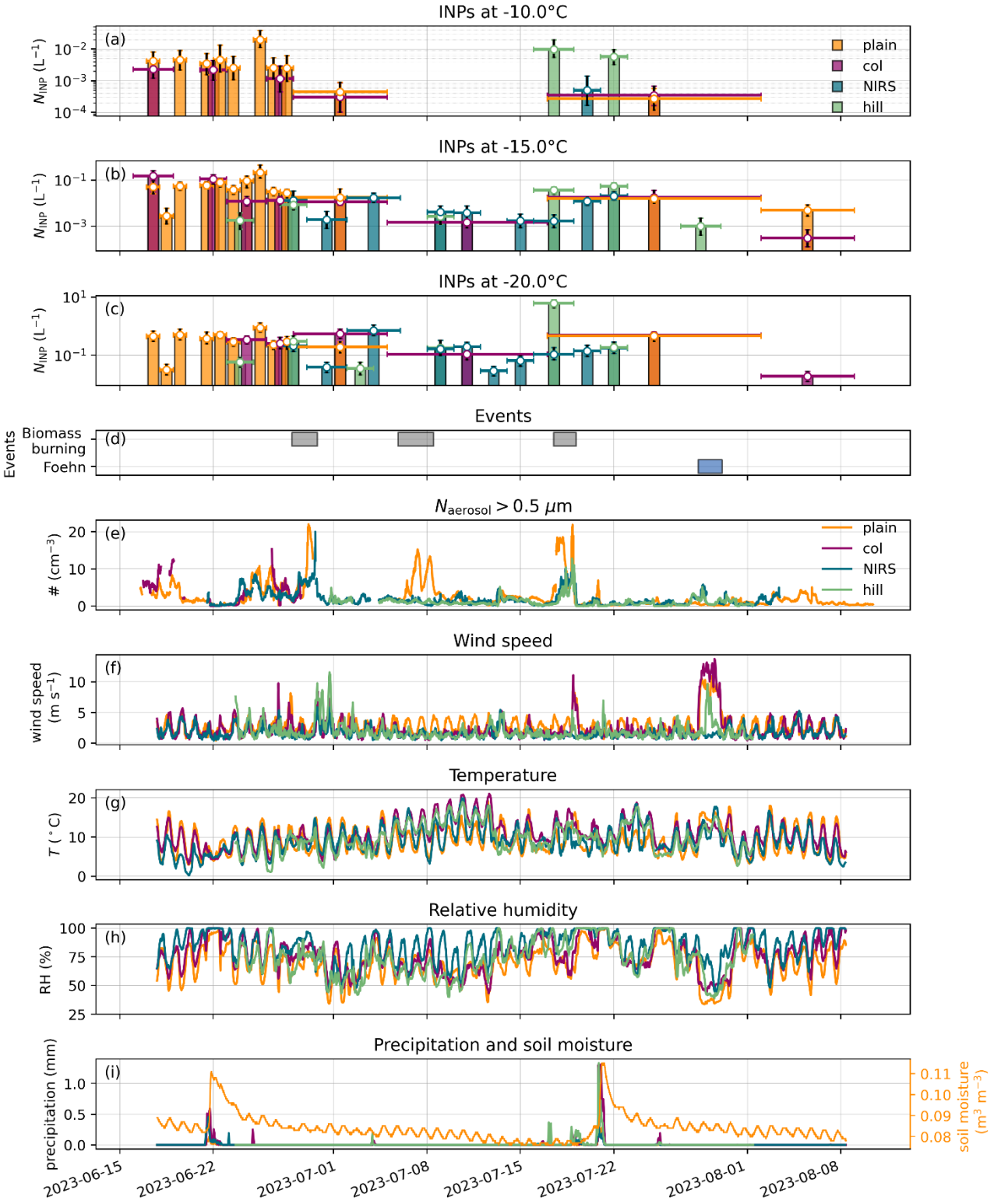

https://doi.org/10.5194/egusphere-2026-484
Preprint. Discussion started: 16 February 2026

Figure 8. Time series of INPs, coarse particles and meteorology. INP concentrations at (a) -10 °C, (b) -15 °C, and (c) -20 °C, the colored horizontal lines indicate the filter sampling period, the vertical errorbars indicate the 95 % confidence intervals. (d) Time periods of events including biomass burning plumes transported from Canada, and a Foehn event. (e) Particle number concentration > 0.5 µm, (f) 2 m wind speed, (g) temperature, (h) relative humidity, (i) precipitation and soil moisture at the different locations including Narsarsuaq plain (*plain*), Narsarsuaq col (*col*), Narsaq International Research station (*NIRS*), and Tasigaaq hill (*hill*) near Narsaq, distinguished by color (legend in panel e). Soil moisture is only measured at the Narsarsuaq *plain* site.

3.2.3 Possible contribution of local dust to atmospheric INPs

The observed differences in INP spectra across sites suggest a potential local influence of the glacial outwash plain on the atmospheric INP population in Narsarsuaq. To further explore the potential sources and relationships among samples, we performed a PCA on all INP measurements, including both atmospheric and bulk dust samples. The PCA was based on the slopes of INP spectra calculated in 2 °C intervals from -8 °C to -20 °C, along with the logarithmic ratios of INP concentrations at each interval relative to -15 °C, similar as in Barry et al. (2023). This allows us to visualize clustering and assess patterns in the variability of INP spectra. Fig. 9 presents the PCA results along the first two principal components (PC1, explaining 50.6 % of the variance and PC2 explaining 15.1 % of the variance). Overall, bulk and filter samples tend to separate along PC1. According to the loading arrows, which indicate the contribution of the original variables to the principal components by their length (magnitude of contribution) and orientation (correlation with the principal components), logarithmic ratios mainly contribute to PC1, whereas slopes contribute to PC2. The samples partially cluster by location, with *NIRS* and *col* samples grouping in a similar region of the plot. Interestingly, most (~10 of 13) of the Narsarsuaq *plain* filter samples cluster together with Narsarsuaq bulk samples, suggesting that some of the bulk dust may indeed contribute to the atmospheric INP population at this location by suspension into the atmosphere. The result can also suggest that the Narsarsuaq *col* INP spectra might already be less affected by the glacial outwash plain dust source, possibly reflecting a more mixed INP composition. The clustering of Narsarsuaq *plain* bulk dust and filter samples persists for heat treated spectra (Fig. B21), though the result is more uncertain due to the much smaller sample size.

https://doi.org/10.5194/egusphere-2026-484
Preprint. Discussion started: 16 February 2026

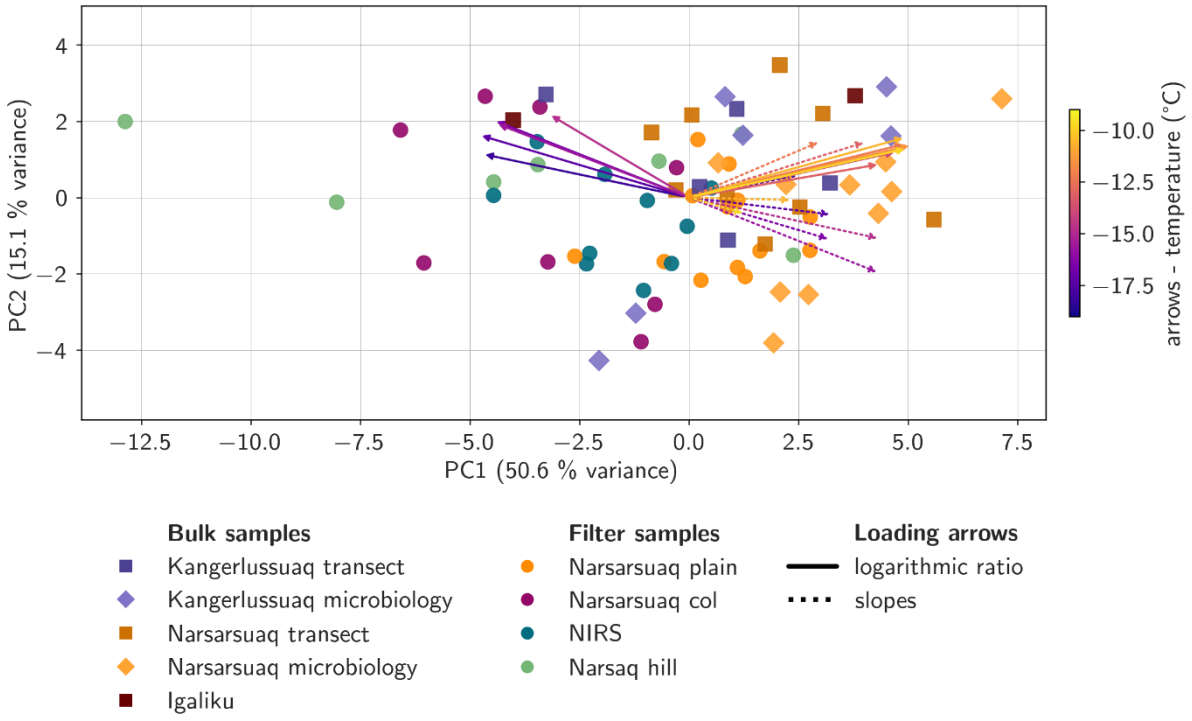

505 **Figure 9. Variability in INP spectra.** Principal component analysis (PCA) for all samples, based on the slopes of INP spectra in 2 °C intervals from -8 °C to -20 °C, and the logarithmic ratios of INP concentrations at each interval relative to -15 °C. The arrows represent the variable loadings, color-coded by temperature, where solid arrows indicate the logarithmic ratios, dotted arrows represent the slopes. Axes represent the first two principal components, note that they are not scaled to the variance explained.

510 Overall, our observations indicate that atmospheric INP concentrations in southern Greenland were driven by a combination of regional background sources and highly localized contributions. The glacial outwash plain in Narsarsuaq likely served as a local HLD INP source under the observed calm summertime conditions, while biogenic INPs, potentially originating from nearby vegetated surfaces, may have contributed to the observed variability at the sampling sites. Further analysis is needed to better constrain the frequency and magnitude of potential elevated dust loading events and PBAP emissions to assess their
515 implications for INP concentrations and cloud glaciation in this region. Improved characterization of HLD sources could focus particularly on the shoulder seasons (spring and autumn), when higher wind speeds and reduced soil moisture are likely to enhance dust emissions. To better understand biological INP sources, complementary measurements such as fluorescent particles, PBAP tracers (e.g., mannitol, arabitol), pollen and spore sampling, or microscopy-based particle detection, could help to constrain their emissions and contribution to INPs in glacial outwash plains and other high-latitude environments.

https://doi.org/10.5194/egusphere-2026-484
Preprint. Discussion started: 16 February 2026

4. Conclusions

We investigated the ice-nucleating activity of glacial dust and the mixed ambient aerosol population in southwestern Greenland to identify possible INP sources and their characteristics, given their relevance for mixed-phase clouds and Arctic climate processes. Glacial dust from outwash plains in southwestern Greenland shows ice-nucleating properties relevant for the mixed-phase cloud regime (n_m of 4.4×10^4 to 1.2×10^7 g^{-1} dust at -15 °C), but lower ice-nucleating activity compared to other high-latitude dust sites, cautioning against the use of highly ice-nucleating dust parameterization schemes for the entire Arctic. Ice-nucleating activity and its variability are primarily driven by small amounts (<0.02-0.74 wt%) of organic material, likely related to local environmental factors such as vegetation and the presence of microbiota. This is supported by both (i) the strong reduction of n_m following heat and hydrogen peroxide treatments (at -15 °C, on average 68 % of the ice-nucleating activity is heat-labile, and over 99 % is attributable to organic material), and (ii) the significant correlation with TOC and microbial abundance. Differences between high-latitude dust regions may be driven by the characteristics of these biogenic INP sources, particularly for relatively warm temperatures (approximately > -15 °C). Atmospheric INP concentrations in southern Greenland (3×10^{-4} to 0.2 L^{-1} at -15 °C) are comparable to other high-latitude summertime observations and exceed those reported for marine-dominated environments. The higher fractions of organic and heat-labile INPs (on average at -15 °C, 87 % heat-labile INPs, 95 % organic INPs) compared to the bulk dust samples further point to a substantial biogenic contribution in the atmosphere. Spatial variability between the four sampling sites suggests high influence from local sources, with the Narsarsuaq outwash plain likely representing a local HLD INP source. This interpretation is supported by the similarity of Narsarsuaq dust and filter samples in the PCA, and the elevated warm-temperature INP (> -15 °C) concentrations observed at the Narsarsuaq outwash plain site, that could arise from a mix of dust and organic material.

These findings provide a characterization of potential and observed INP sources in southern Greenland and highlight the important role of biogenic contributions. Interestingly, the DeMott et al. (2015) global desert dust parameterization describes the observed INP activity at all sites quite well and could be used as proxy. On small scales, detailed investigations into the specific organisms and compounds that influence the dust's ice-nucleating activity could help to further understand differences among regions and improve our understanding on how INP sources may evolve in a warming and increasingly vegetated Arctic. On broader spatial and temporal scales, assessing the influence of outwash plains on cloud glaciation and the regional radiation budget requires more precise, year-round quantification of INP emission fluxes, including both dust and biological particles. Developing and evaluating regionally constrained INP parameterizations, informed by different INP sources as well as observational and modelling efforts, could improve the representation of mixed-phase cloud processes and their climatic impacts.

https://doi.org/10.5194/egusphere-2026-484
Preprint. Discussion started: 16 February 2026

Appendix A: The Sion Particle Ice Crystallization Experiment (SPICE)

A1 General working principle

The Sion Particle Ice Crystallization Experiment (SPICE) is an offline droplet freezing technique for quantifying immersion-mode ice-nucleating activity of aerosol or other environmental samples. SPICE is built based on the design of the Karlsruhe Institute of Technology (KIT) INSEKT (Schneider et al., 2021) and the Colorado State University (CSU)-IS (Hill et al., 2016), and similar methods and set-ups that are widely used in ice nucleation research (e.g., Chen et al., 2018; David et al., 2019; Miller et al., 2021). In these droplet freezing assays, microliter- to nanoliter-sized droplets containing the sample are cooled at a controlled rate until freezing is observed. From the fraction of frozen droplets as a function of temperature, the cumulative concentration of ice-nucleating particles (INPs) active at a given temperature is inferred using statistical methods (Vali, 1971). We first describe the instrument design in Sect. A1.1, followed by the typical workflow of INP measurements in Sect. A1.2 and the associated data processing and INP calculations in Sect. A1.3. Sect. A2 provides details regarding the temperature calibration and uncertainty (Sect. A2.1), the water background signal and limit of detection (Sect. A2.2), and the validation of the instrument using measurements of two ice-nucleating materials and comparison to the literature (Sect. A2.3).

A1.1 Instrument Design

The general set-up of the SPICE is shown in Fig. A1a with its three main components: a chiller (Lauda RP 245 E, Germany), the central part with the cooling block and camera assembly, and a computer for data acquisition and processing. The central part (Fig. A1b) consists of two aluminum incubation blocks (Cat. No. Z743474, Sigma Aldrich, USA) designed to hold 96-well PCR trays (Cat. No. 781368, BRAND, Germany). The aluminum blocks have been modified to allow the cooling liquid (silicon oil KRYO 51, Lauda, Germany) to flow from the chiller through milled channels (9.5 width, 15.5 mm height, Fig. A1c), to ensure an approximately uniform temperature control. The blocks are insulated with polystyrene plates and housed in a custom-made PVC box. Each of the two blocks contains four evenly distributed PT100 sensors (TC Direct, Germany) to monitor the temperature (Fig. A1c). The set-up is housed in a metal-box to reduce external influence (e.g., light, dust or humidity) on the measurements.

For experiments, PCR trays containing the sample are placed in the aluminum blocks. The PVC housing is closed with a glass pane. To avoid condensation, synthetic filtered air can be passed through 20 small tubes positioned above and below the glass pane. To record freezing events visually, a camera (USB3 Vision industrial camera U3-3880LE Rev.1.2, IDS, Germany) with a polarizing filter, and an LED lamp are mounted 35 cm above the aluminum blocks.

The temperature is controlled via the chiller, typically using a linear cooling ramp from +2 °C to −35 °C at a rate of 0.33 °C min^{-1}. The PT100 sensors log at 1 s resolution using a Madgetech 4 data logger (MadgeTech, USA). Images are simultaneously acquired at 1 Hz and stored locally. When the experiment is finished, a custom-made Python script synchronizes the image and temperature data (https://github.com/EERL-EPFL/freezing-droplets), and detects freezing events through brightness changes in circular regions corresponding to each droplet. All experimental data and metadata are archived in a dedicated INP

https://doi.org/10.5194/egusphere-2026-484
Preprint. Discussion started: 16 February 2026

database (https://github.com/EERL-EPFL/spice-ui, https://github.com/EERL-EPFL/spice-api, https://github.com/EERL-EPFL/spice-client).

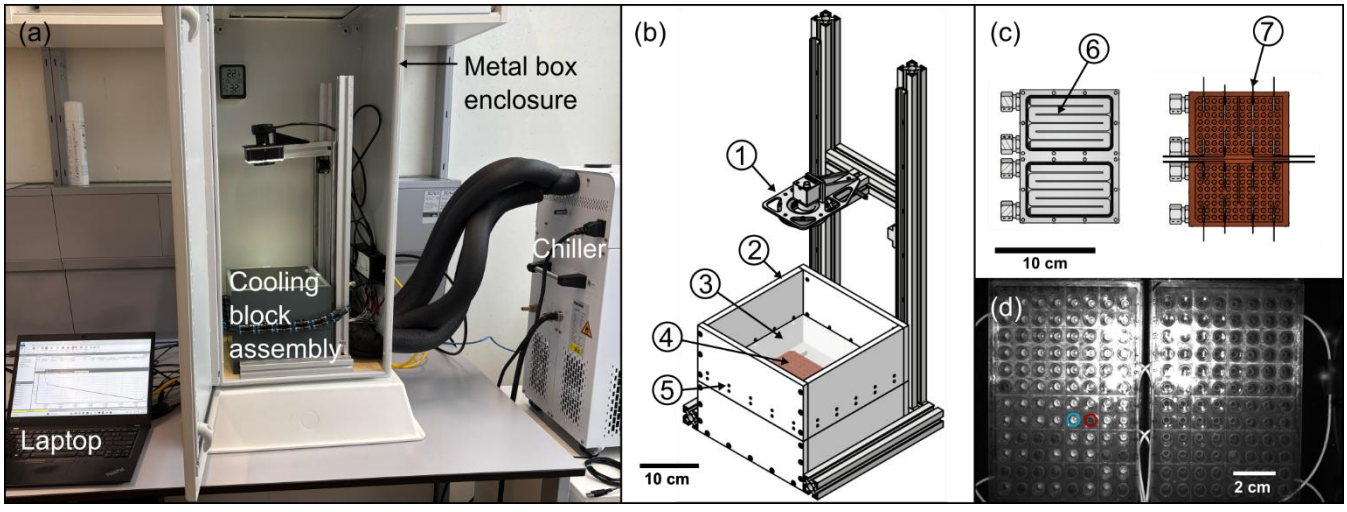

Figure A1. SPICE. (a) Photograph of the SPICE set-up. (b) Model of the cooling block assembly. The numbered items correspond to (1) the camera and LED lamp, (2) the PVC box, (3) the glass pane, (4) the aluminum cooling blocks, (5) holes for filtered air-flow tubes. (c) Details of the aluminum block including (6) milled channels for cooling liquid (when red part of the block removed), and (7) placement of temperature sensors. (d) Example of an image during the freezing experiment including an example of a frozen (red circle) and unfrozen (blue circle) droplet.

A1.2 Experimental workflow of a typical experiment

The workflow of a typical experiment is illustrated in Fig. A2. It generally consists of preparing a sample suspension (1), applying optional treatments (1a, 1b), creating dilutions (2), pipetting droplets into PCR trays (3), running the freezing experiment (4), and data processing and quality control (5, Sect. A1.3). All preparation steps are performed under a laminar flow hood.

- Sample preparation (1 & 2): For filter samples (we use Nuclepore™ polycarbonate filters with 47 mm diameter, 0.2 µm pore diameter), the filter is inserted in washing water (typically 5-12 mL of bio-molecular-biology-free reagent water from Sigma Aldrich (Cat. No. W4502, Sigma Aldrich, USA), hereafter referred to as SA water) and placed in a tube rotator for 20 min to extract the aerosols. For bulk samples, an initial suspension is prepared by weighing a defined mass of the material and adding SA water to reach the desired concentration, typically we use an initial concentration of approximately 2 g L^{-1}. The initial suspension is typically shaken by hand, or also placed in the tube rotator for a couple of minutes. Depending on sample characteristics, dilution series are then created, e.g., two 15-fold dilutions for filter samples, and four 10-fold dilutions for bulk samples, as applied in this study.

https://doi.org/10.5194/egusphere-2026-484
Preprint. Discussion started: 16 February 2026

- Treatments (1a, b): If treatments are applied, they are performed on a smaller subsample of the initial suspension. The dilution series is subsequently prepared from this treated suspension.
    a) For heat treatments, the tube with typically 3 mL of the initial suspension is immersed in a boiling water bath for 20 min.
    b) For hydrogen peroxide treatments, 1 ml of 30 % H_2O_2 is added to 2 mL of sample and the tube is placed in a boiling water bath illuminated with UV radiation for 20 min. Residual H_2O_2 is then digested by adding small volumes (typically around 90-130 µL) of catalase (Cat. No. MPB-210042910-10ML, MP Biomedicals, USA).
- Droplets in PCR tray (3): The prepared suspensions and dilutions are pipetted into PCR trays, with a droplet volume of 50 µL per well. Each dilution is distributed across a designated region of the tray, using a minimum of 32 wells per dilution. One region is reserved as negative control with only SA water, to determine background freezing. Air bubbles are removed with the pipette tip to avoid artefacts in freezing behavior.
- Freezing experiment (4): The PCR trays are then sealed with foil (Cat. No. AXYPCR-TS, Axygen, Corning Inc., USA), and inserted into the cooling blocks. The experiment is run by starting the temperature logging, image acquisition, as well as the cooling program.
- Data processing (5): Following the experiment, the data is processed and quality controlled, as described in the next section (A1.3).

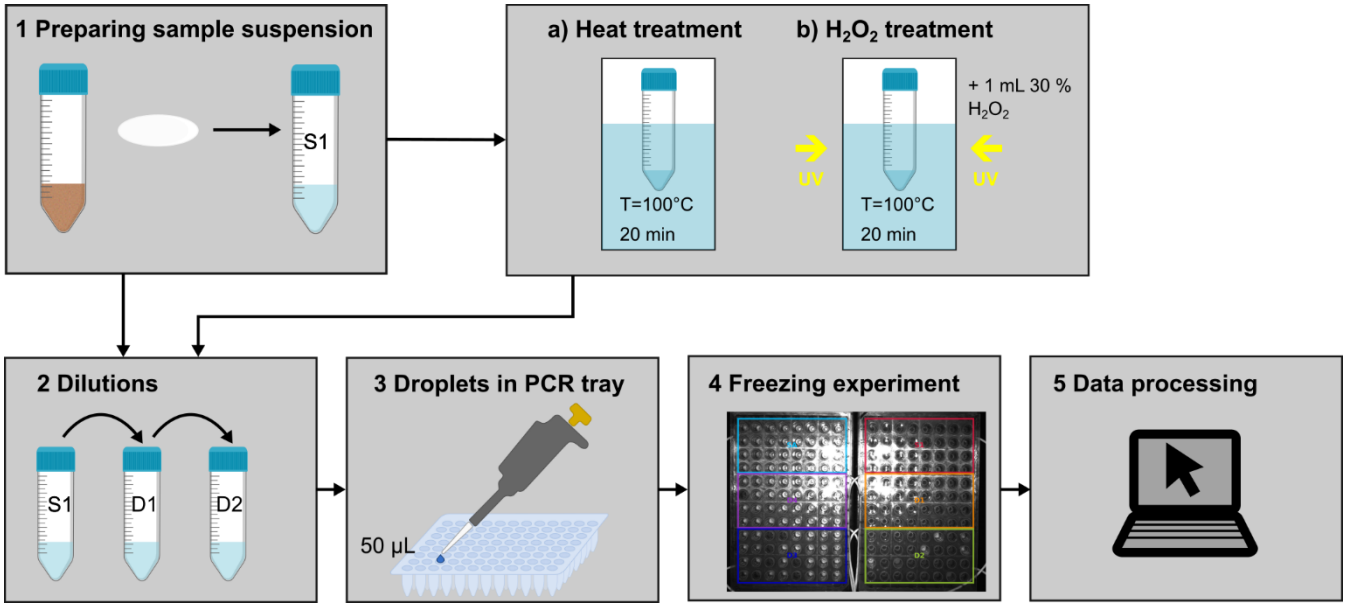

Figure A2. INP freezing assay workflow. (1) Preparing sample suspension (S1) from, e.g., a bulk dust or a filter sample. Optionally, treatments can be performed on the initial suspension, such as (a) heat or (b) H_2O_2 treatment. From the initial suspension, (2) a dilution series is created (e.g., dilutions D1 and D2) and (3) pipetted into PCR trays, with a typical droplet volume of 50 µL. (4) The freezing experiment is performed, and followed by (5) data processing.

https://doi.org/10.5194/egusphere-2026-484
Preprint. Discussion started: 16 February 2026

A1.3 Data processing and INP calculations

To acquire the data from each experiment, the image and temperature data are first synchronized using the Python-based freezing-droplets routine. In the following, we describe the typical steps used to process the data and calculate INP concentrations.

Temperature data are first checked for outliers. In case of electrical noise or unrealistic data points, a despiking function is applied, or the faulty sensor excluded. Temperatures are then averaged across all sensors and adapted using the calibrations described in Sect. A2.1. Data are aggregated into 0.5 °C intervals, and the frozen fraction, the proportion of frozen droplets at each temperature, is computed for every dilution. The 95 % confidence intervals are calculated based on binomial sampling uncertainty, using equation 2 in Agresti and Coull (1998), which is appropriate for a small sample size (Brown et al., 2001) and typically used in INP calculations (e.g., Hill et al., 2016; Schneider et al., 2021):

$$CI_{\text{upper,lower}} = \left(FF + \frac{z_{\alpha/2}^2}{2n} \pm z_{\alpha/2} \sqrt{\frac{FF(1-FF) + \frac{z_{\alpha/2}^2}{4n}}{n}} \right) \frac{1}{1 + \frac{z_{\alpha/2}^2}{n}} \quad \text{(A1)}$$

Where FF is the frozen fraction ($\hat{p}$ in the original formula) and n corresponds to the number of wells. For 95 % confidence intervals, $z_{\alpha/2}$ has a value of 1.96, based on the $1 - \frac{\alpha}{2}$ quantile for $\alpha = 0.05$ of a standard normal distribution.

Further quality checks are performed, similar to Böhmländer et al. (2025):

1. Temperature difference to the water background: The temperature difference at a given frozen fraction ΔT_{FF} between background water and sample must exceed 1 °C; otherwise, a warning flag is assigned.
2. Temperature difference between dilutions: ΔT_{FF} between consecutive dilutions must be larger than 1 °C; otherwise, a warning flag is assigned.
3. Freezing sequence: Dilutions must freeze in the expected order, with highest concentration first and lowest concentration last; otherwise, an error flag is assigned.
4. Confidence intervals: $\frac{CI_{95\%\,\text{upper}}}{CI_{95\%\,\text{lower}}} < x$, where x is a user-defined threshold to flag data points with large confidence intervals (here, x=5). Data exceeding this threshold are assigned a warning flag.

Data with error flags are removed, while data with warning flags may be removed following manual inspection. For checks 1-3, we assess the frozen fractions of 0.25, 0.5, and 0.75.

The cumulative INP concentrations as a function of temperature T are derived following Vali (1971) and the equations presented here correspond to the formulations commonly applied in droplet freezing studies (e.g., DeMott et al., 2017; Kanji et al., 2017). The calculations are based on the assumption that freezing is only a function of temperature and time-independent,

https://doi.org/10.5194/egusphere-2026-484
Preprint. Discussion started: 16 February 2026

and that INPs are distributed randomly and independently across droplets, following a Poisson distribution. The cumulative INP concentration in the suspension as a function of temperature can thus be derived as follows:

$$INP_{\mathrm{sus}}(T) = -\frac{\ln\left(1 - FF(T)\right)}{V_{\mathrm{d}}} \tag{A2}$$

where *FF(T)* is the fraction of frozen droplets at temperature *T*, and V_{d} is the droplet volume (50 µL in this study).

To cover a wider temperature range, it is common to dilute the sample, thereby reducing the number of INPs in each droplet:

$$INP_{\mathrm{sus}}(T) = -\ln\left(1 - FF(T)\right)\frac{d}{V_{\mathrm{d}}} \tag{A3}$$

where *d* is the dilution factor.

Since some INPs can also originate from the background water or other contaminations (PCR trays, pipette tip, handling, etc.) used to create the suspension and dilutions, the INP concentration in the suspension is corrected based on the frozen fraction of the water background.

$$INP_{\mathrm{sus,corr}}(T) = -ln\left(\frac{1 - FF(T)}{1 - FF_{\mathrm{background}}(T)}\right)\frac{d}{V_{\mathrm{d}}} \tag{A4}$$

Depending on the properties of the sample, the ice-nucleating activity is expressed or calculated differently. For atmospheric filter samples, we calculate the atmospheric INP concentrations as:

$$N_{\mathrm{INP}}(T) = INP_{\mathrm{sus,corr}}(T)\frac{V_{\mathrm{wash}}}{V_{\mathrm{air}}} \tag{A5}$$

where V_{wash} is the volume of washing water to extract the aerosols in the initial suspension, and V_{air} is the total air volume that passed through the filter sample.

For bulk samples, the ice-nucleating activity is often normalized to the mass of the sample, and expressed as ice-active mass site densities n_{m}:

$$n_{\mathrm{m}}(T) = INP_{\mathrm{sus,corr}}(T)\frac{1}{C_{\mathrm{m}}} \tag{A6}$$

where C_{m} is the mass concentration of the bulk sample in the suspension.

Alternatively, the ice-nucleating activity can also be normalized to the surface area of the sample, which is referred to as ice-active surface site densities n_{s}:

$$n_{\mathrm{s}}(T) = INP_{\mathrm{sus,corr}}(T)\frac{1}{C_{\mathrm{m}}SSA} \tag{A7}$$

Where *SSA* is the specific surface area of the sample, obtained through direct measurements, or estimated geometrically.

To create one INP spectrum, INP concentrations of different dilutions are averaged for overlapping temperatures, and confidence intervals are adjusted taking into account asymmetric uncertainties, by applying the code of Laursen et al. (2019).

https://doi.org/10.5194/egusphere-2026-484
Preprint. Discussion started: 16 February 2026

A2 Characterization and validation

A2.1 Temperature calibration and uncertainty

Accurate temperature measurements are essential for quantifying the ice-nucleating activity in droplet freezing assays. The freezing temperatures reported for each experiment are based on the mean of the eight PT100 sensors positioned in the aluminum block that is cooled via the circulating chiller fluid. This section describes the intercomparison and calibration of the eight sensors relative to one another, the calibration of the block temperature against the temperature inside the wells, and the quantification of the overall temperature uncertainty.

To ensure accurate temperature measurements in the aluminum block, the PT100 temperature sensors were intercompared by positioning them together inside the block and placing the assembly in a cooling chamber. The chamber was cooled to -24 °C, and let to warm up from -24 °C to +18 °C over 64 hours to provide a stable and homogeneous thermal environment. For each sensor, the measured temperature was compared to the mean temperature of all sensors within the stable range (−15 °C to 18 °C, temperatures below -15 °C showed small fluctuations due to a faster warming rate). A linear fit of each sensor's temperature anomaly relative to the ensemble mean was used to determine a constant calibration offset (as slopes were equal to 1). The offsets, summarized in Table 1, were applied as corrections to the raw temperature data from the PT100 sensors.

Table 1. Calibration constants for PT100 temperature sensors.

Temperature sensor	1	2	3	4	5	6	7	8
Intercept (°C)	-0.08	0	0.03	0.07	-0.03	-0.06	0.1	-0.03

Due to the sensor positions and spatial differences in heat transfer from the cooling liquid, small temperature gradients across the block are expected. The minimum and maximum standard deviations of 212 experiments are shown in Fig. A3, and show that the temperature spread is not constant over time. Variability is notably larger prior to 20 March 2025 and decreased thereafter. This change coincided with improvements to the laboratory air conditioning, which created a colder and drier laboratory environment. In addition to the colder ambient temperatures, SPICE could be operated with minimal or no filtered airflow, whereas previously stronger airflow was required to prevent condensation, an approach that also contributed to increased temperature variability.

As these changes affect temperature stability, the sample measurement period is separated into period 1 and period 2 (shaded regions in Fig. A3), for which temperature uncertainty is quantified independently. Fig. A4 shows the median, interquartile range, and full range of temperature standard deviations as a function of temperature for both periods. Temperature variability increases toward colder temperatures in both cases, but more strongly in period 1. At -30 °C, the maximum standard deviation reaches 0.57 °C in period 1, compared to 0.28 °C in period 2, which is similar to comparable set-ups (e.g. 0.6 °C in David et al., 2019; 0.5 °C in Miller et al., 2021).

https://doi.org/10.5194/egusphere-2026-484
Preprint. Discussion started: 16 February 2026

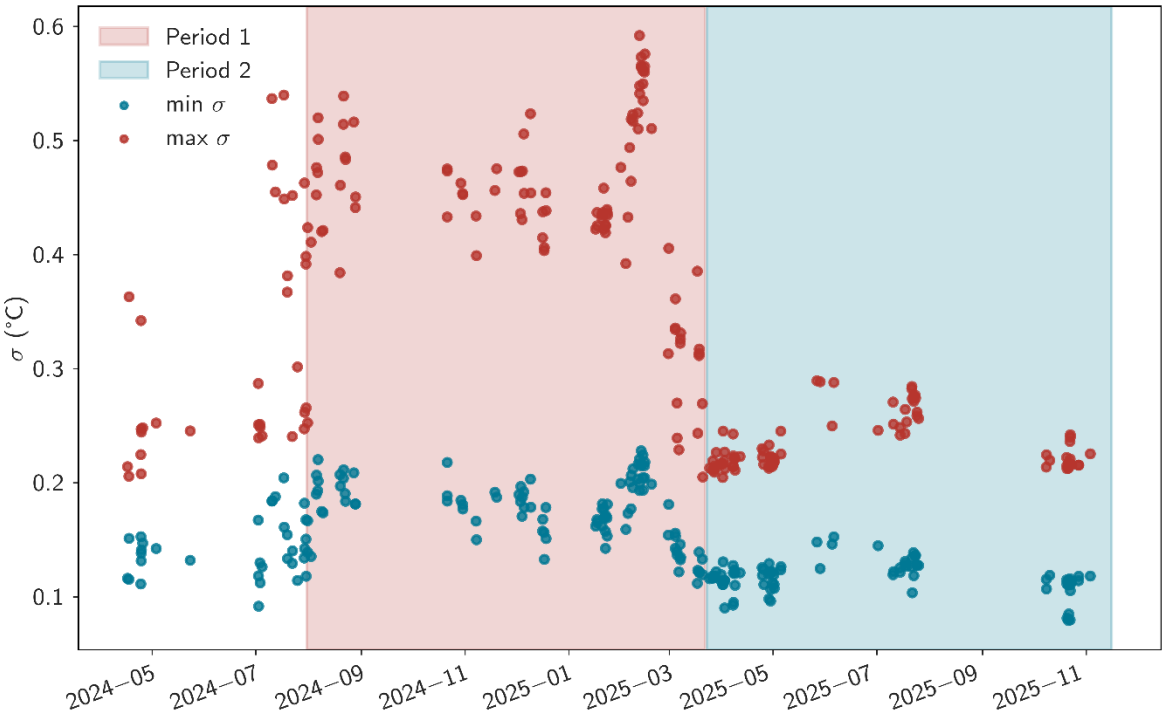

Figure A3. Temperature standard deviation over time. Minimum and maximum temperature standard deviations (σ) for each experiment. The laboratory environmental conditions varied over time with a change in laboratory air conditioning in March 2025, which is why we have split the sample experiments into period 1 and 2, that show different temperature variability. The unmarked period before period 1 corresponds to various test experiments.

https://doi.org/10.5194/egusphere-2026-484
Preprint. Discussion started: 16 February 2026

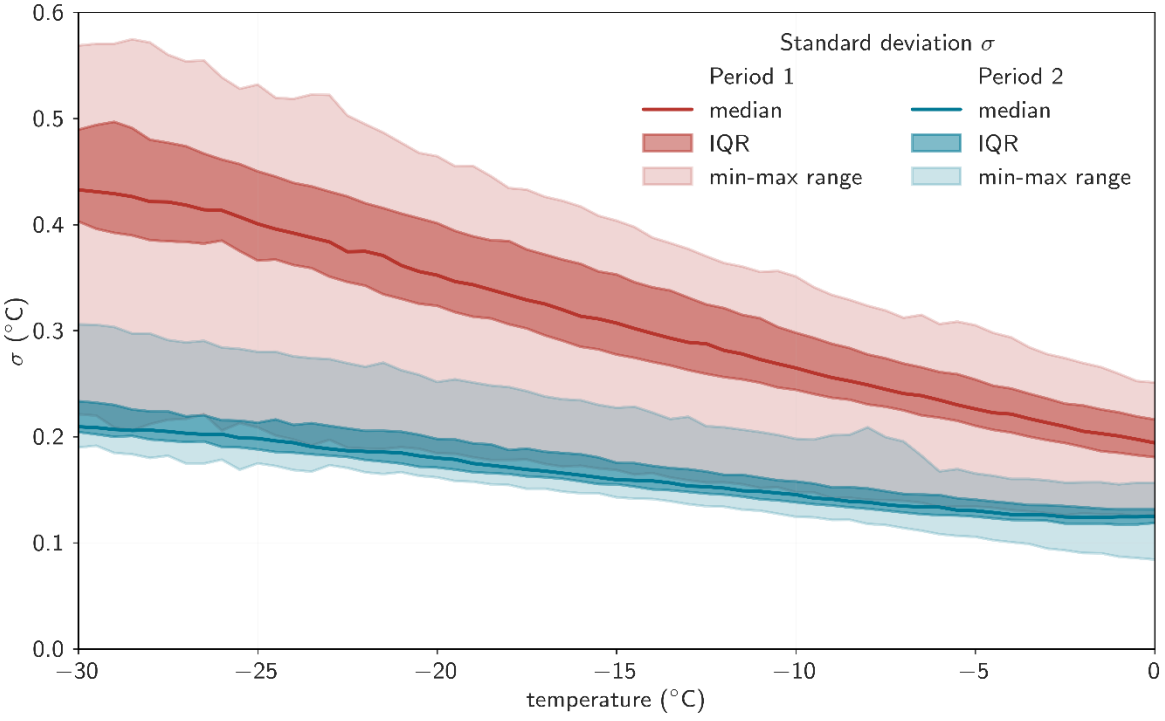

Figure A4. Temperature standard deviation as a function of temperature. Median, interquartile range (IQR) and minimum-maximum range temperature standard deviations derived from eight PT100 temperature sensors across 212 experiments, separately for period 1 and period 2, illustrating the variability in temperature homogeneity within the aluminum block as a function of temperature.

Some heat loss is expected between the temperature sensors embedded in the aluminum block and the actual droplet positions in the PCR trays. To quantify this offset, temperature calibration experiments were carried out using the following setup: eight K-type thermocouples (TW-KT3P-1000, Thermosense, UK) were placed into wells filled with ethanol (Fig. 5c), and a standard freezing experiment was performed with a cooling rate of 0.33 °C min^{-1}. Thermocouple temperatures were recorded using an external data logger (HH-4208SD, Thermosense, UK). A linear regression was applied between the average temperature measured by the PT100 sensors in the block ($T_{\mathrm{block,avg}}$) and the average temperature in the wells measured by the thermocouples ($T_{\mathrm{well,avg}}$).

Given the temperature variability over time, which also affects differences in block and well temperatures, we applied separate calibrations for period 1 and period 2. For period 1, three calibration experiments were conducted with filtered airflow, using different thermocouple placements to ensure representative spatial coverage across the PCR trays. The combined calibration (Fig. 5a, average of slopes and intercepts of the three experiments) yields the relationship:

$$T_{\mathrm{well,avg}} = 0.96 \times T_{\mathrm{block,avg}} + 0.63 \quad \text{(A8)}$$

The calibration uncertainty is approximated by the standard deviations of slopes ($\sigma_{\mathrm{m}}: \pm 0.008$) and intercepts ($\sigma_{\mathrm{b}}: \pm 0.26$). Combined with the maximum block-temperature uncertainty ($\sigma_{T_{\mathrm{block}}}: \pm 0.57$), the uncertainty in well temperatures is estimated by propagating the uncertainties:

https://doi.org/10.5194/egusphere-2026-484
Preprint. Discussion started: 16 February 2026

$$\sigma T_{\text{well}} = \sqrt{[\left(\left(\frac{\sigma_m}{m}\right)^2 + \left(\frac{\sigma_T}{T}\right)^2\right) \cdot |mT|]^2 + \sigma_b^2} \quad \text{(A9)}$$

For period 1, this results in a total well-temperature uncertainty of $\sigma_{T_{\text{well}}} = \pm 0.65$ °C.

For period 2, three additional calibration experiments were performed with the same setup, but without the filtered airflow. The combined calibration (Fig. 5b) results in the following equation:

$$T_{\text{well,avg}} = 0.96 \times T_{\text{block,avg}} + 0.12 \quad \text{(A 10)}$$

The smaller offset between block and well temperatures, together with reduced temperature variability, leads to a lower total uncertainty of $\sigma_{T_{\text{well}}}$=±0.28 °C, based on Eq. A9 (σ_m: ± 0.001, maximum $\sigma_{T_{\text{block}}}$: ± 0.28, σ_b: ± 0.054). Although Eq. A9 assumes independent uncertainties, which may not strictly be true, the resulting estimates remain conservative because we use the maximum observed temperature standard deviations across all experiments.

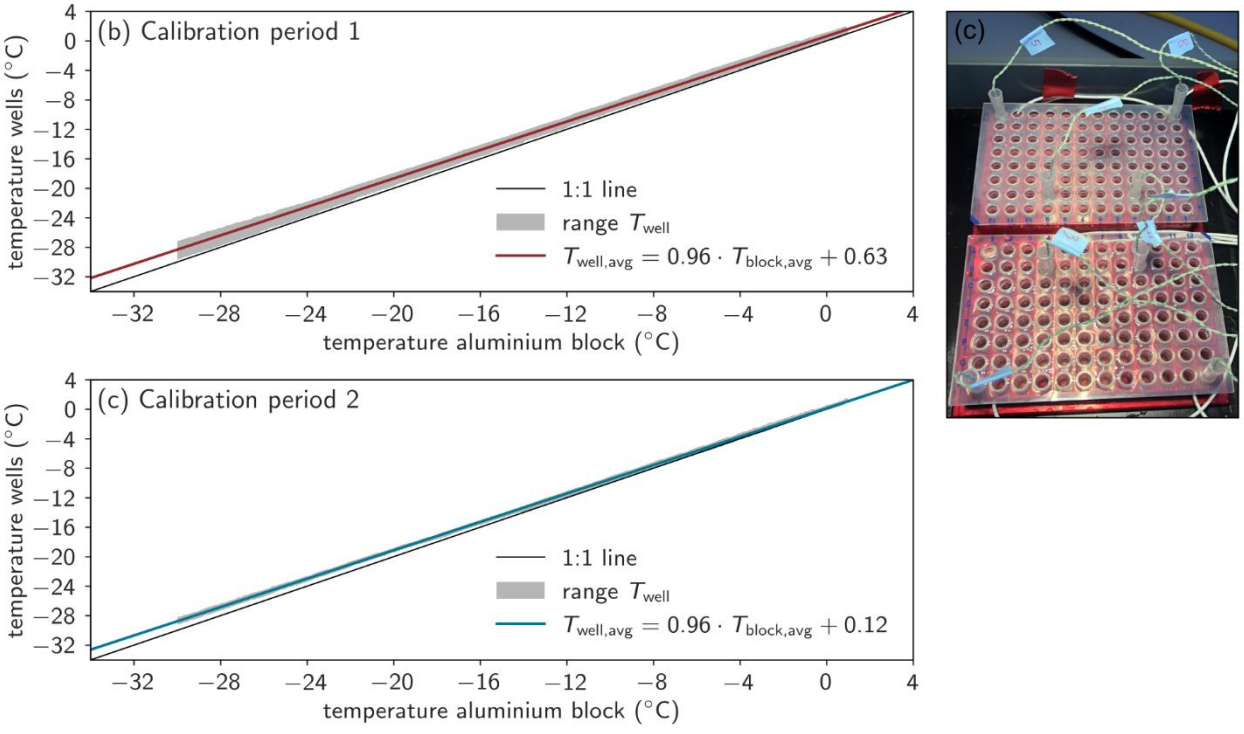

Figure A5. SPICE temperature calibration. (a) Calibration for period 1, conducted with airflow and under warmer laboratory conditions, and (b) for period 2, conducted without airflow and under colder laboratory conditions. For each period, three calibration experiments with different thermocouple placements were performed. Grey shading indicates the range of temperatures measured in the wells, while the linear fit represents the mean slope and intercept derived from the three calibration experiments. (c) Experimental setup illustrating the thermocouples inserted into the wells of the PCR trays.

https://doi.org/10.5194/egusphere-2026-484
Preprint. Discussion started: 16 February 2026

A2.2 Water background and limit of detection

All experiments include negative controls of the background water to quantify potential background freezing events caused by impurities in the water, contamination during handling, or the PCR tray material itself. We use SA water for our experiments, which has previously been shown to exhibit low and more reproducible freezing behavior than other purified waters (David et al., 2019; Miller et al., 2021), consistent with our comparison in the laboratory (Fig A6a). We define the limit of detection as the median of the median freezing temperature ($T_{50,}$ where frozen fraction = 0.5) of 152 experiments (Fig. A6b, including both dedicated water testing experiments and negative controls within sample freezing assays), which is -24.71 °C (interquartile range of 0.88 °C). The water background and limit of detection is therefore similar to other INP freezing set-ups (e.g., Chen et al., 2018; David et al., 2019; Miller et al., 2021). For the negative controls within sample freezing assays, we typically use the same PCR tray region, which might introduce a small bias, though it is below the reported temperature uncertainty. The cumulative INP concentrations reported for samples are corrected with the water background of each individual experiment, as described in Eq. A4.

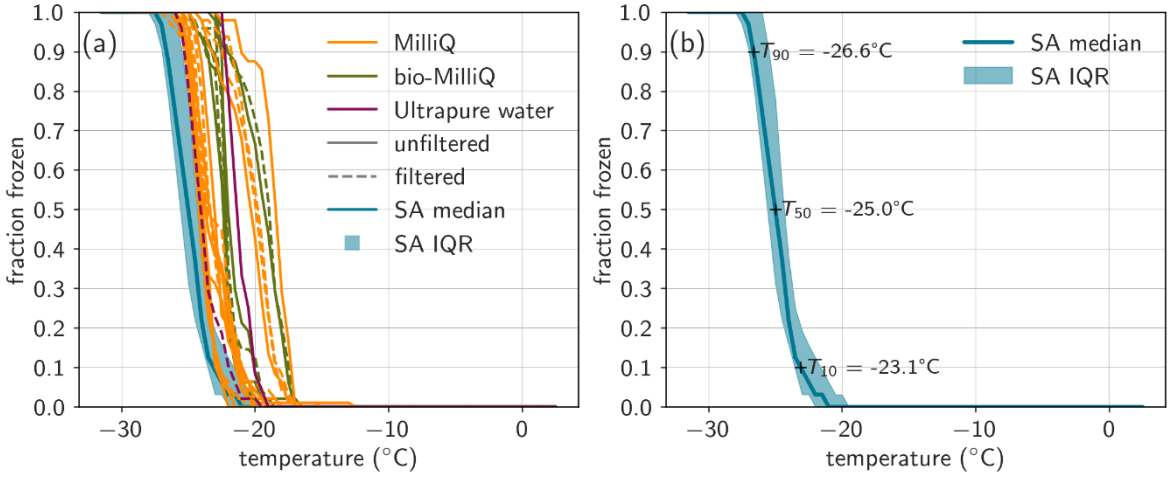

Figure A6. Background freezing. (a) Frozen fraction of different purified water types: Milli-Q (Millipak®, Merck, Germany), bio-Milli-Q (Biopak®, Merck, Germany), and Ultrapure water (Cat. No. 022934.K2, Thermo Scientific, USA), shown either unfiltered (solid line) or filtered through a 0.1 µm syringe filter (Whatman® Puradisc 25 TF, dashed lines), and bio-molecular-biology-free reagent water from Sigma Aldrich (SA) water (median and IQR of 152 experiments). (b) Median and IQR of SA water including freezing temperatures where a fraction of 0.1, 0.5, and 0.9 of droplets are frozen (T_{10}, T_{50}, T_{90}).

A2.3 Validation experiments

To validate SPICE, we tested two commercially available materials with published ice-nucleation freezing spectra, NX-illite and lignin. NX-illite is a clay mineral with well-documented freezing activity (e.g., Beall et al., 2017; David et al., 2019; Harrison et al., 2018; Hiranuma et al., 2015; Miller et al., 2021) and can be representative of atmospheric dust which contains a high illite fraction (approx. 40 %, Broadley et al., 2012; Murray et al., 2012). Following David et al. (2019) and Miller et al. (2021), suspensions of 0.1, 0.05, and 0.001 g L^{-1} NX-illite (Adolf Gottfried Tonwerke GmbH, Germany) were prepared using

https://doi.org/10.5194/egusphere-2026-484
Preprint. Discussion started: 16 February 2026

SA water, and $n_{s,BET}$ was calculated with Eq. A7 using a Brunauer-Emmett-Teller (BET) specific surface area of 124.4 m^2 g^{-1} for NX-illite (Hiranuma et al., 2015). The resulting $n_{s,BET}$ spectra are shown in Fig. A7, including results obtained with the same concentrations from DRINCZ, FINC, and LINDA (Miller et al., 2021), as well as measurements from IR-NIPI (Harrison et al., 2018), SIO-AIS (Beall et al., 2017), and the range and wet suspension parameterization from the intercomparison campaign described in Hiranuma et al. (2015). The parameterization by Hiranuma et al. (2015) agrees reasonably well with the SPICE measurements around -15 °C, but predicts $n_{s,BET}$ values 2-10 times higher at colder temperatures. The SPICE $n_{s,BET}$ values fall within the broad range reported by Hiranuma et al. (2015), though generally towards the lower end. They are also 1-2 orders of magnitude lower than NX-illite $n_{s,BET}$ values measured by Beall et al. (2017) and Harrison et al. (2018).

SPICE measurements are in better agreement with $n_{s,BET}$ spectra reported in Miller et al. (2021), but depend on both temperature and particle concentration. For suspensions of 0.01 g L^{-1} and 0.05 g L^{-1}, the SPICE measurements agree well with Miller et al. (2021) at temperatures colder than about –21 °C and –18 °C, respectively, but are around a factor of two lower at higher temperatures. At 0.1 g L^{-1}, the measurements match closely below –14 °C, but SPICE shows up to two times higher $n_{s,BET}$ at warmer temperatures.

Despite the large variability in published NX-illite freezing spectra, the SPICE measurements lie within the overall reported range and show broadly consistent behavior. The spread among different datasets could reflect variability introduced by differences in sample properties, e.g., including particle dispersion, sedimentation, and size distribution characteristics, as well as differences in sample preparation and measurement methods (Hiranuma et al., 2015; Miller et al., 2021). Unlike the coordinated comparisons in Miller et al. (2021) and Hiranuma et al. (2015), the NX-illite sample used in this study was purchased independently, which may further contribute to deviations between datasets.

Commercial lignin has been proposed by Miller et al. (2021) as an ice-nucleation reference material because it showed better agreement among three different droplet-freezing instruments compared to NX-illite, displayed consistent results across production batches, and remained stable over time. Lignin is a natural, biosphere-abundant polymer, and the commercial material used here is sourced as a by-product of the pulp and paper industry. For this study, we used alkali low-sulfonate kraft lignin (CAS 8068-05-1, Sigma Aldrich, product code 471003) to prepare suspensions equivalent to 20 g C L^{-1}, and calculated the ice-nucleating active site density per unit carbon mass (n_m) following Miller et al. (2021):

$$n_m(T)[\mathrm{mg}^{-1}] = INP_{sus,corr}(T)\frac{1}{C_m(TOC)} \quad \text{(A 11)}$$

where $C_m(TOC)$ is the mass concentration of carbon in the solution. For the lignin used here, this concentration is determined from the lignin mass (40 mg L^{-1}) and the manufacturer-reported carbon content (50.3 %).

The SPICE freezing spectra of lignin show high reproducibility across repeated experiments, and are in good agreement with the results reported by Miller et al. (2021). While the parameterization based on multiple instruments shows up to a factor of 2-3 difference in the -15 °C to -20 °C temperature range, the SPICE measurements closely match the batch-specific measurements in Miller et al. (2021, upper green range in Fig. A8). In addition, we participated in an offline INP comparison

https://doi.org/10.5194/egusphere-2026-484
Preprint. Discussion started: 16 February 2026

initiative coordinated by the Centre for Cloud Ice nucleation (CCIce) within the Aerosol, Clouds, Trace Gases Research Infrastructure (ACTRIS) framework in 2025. SPICE compared well to the other instruments and fell within the statistical uncertainty of the ensemble of measurements (Höhler, Lacher et al., in preparation).

Overall, the high reproducibility of our measurements and their good agreement with published data for NX-illite, lignin, and other droplet freezing instruments demonstrate that SPICE provides robust and reliable measurements of immersion-mode INPs.

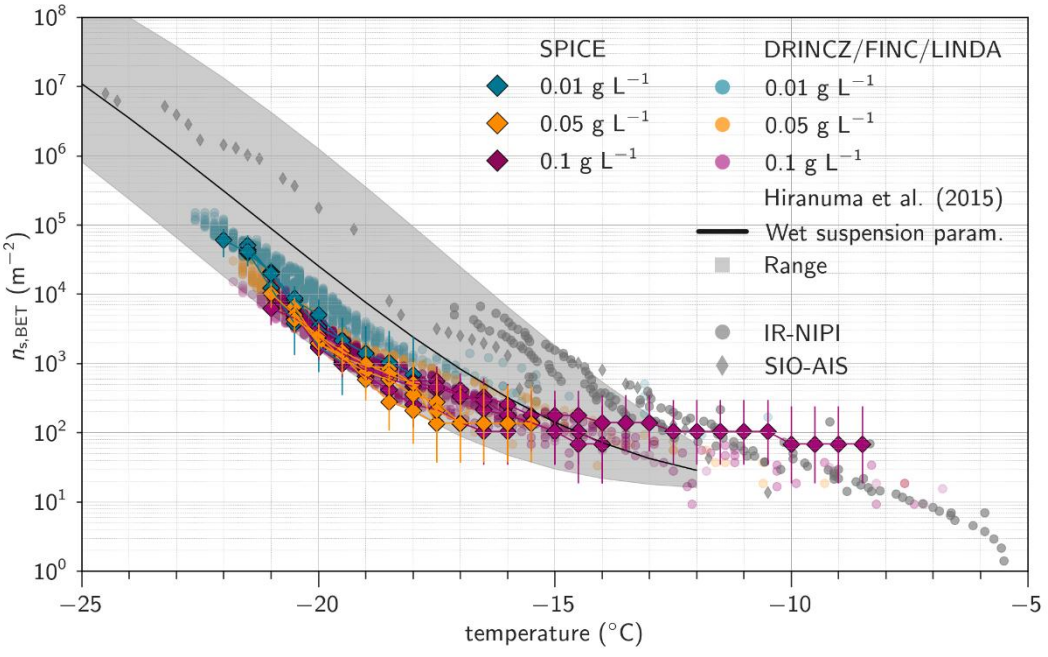

Figure A7. NX-illite comparison. Ice-active surface site densities ($n_{s,BET}$) of NX-illite suspensions with concentrations of 0.01, 0.05, and 0.1 g L^{-1} measured with SPICE. $n_{s,BET}$ was calculated using an BET surface area of 124.4 m^2 g^{-1} for NX-illite (Hiranuma et al., 2015). For comparison, results obtained with the same concentrations from DRINCZ, FINC, and LINDA (Miller et al., 2021), as well as measurements from IR-NIPI (Harrison et al., 2018) and SIO-AIS (Beall et al., 2017), are shown. The shaded region and solid line indicate the range and wet-suspension parameterization from Hiranuma et al. (2015).

https://doi.org/10.5194/egusphere-2026-484
Preprint. Discussion started: 16 February 2026

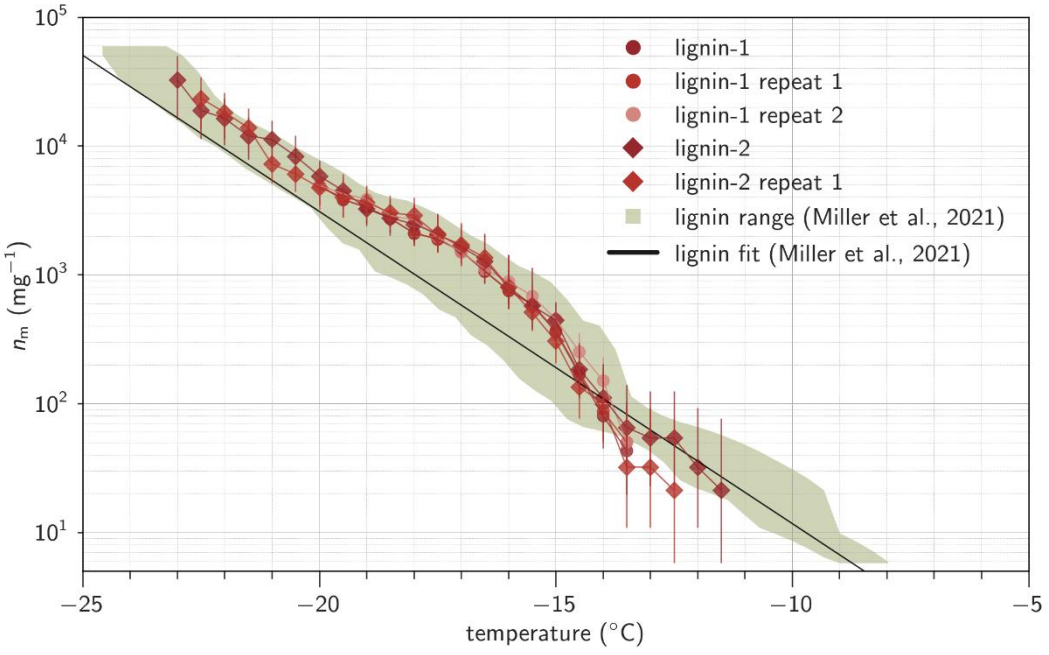

Figure A8. Lignin comparison. Ice-active mass site densities (n_m) of lignin suspensions measured with SPICE. The first suspension (lignin-1) with 20 mg C L^{-1} solution was measured three times. The second suspension (lignin-2) was measured twice, including the solution of 20 mg C L^{-1} and a 10-fold dilution. The shaded region and solid line indicate the range and parameterization from Miller et al. (2021).

https://doi.org/10.5194/egusphere-2026-484
Preprint. Discussion started: 16 February 2026

Appendix B - Additional figures for methods and results sections

Figure B1. Photos of samples and stations. Example photos of (a) *transect* and (b) *microbiology* samples (the diameter of the ring is 24 cm). (c) Atmospheric stations at Narsarsuaq plain, col, Narsaq International Research station (NIRS), and Tasigaaq hill near Narsaq.

https://doi.org/10.5194/egusphere-2026-484
Preprint. Discussion started: 16 February 2026

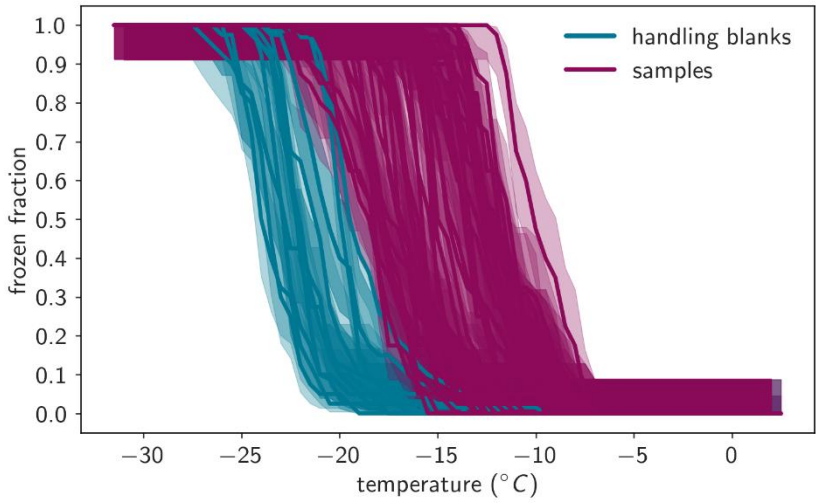

Figure B2. Comparison of frozen fraction of handling blanks and samples. Note that the washing water volume for handling blanks was 8 mL, and for filter samples 12 mL.

Table B1. Mineral abundances. Phase fractions of known ice-nucleating minerals in a subset of dust samples. The phase fractions are based on XRD measurements and reported in weight percent. Refinements were conducted both with (left of /) and without (right of /) correction for preferred orientation of crystallites, the correction using spherical harmonics.

Location	Sample	Quartz (%)	Albite (%)	K-Feldspar (%)	Illite (%)
Narsarsuaq	N1	11 / 23	62 / 35	16 / 22	1 / 9
Narsarsuaq	N5	11 / 22	61 / 34	16 / 21	2 / 7
Kangerlussuaq	K1	8 / 12	52 / 49	28 / 25	4 / 4
Kangerlussuaq	K4	8 / 8	48 / 46	26 / 29	4 / 5
Igaliku	I1	7 / 9	56 / 53	20 / 22	3 / 4

https://doi.org/10.5194/egusphere-2026-484
Preprint. Discussion started: 16 February 2026

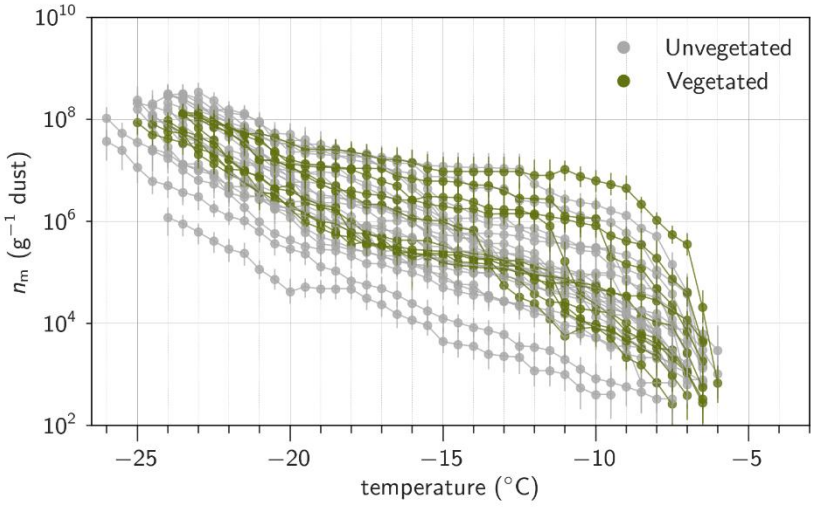

Figure B3. Ice-active mass site densities (n_m) for unvegetated and vegetated samples. Note that all *transect* samples are unvegetated and only some *microbiology* samples are vegetated.

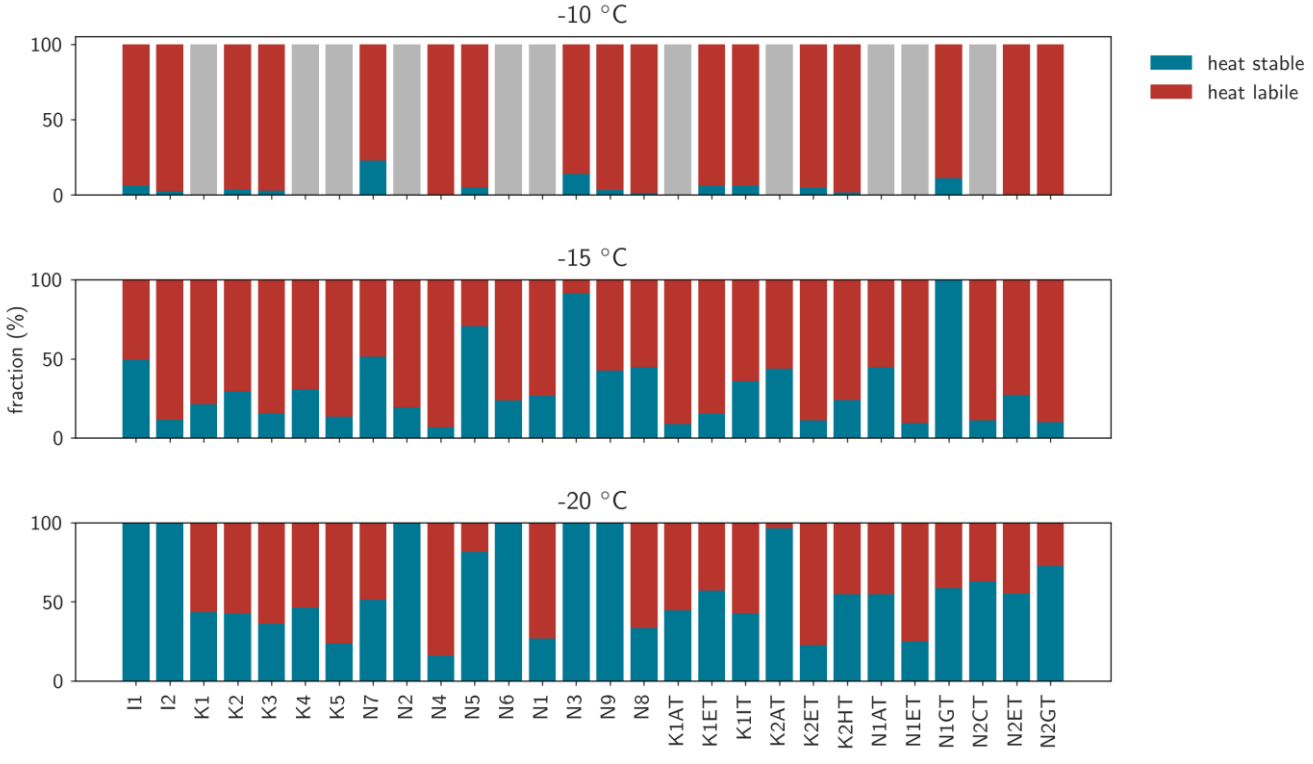

Figure B4. Heat-stable and heat labile fractions. Heat labile and heat stable fraction at (a) -10 °C, (b) -15 °C, and (c) -20 °C. Grey bars indicate no data, but are likely primarily heat-labile INPs.

https://doi.org/10.5194/egusphere-2026-484
Preprint. Discussion started: 16 February 2026

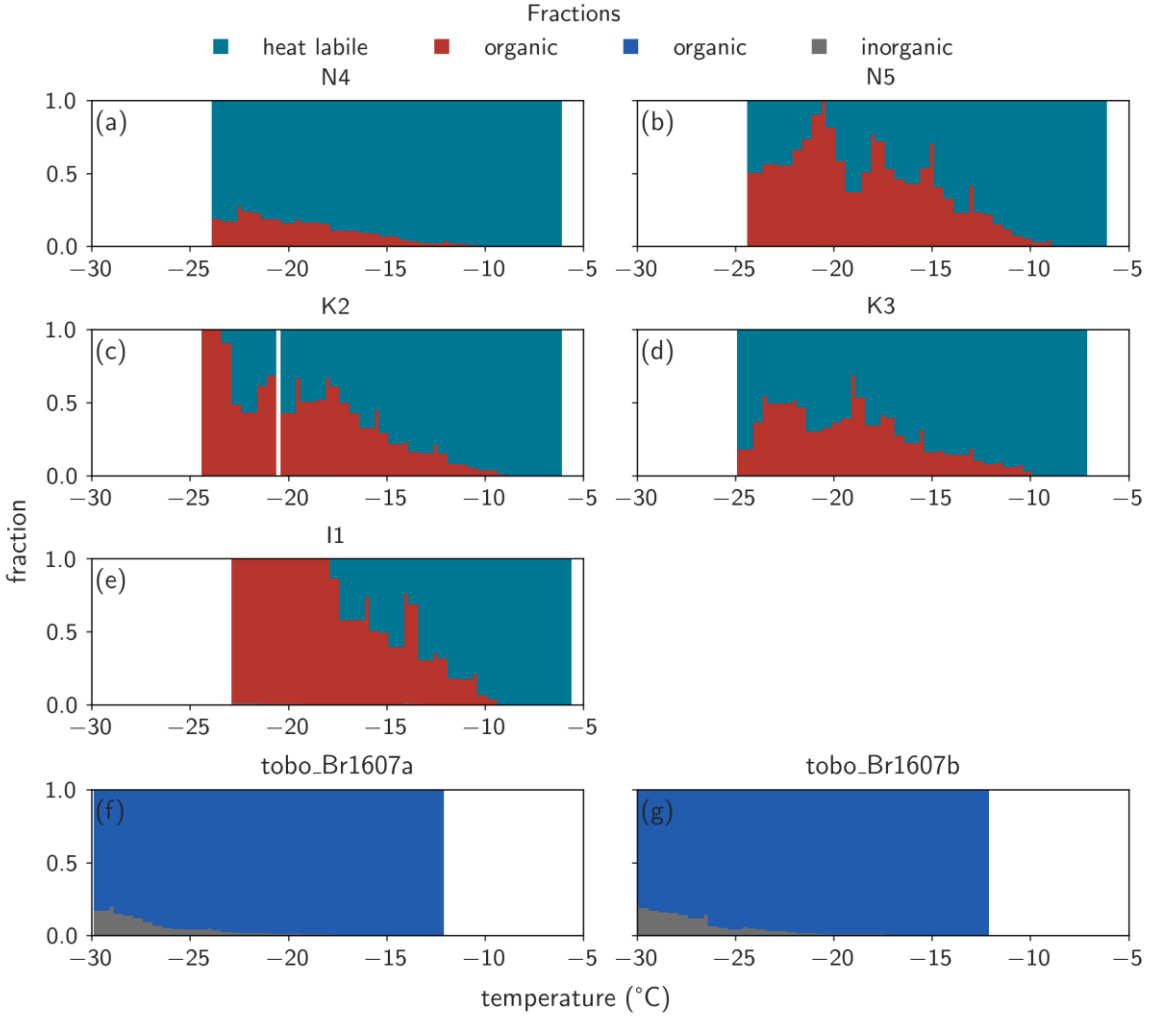

845 **Figure B5. Composition information.** Fraction of heat labile, heat stable, and inorganic INPs per gram of dust for samples in Narsarsuaq (a, b), Kangerlussuaq (c, d), and Igaliku (e). Fraction of organic (which includes heat labile and heat stable organics) and inorganic INPs per gram of dust for samples from Svalbard (Tobo et al., 2019).

https://doi.org/10.5194/egusphere-2026-484
Preprint. Discussion started: 16 February 2026

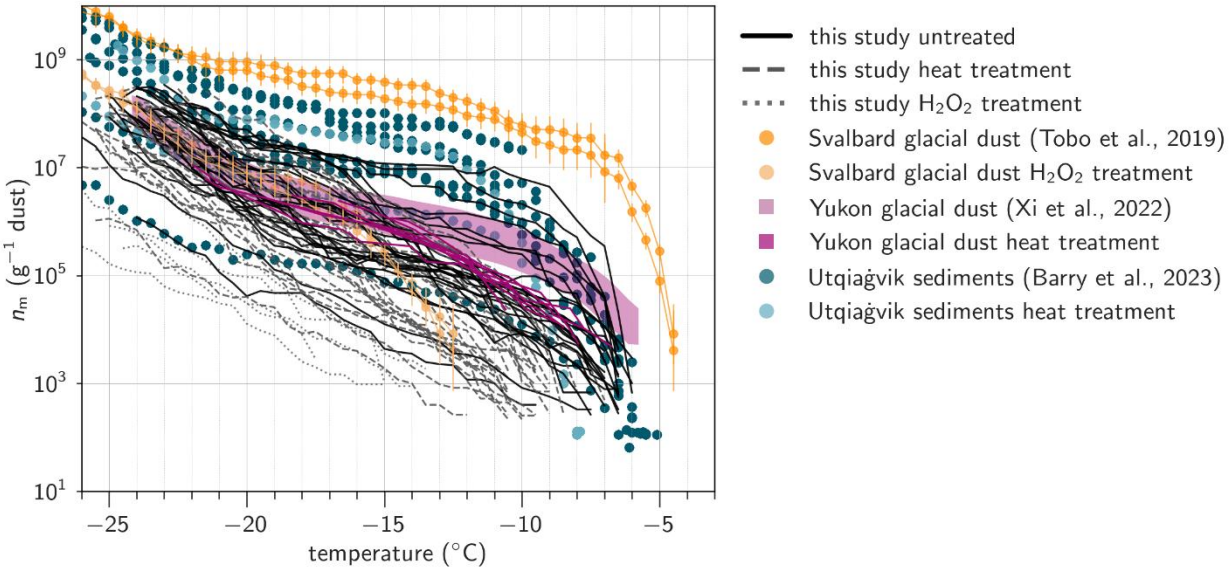

Figure B6. Literature comparison including heat and peroxide treatment. Ice-active mass site densities (n_m) of bulk dust samples for this study without treatment, and including heat and peroxide treatment. Other high-latitude sites are added including untreated and hydrogen peroxide treated bulk dust samples by Tobo et al. (2019), untreated and heat treated (heating to 100 °C for 1 h) dust aerosol samples by Xi et al. (2022), and untreated and heat treated (heating to 95 °C for 20 min) sediment samples by Barry et al. (2023).

https://doi.org/10.5194/egusphere-2026-484
Preprint. Discussion started: 16 February 2026

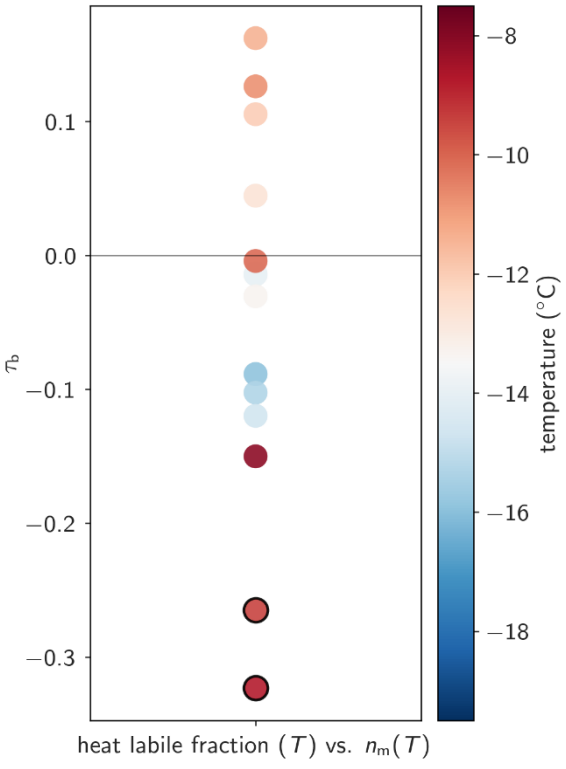

Figure B7. Correlation coefficients of heat labile fraction vs. n_m as a function of temperature. Kendall's tau correlation coefficient (τ_b, chosen due to ties in the data) between heat labile fraction and n_m values as a function of temperature. Correlation coefficients are only shown for temperatures with more than 23 datapoints (-7 to -19.5 °C). Black circles indicate statistical significance ($p < 0.05$).

https://doi.org/10.5194/egusphere-2026-484
Preprint. Discussion started: 16 February 2026

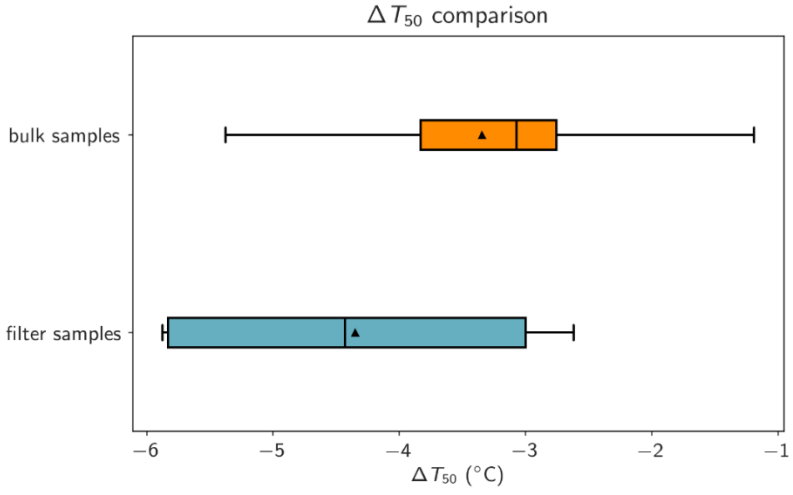

Figure B8. ΔT_{50} comparison. Difference of median freezing temperature T_{50} (temperature where 50 % of droplets are frozen) for the untreated and heat-treated initial suspension (undiluted).

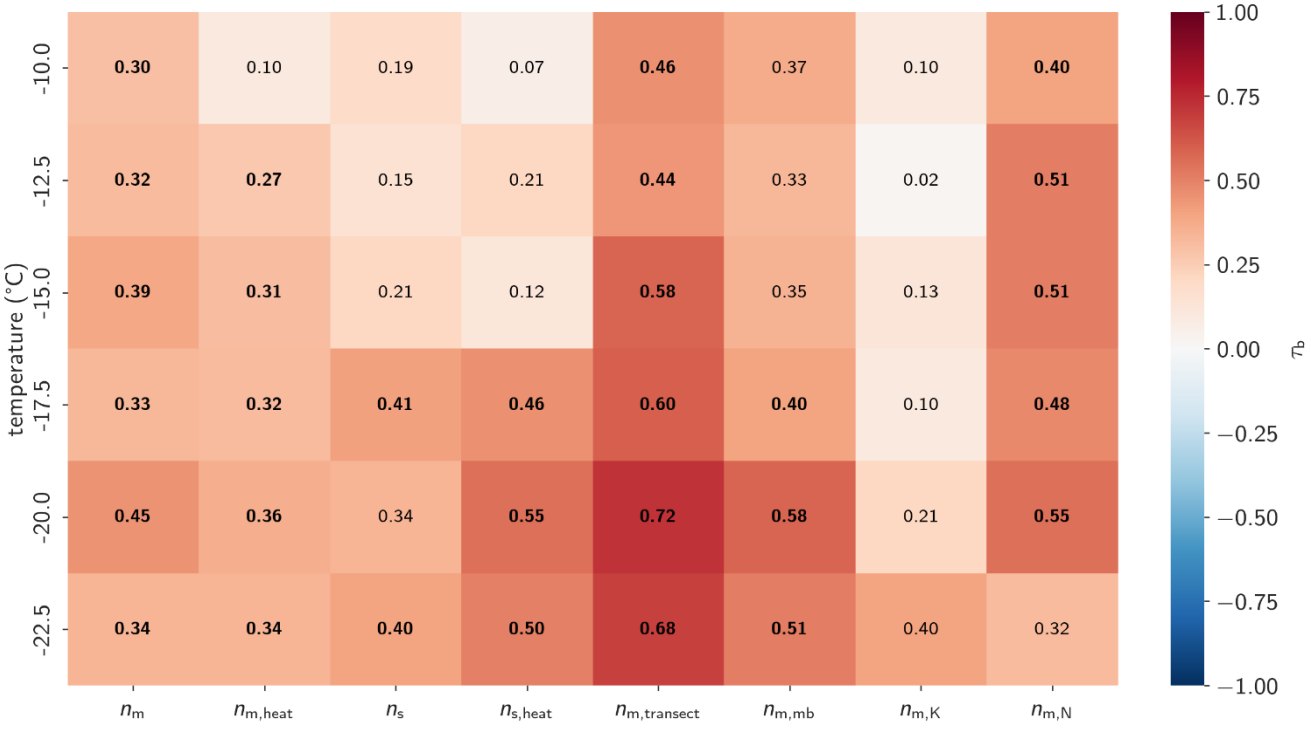

Figure B9. Correlation coefficient TOC and different variables. Kendall's tau correlation coefficient (τ_b) of total organic carbon (TOC) and different INP characteristic, including ice-active mass site densities (n_m), n_m following heat treatment ($n_{m,heat}$), ice-active surface site densities (n_s), n_s following heat treatment ($n_{s,heat}$), n_m of transect samples ($n_{m,transect}$), n_m of microbiology samples ($n_{m,mb}$), n_m in Kangerlussuaq ($n_{m,K}$), and n_m in Narsarsuaq ($n_{m,N}$). The correlation coefficient is written in bold when statistically significant ($p < 0.05$).

https://doi.org/10.5194/egusphere-2026-484
Preprint. Discussion started: 16 February 2026

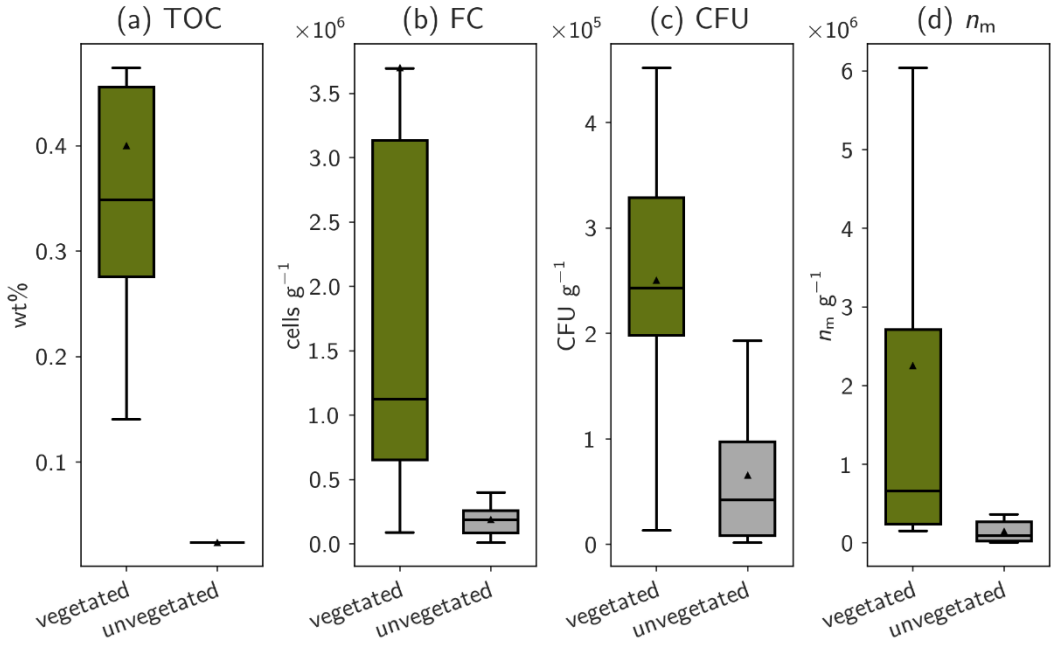

Figure B10. Influence of vegetation. Comparison of (a) TOC, microbial abundance based on (b) flow cytometry (FC) and (c) colony forming units (CFU), and (d) ice-active mass site densities (n_m) at -15 °C for vegetated (n=10) and unvegetated (n=6) *microbiology* samples.

https://doi.org/10.5194/egusphere-2026-484
Preprint. Discussion started: 16 February 2026

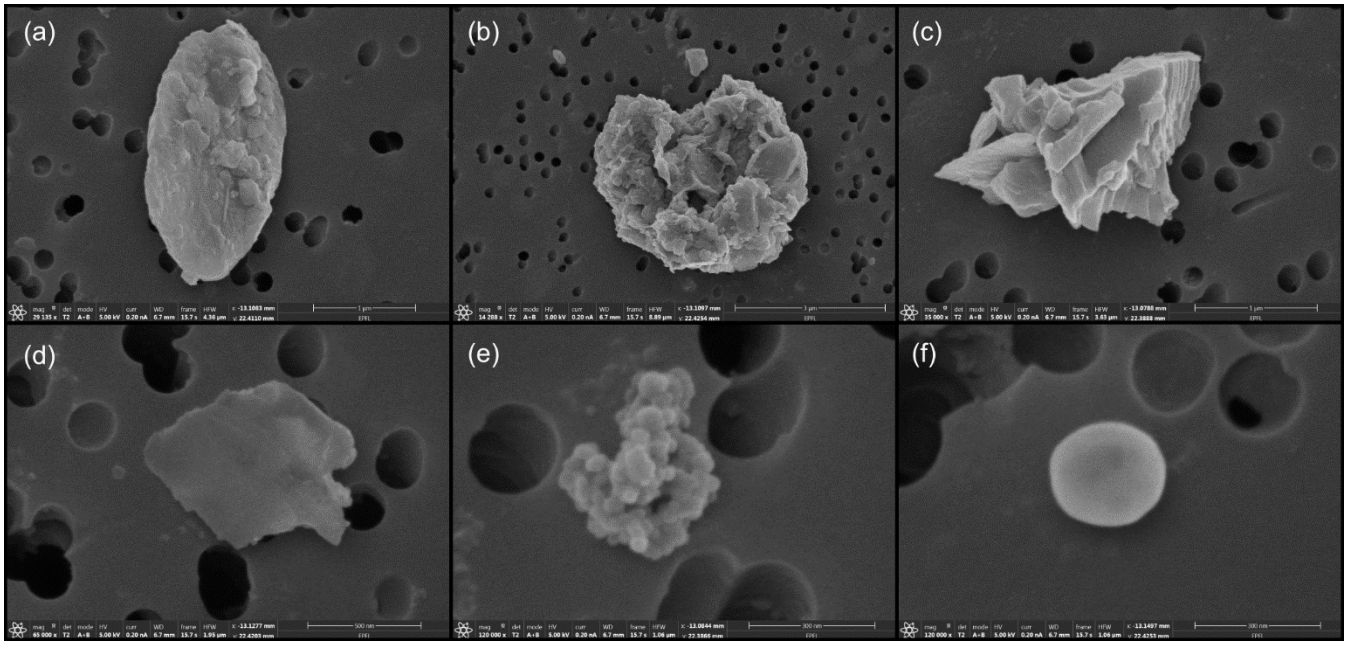

880 **Figure B11. Images of aerosol particles at Narsarsuaq *plain* site.** Particles were analyzed with a Teneo® field-emission Scanning Electron Microscope (FEI/Thermo Fisher Scientific, USA) on Nuclepore™ polycarbonate filters (47 mm diameter, 0.2 µm pore diameter) sampled from 16.06.2023 13:03 – 17.06.2023 11:12. The majority of observed particles were mineral dust particles, with examples shown in a-d. Other observed particle types were potentially from marine origin (e) or long-range transported (f). The filter was coated with a 7 nm Iridium layer to avoid charge accumulation.

885

https://doi.org/10.5194/egusphere-2026-484
Preprint. Discussion started: 16 February 2026

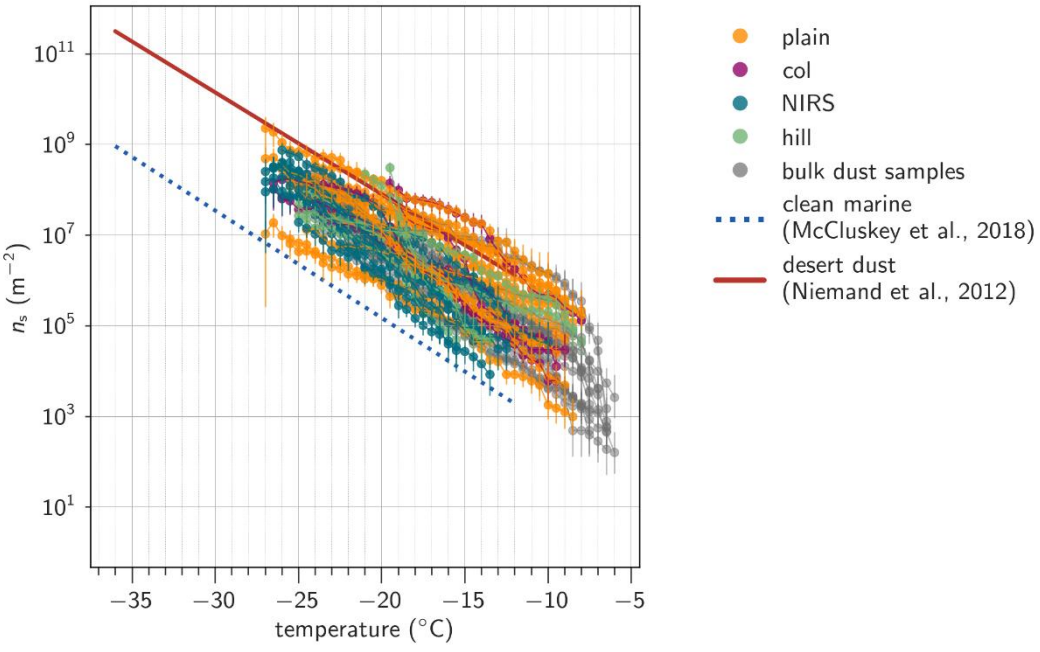

Figure B12. INP spectra normalized by surface area. Atmospheric INP concentrations normalized by the total aerosol surface area for particles larger than ~190 nm, derived from optical particle counter measurements (Sect. 2.1.2). For comparison, INP spectra of bulk *transect* samples normalized by BET surface area are shown, together with parameterizations for clean marine environments (McCluskey et al., 2018b) and desert dust (Niemand et al., 2012).

https://doi.org/10.5194/egusphere-2026-484
Preprint. Discussion started: 16 February 2026

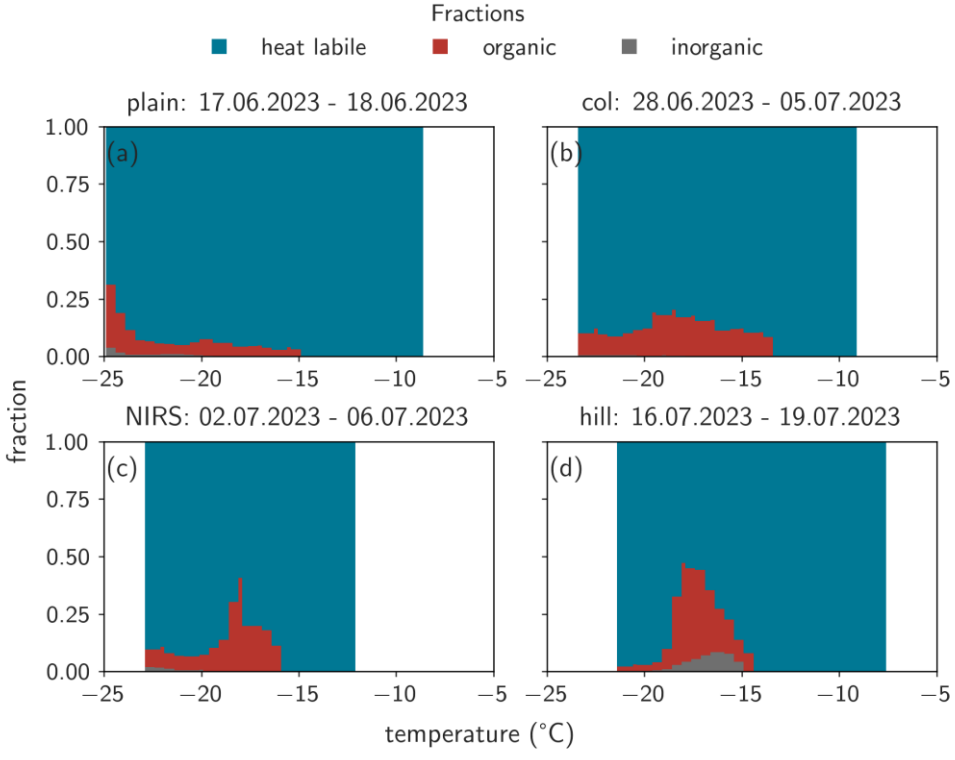

Figure B13. Composition information of filter samples. Fraction of heat labile, heat stable, and inorganic INPs for a filter sample at the (a) Narsarsuaq plain, (b) Narsarsuaq col, (c) Narsaq International Research Station (NIRS), and (d) Tasigaaq hill near Narsaq. The sampling period of each filter is indicated in the title.

https://doi.org/10.5194/egusphere-2026-484
Preprint. Discussion started: 16 February 2026

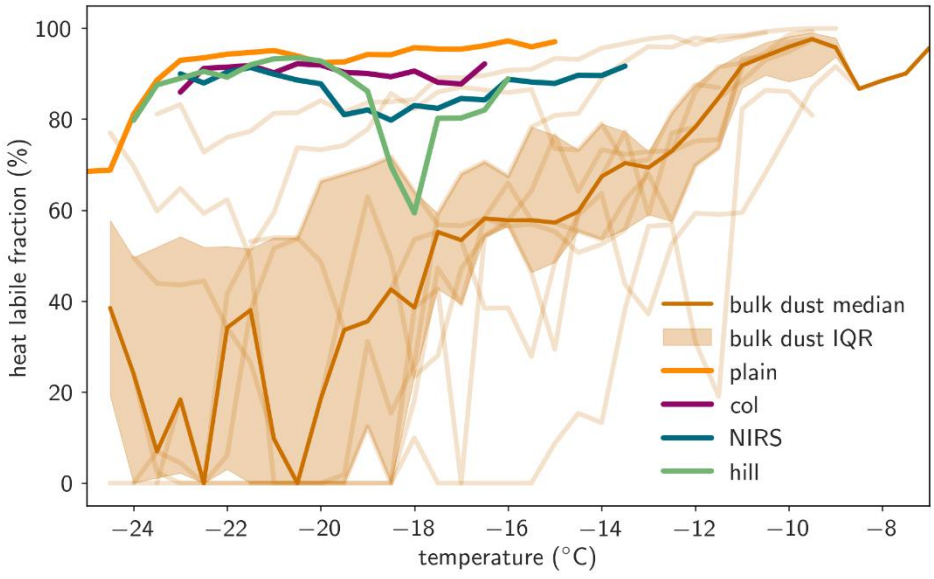

Figure B14. Heat labile fractions. Heat labile fractions of Narsarsuaq bulk dust samples (including median and IQR) and aerosol filter samples for the different locations as a function of temperature.

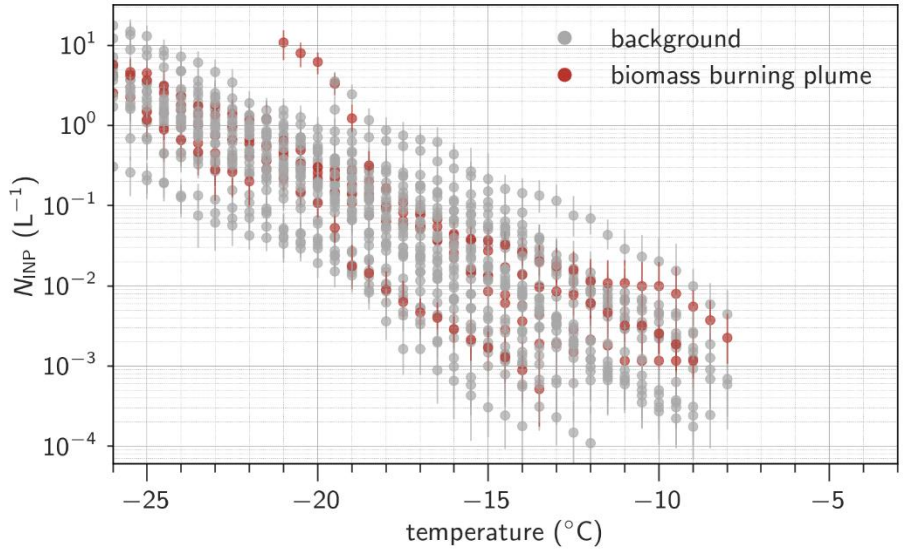

Figure B15. Biomass burning plume. INP spectra with filters during biomass burning plumes marked in red.

https://doi.org/10.5194/egusphere-2026-484
Preprint. Discussion started: 16 February 2026

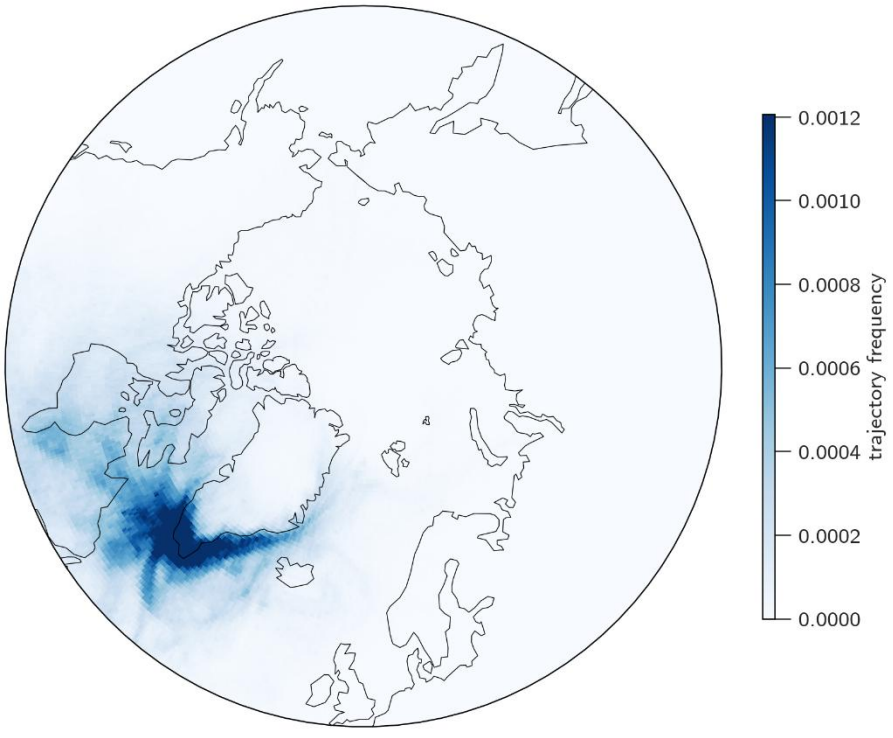

910

Figure B16. Trajectory frequency. Relative frequency of 5-day backward trajectories (Lagranto, Sprenger and Wernli, 2015) initialized near the surface at Narsaq at 3-hour intervals beween 16.06.2023 – 02.08.2023 using ERA5 meteorology.

https://doi.org/10.5194/egusphere-2026-484
Preprint. Discussion started: 16 February 2026

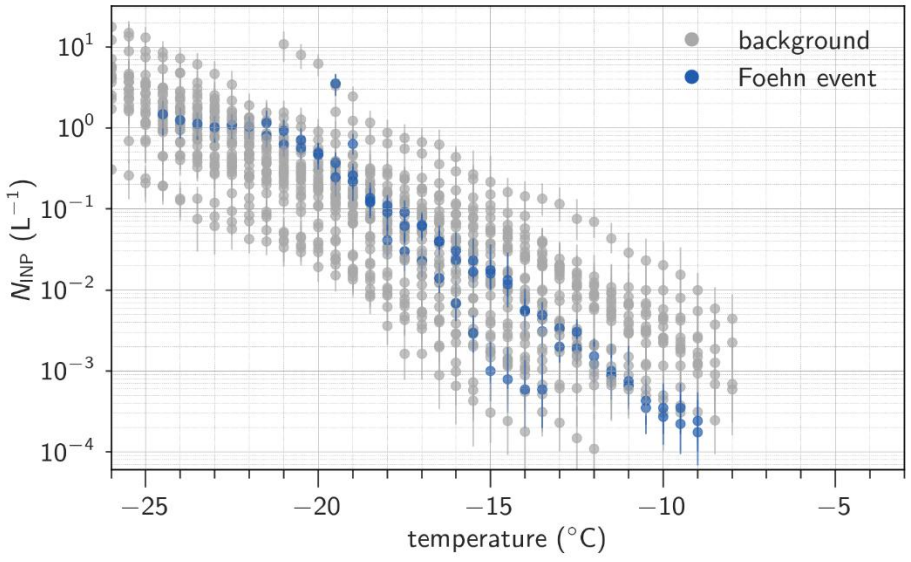

Figure B17. Foehn event. INP spectra with filters during Foehn event marked in blue.

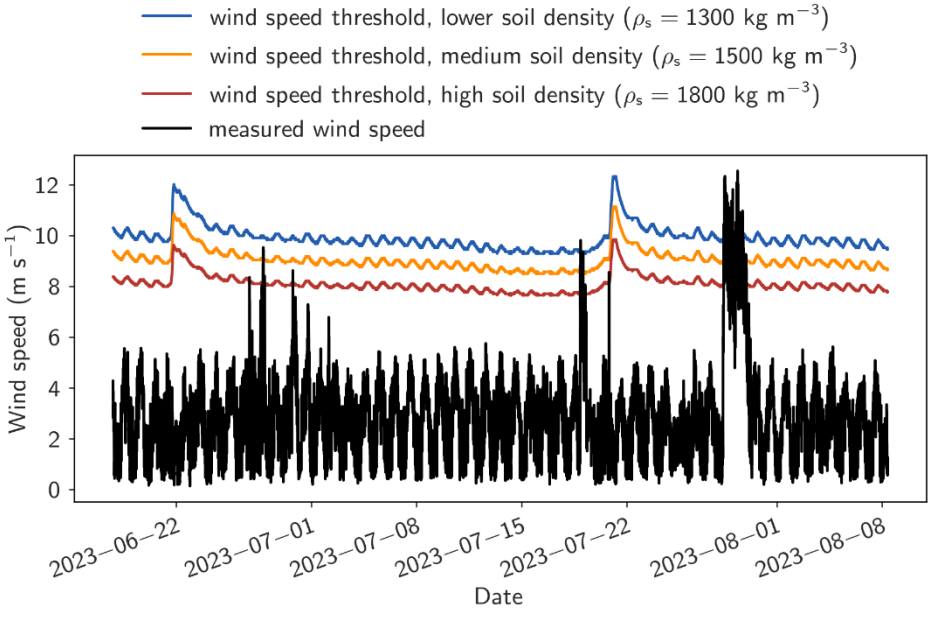

Figure B18. Wind speed threshold for dust emission. Wind speed threshold estimates are based on Fig. 3 in Fécan et al. (1999). Measured volumetric soil moisture at the plain station was converted to gravimetric soil moisture assuming different soil densities (colored lines), measured wind speed at the Narsarsuaq plain station is shown in black.

https://doi.org/10.5194/egusphere-2026-484
Preprint. Discussion started: 16 February 2026

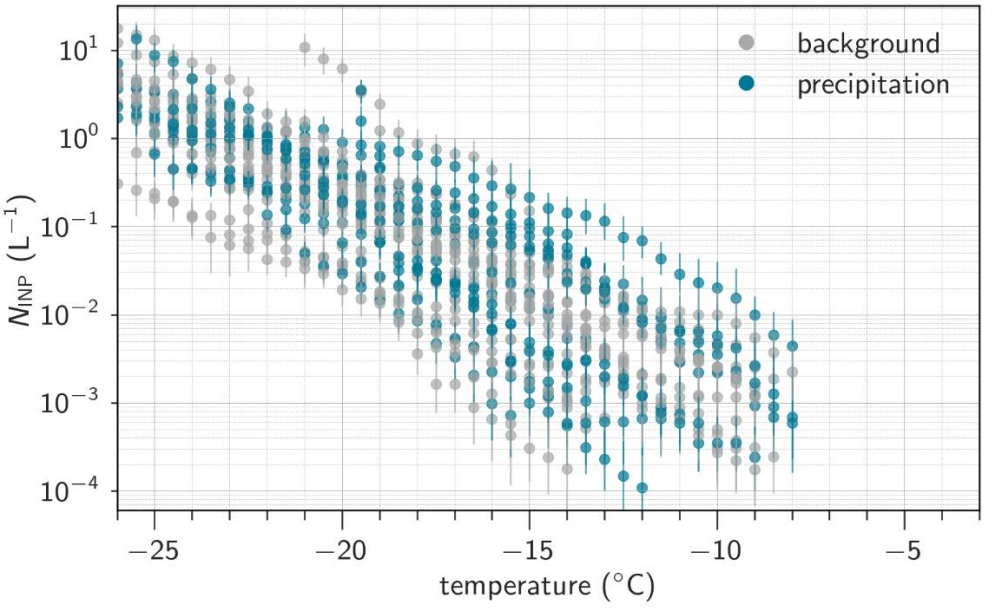

Figure B19. Precipitation. INP spectra with filters during precipitation during the sampling period marked in blue.

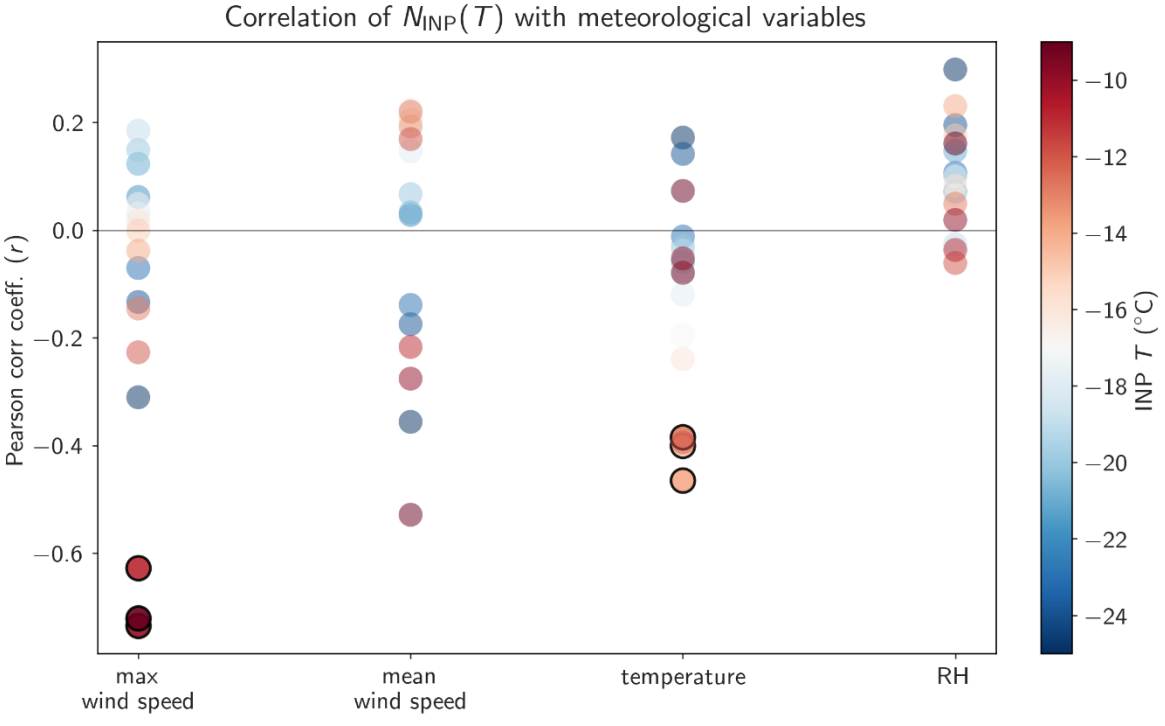

Figure B20. Correlation of N_{INP} and meteorological variables. Pearson correlation coefficient of atmospheric INP concentrations (N_{INP}) with maximum and mean wind speed during the filter period, mean temperature, and relative humidity (RH) at all atmospheric stations.

https://doi.org/10.5194/egusphere-2026-484
Preprint. Discussion started: 16 February 2026

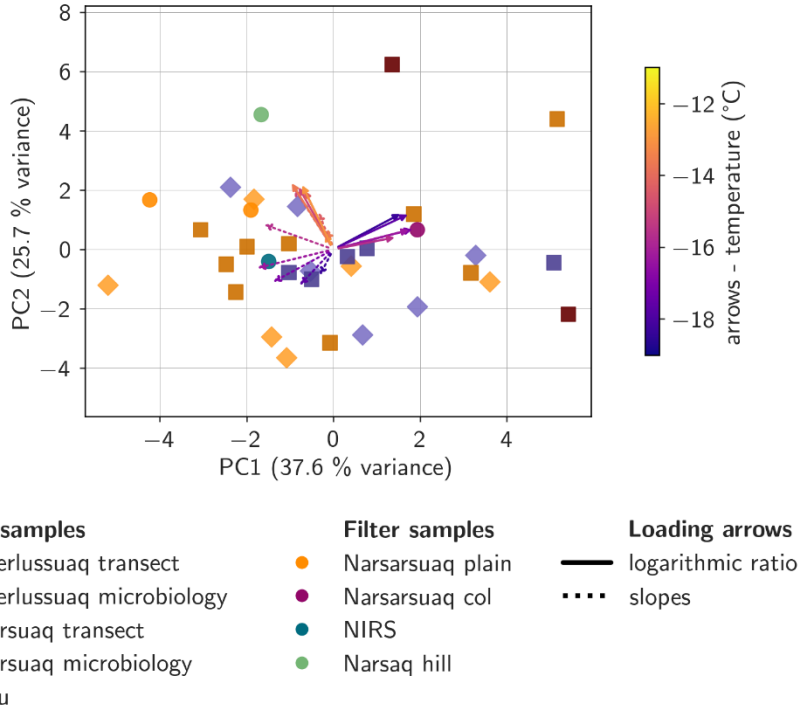

930 **Figure B21. Variability in heat treated INP spectra.** Principal component analysis (PCA) for all samples, based on the slopes of heat treated INP spectra in 2 °C intervals from -10 °C to -20 °C, and the logarithmic ratios of INP concentrations at each interval relative to -15°C. The arrows represent the variable loadings, color-coded by temperature, where solid arrows indicate the logarithmic ratios, dotted arrows represent the slopes. Axes represent the first two principal components scaled to the variance explained.

https://doi.org/10.5194/egusphere-2026-484
Preprint. Discussion started: 16 February 2026

Appendix C. INPs in glacial outwash plains in the Swiss Alps

To compare the ice-nucleating properties of glacial dust from Greenland with those from other glaciated regions, we additionally collected dust samples from three glacial outwash plains in the Swiss Alps (canton of Valais, southwestern Switzerland). Although the Alpine outwash plains are considerably smaller in extent and are unlikely to represent a major regional INP source, the underlying processes governing dust generation and composition may be comparable to those in Greenland. Samples were collected along transects at each site, as summarized in Table C1 and shown in Fig. C1. Sample preparation and INP measurements were conducted following the same procedures as for the Greenland *transect* samples, described in Sect. 2.1.1 and Sect. 2.2.

Table C1. Overview of bulk dust samples.

Location	ID	Latitude (°)	Longitude (°)	Date (YYYY-MM-DD)	INP treatments
Lämmerenboden	L1	46.3969735	7.6026584	2025-07-02	heat, H_2O_2
	L2a	46.3968498	7.5998052	2025-07-02	
	L2b	46.39613	7.59511	2025-07-02	
	L3	46.39613	7.59511	2025-07-02	
Lac du Grand Désert	LG1	46.5157812	7.20105486	2025-07-11	
	LG2	48.0860320	7.3373169	2025-07-11	heat, H_2O_2
	LG3	46.0784114	7.3379723	2025-07-11	
	LG4	46.0761233	7.338429	2025-07-11	
Ferpècle	F1	46.39613	7.59511	2025-07-04	
	F2	46.39613	7.59511	2025-07-04	heat, H_2O_2
	F3	46.39613	7.59511	2025-07-04	
	F4	46.39613	7.59511	2025-07-04	

https://doi.org/10.5194/egusphere-2026-484
Preprint. Discussion started: 16 February 2026

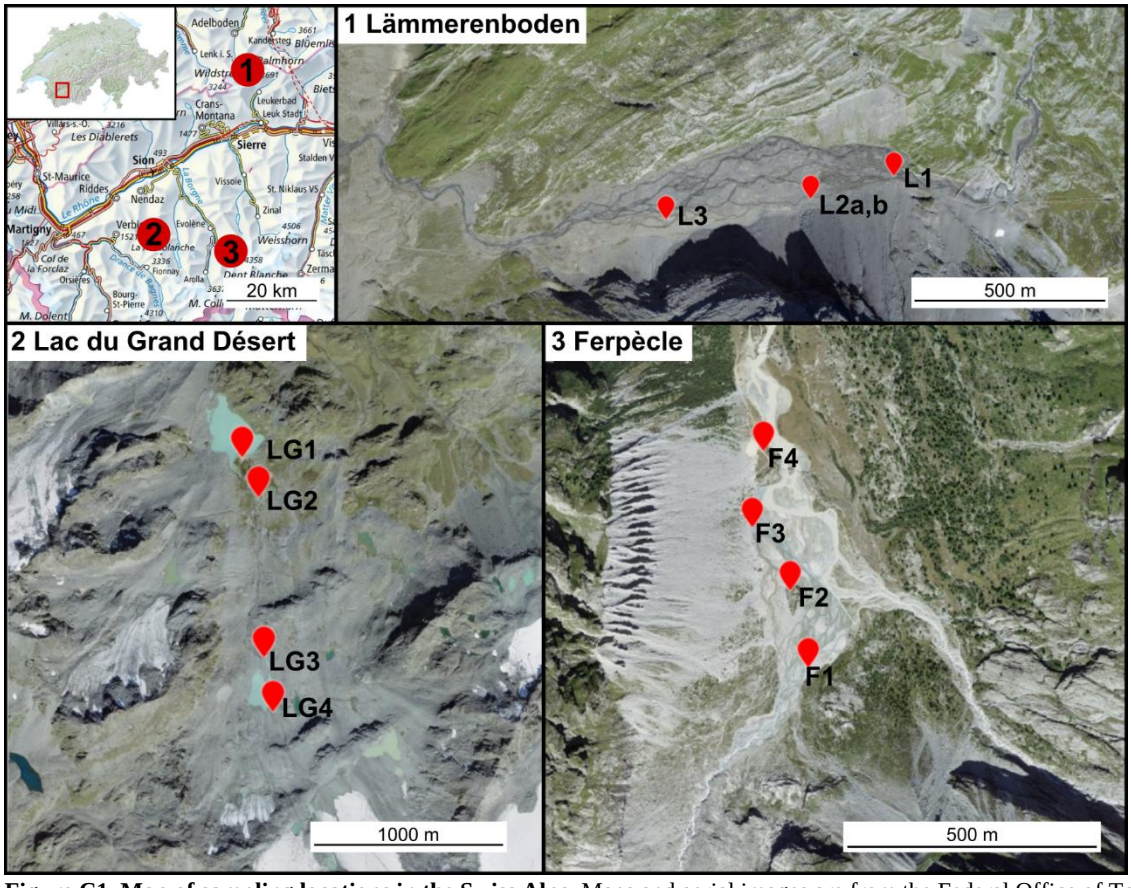

Figure C1. Map of sampling locations in the Swiss Alps. Maps and aerial images are from the Federal Office of Topography swisstopo.

950

https://doi.org/10.5194/egusphere-2026-484
Preprint. Discussion started: 16 February 2026

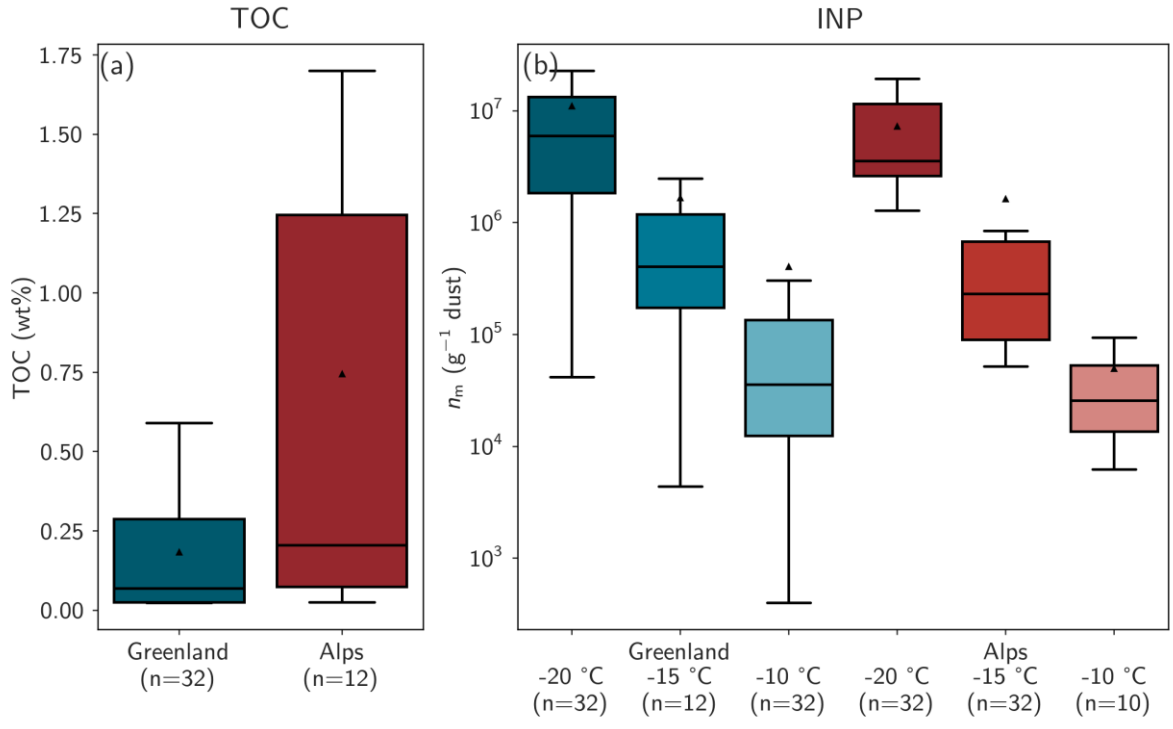

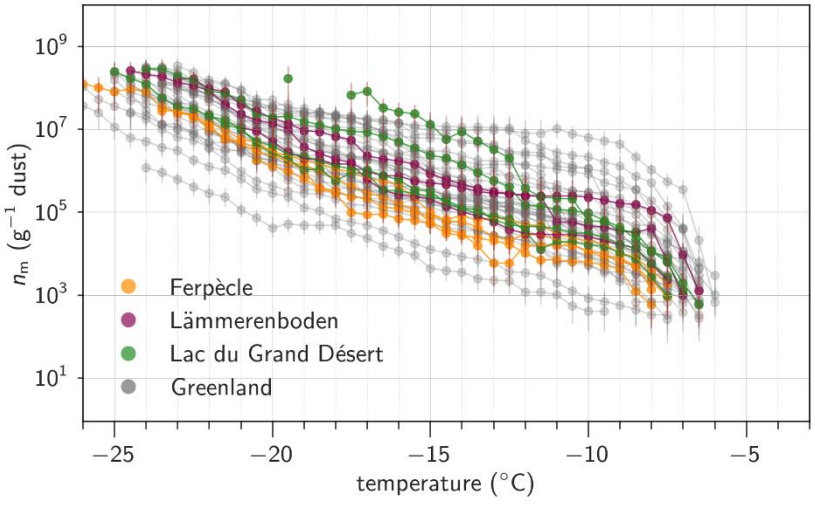

Figure C2. Bulk dust ice-nucleating activity. Ice-active mass site densities (n_m) of dust samples in glacial outwash plains in the Swiss Alps (Ferpècle, Lämmerenboden, Lac du Grand Désert) and Greenland.

https://doi.org/10.5194/egusphere-2026-484
Preprint. Discussion started: 16 February 2026

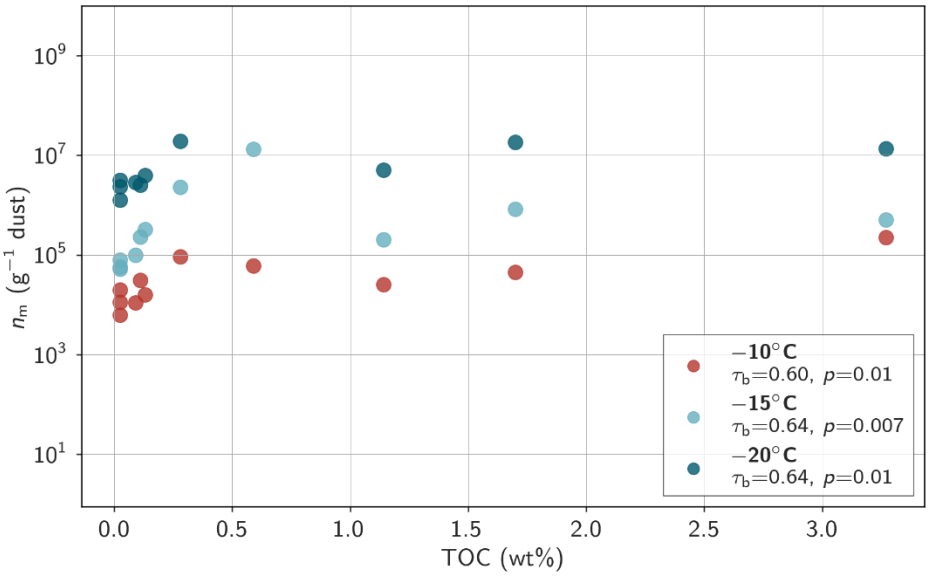

Figure C3. TOC and ice-nucleating activity. Scatterplot of total organic carbon (TOC) content vs ice-active mass site densities (n_m) for the temperatures -10 °C, -15 °C, and -20 °C. For each temperature, Kendall's tau correlation coefficient (τ_b) and p-value are annotated.

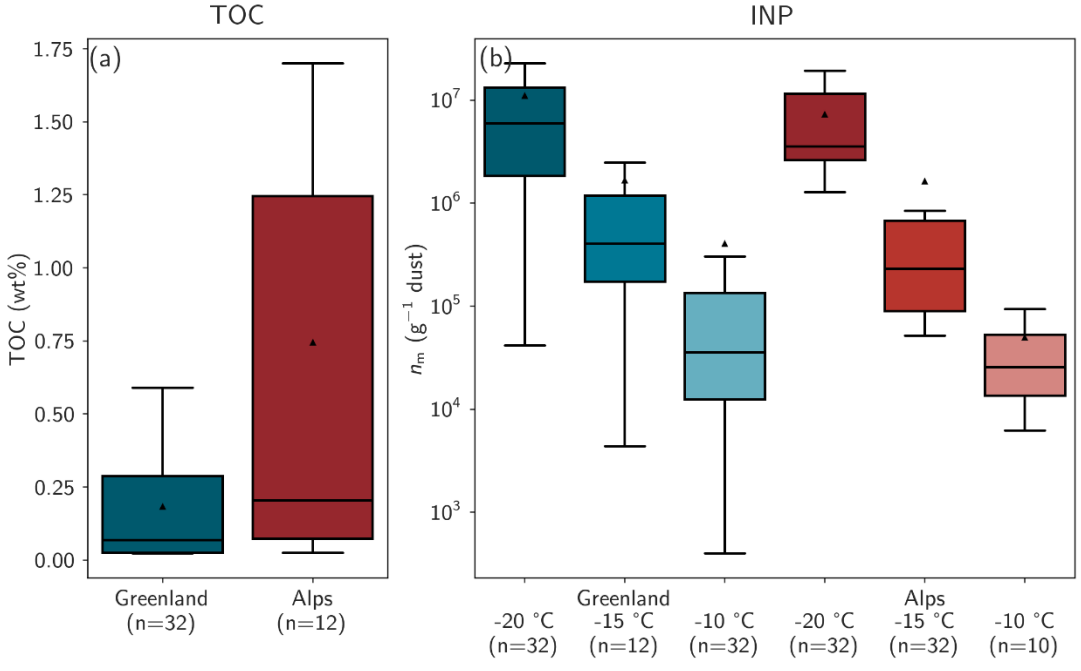

Figure C4. Comparison TOC and INPs. Comparison of (a) TOC values and (b) ice-active mass site densities (n_m) at -20 °C, -15 °C, and -10 °C between dust samples from glacial outwash plains in Greenland and the Swiss Alps.

https://doi.org/10.5194/egusphere-2026-484
Preprint. Discussion started: 16 February 2026

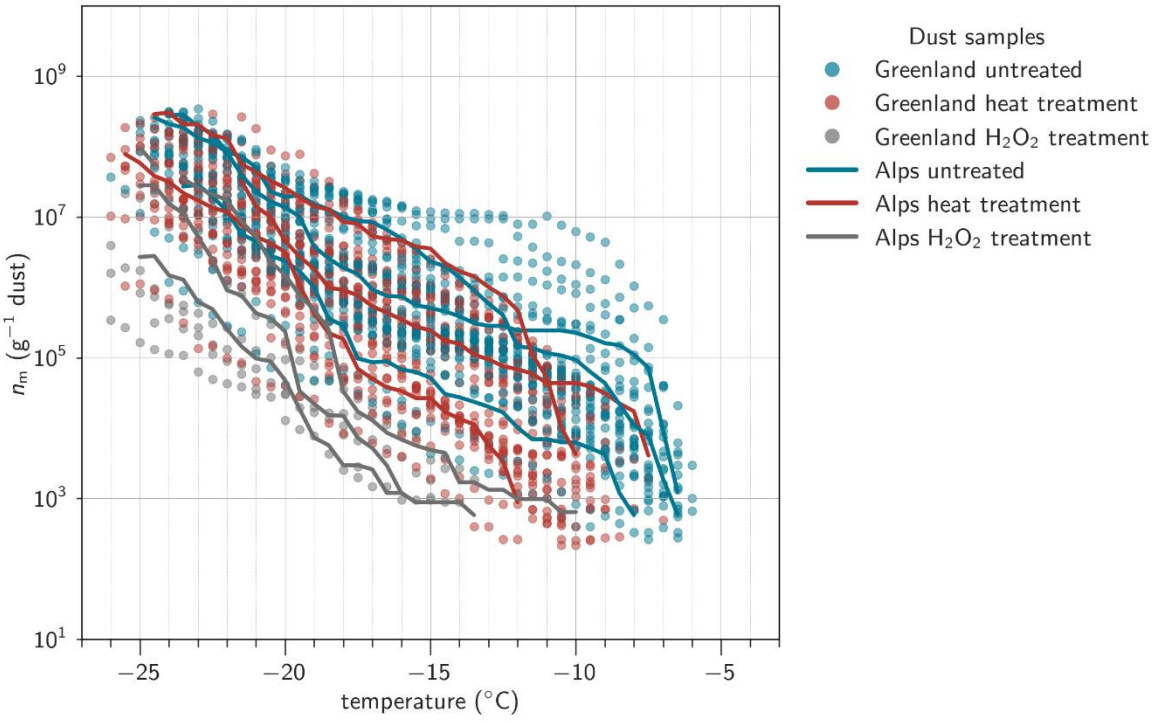

Figure C5. INP composition of dust samples. n_m spectra of bulk dust sample including heat and hydrogen peroxide treatment from glacial outwash plains in Greenland and the Swiss Alps.

https://doi.org/10.5194/egusphere-2026-484
Preprint. Discussion started: 16 February 2026

970

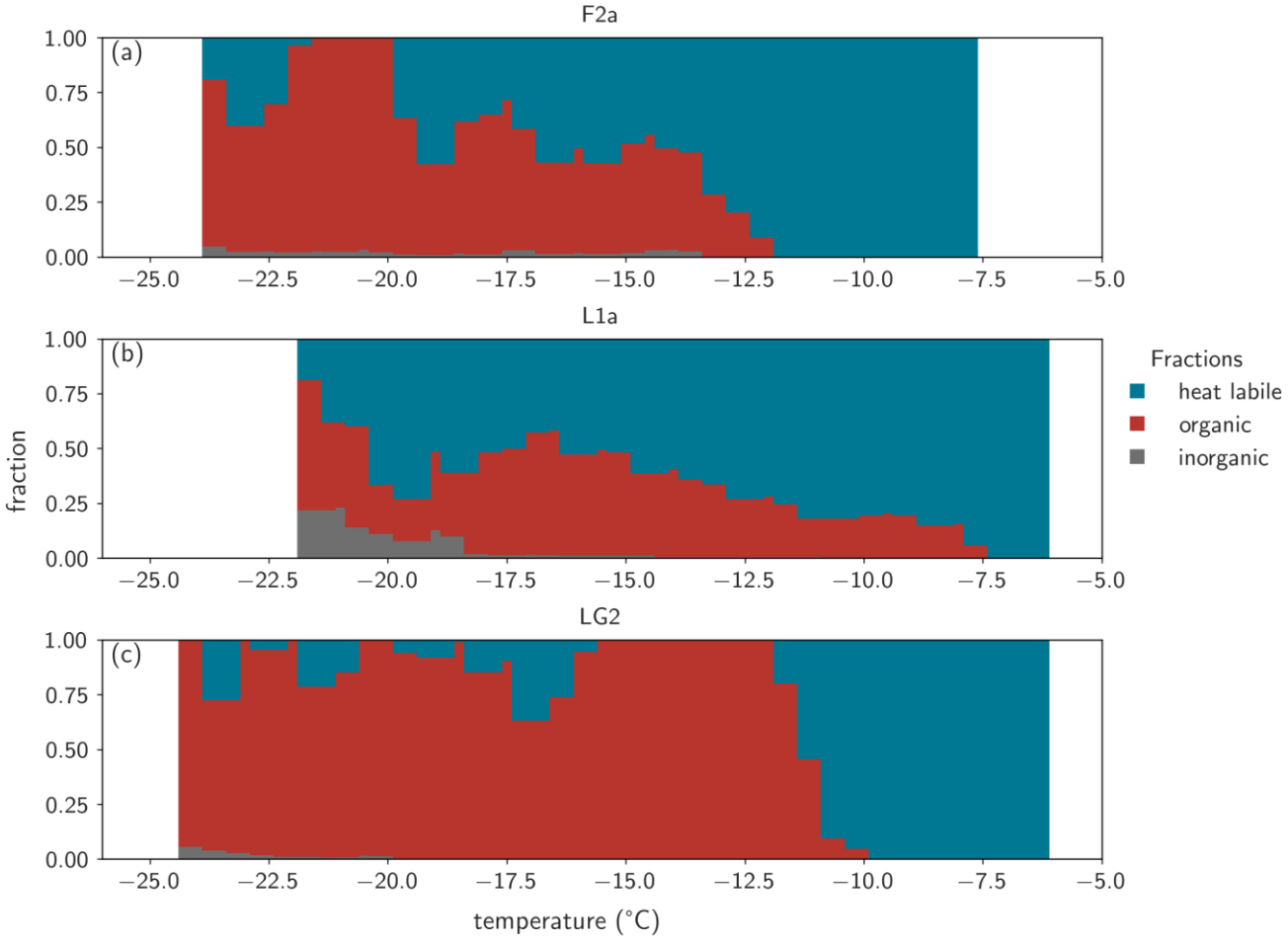

Figure C6. Composition information. Fraction of heat labile, heat stable, and inorganic INPs per gram of dust for samples from (a) Ferpècle, (b) Lämmerenboden, and (c) Lac du Grand Désert (Swiss Alps).

https://doi.org/10.5194/egusphere-2026-484
Preprint. Discussion started: 16 February 2026

Data availability

INP data:

Bergner, N., Marsh, G., Altshuler, I., Bröder, L., Farinotti, D., Guillosson, C. & Schmale, J. (2026). Ice-nucleating activity of glacially sourced dust collected in glacial outwash plains in Narsarsuaq, Igaliku, and Kangerlussuaq, Greenland [Data set]. Zenodo. https://doi.org/10.5281/zenodo.18375165

Bergner, N., Alden, J., Farinotti, D., Favre, L., Heutte, B., Pohorsky, R., Weng, J. & Schmale, J. (2026). Ice-nucleating particle concentrations from June-August 2023 in Narsaq and Narsarsuaq in southern Greenland [Data set]. Zenodo. https://doi.org/10.5281/zenodo.18376580

Meteorological data:

Alden, J., Bergner, N., Heutte, B., Farinotti, D., Favre, L., & Schmale, J. (2025). Meteorological data from multiple weather stations in Narsarsuaq and Narsaq, South Greenland during Greenfjord 2023 [Data set]. Zenodo. https://doi.org/10.5281/zenodo.15388080

Aerosol data:

Bergner, N., Alden, J., Heutte, B., Weng, J., Violaki, K., Favre, L., & Schmale, J. (2025). Fidas measurements of total aerosol number concentration and number size distributions in summertime in Narsaq, South Greenland during Greenfjord 2023 [Data set]. Zenodo. https://doi.org/10.5281/zenodo.15387340

Bergner, N., Alden, J., Heutte, B., Favre, L., Farinotti, D., & Schmale, J. (2025). Portable Optical Particle Sizer (POPS) measurements of aerosol particle number concentration and size distribution in summertime in Narsarsuaq and Narsaq, South Greenland during Greenfjord 2023 [Data set]. Zenodo. https://doi.org/10.5281/zenodo.15388013

Author contributions

NB, GM, JA, IA, LB, DF, LF, BH, JW and JS took part in the field campaign to collect samples and perform measurements. JS conceptualized the campaign and acquired funding. AB, KH, LL and KB provided their expertise on INP measurements. RP and LF built the INP filter sampler. NB analyzed the samples with help from CG. GM conducted microbiology measurements. CA and NB collected and analyzed dust samples in the Alps. NB analyzed the data and wrote the manuscript with contributions and feedback from all authors.

Competing interests

The authors declare that there are no competing interests affecting the research presented in this paper.

Acknowledgements

This work was supported by funding from the ENAC Flagship 2022 ECO-Plains, the Swiss Polar Institute grant no. SPI-FLAG-2021-002 Greenfjord, and the Swiss National Science Foundation grant no. 200021_212101. This project has received

https://doi.org/10.5194/egusphere-2026-484
Preprint. Discussion started: 16 February 2026

funding from the European Union's Horizon 2020 research and innovation program under grant agreement no. 101003826 via the project CRiceS (Climate Relevant interactions and feedbacks: the key role of sea ice and Snow in the polar and global climate system). J.S holds the Ingvar Kamprad chair for Extreme Environments Research sponsored by Ferring Pharmaceuticals. We thank the Narsaq International Research Station team, especially Lise Autogena, and the residents of Narsaq and Narsarsuaq for their generosity, curiosity, and close collaboration throughout our work. We are grateful to the Kujalleq commune for their support and for granting the land-use permissions that made this research possible. We recognize that our study took place on the traditional lands of the people of Kalaallit Nunaat and deeply appreciate the opportunity to carry out this research in a spirit of respect and cooperation with the community. We would like to thank Son Pham-Ba and Evan Thomas for the development of the SPICE image analysis and database. We thank Pascal Schouwink for the XRD measurements, and Emad Oveisi for SEM-EDX measurements. We thank Bence Dienes for the guidance in BET measurements.

References

Adams, M. P., Tarn, M. D., Sanchez-Marroquin, A., Porter, G. C. E., O'Sullivan, D., Harrison, A. D., Cui, Z., Vergara-Temprado, J., Carotenuto, F., Holden, M. A., Daily, M. I., Whale, T. F., Sikora, S. N. F., Burke, I. T., Shim, J.-U., McQuaid, J. B., and Murray, B. J.: A Major Combustion Aerosol Event Had a Negligible Impact on the Atmospheric Ice-Nucleating Particle Population, Journal of Geophysical Research: Atmospheres, 125, e2020JD032938, https://doi.org/10.1029/2020JD032938, 2020.

Agresti, A. and Coull, B. A.: Approximate Is Better than "Exact" for Interval Estimation of Binomial Proportions, The American Statistician, 52, 119–126, https://doi.org/10.2307/2685469, 1998.

Alden, J., Bergner, N., Heutte, B., Favre, L., Surdu, M., Weng, J., Augugliaro, M., Winiger, P., Dönmez, B., Pohorsky, R., Calmer, R., Chatterjee, C., Violaki, K., Nenes, A., Gregor, L., Henning, S., and Schmale, J.: Vertically-resolved source contributions to climate-relevant aerosol properties in Southern Greenlandic fjord systems, EGUsphere, 1–43, https://doi.org/10.5194/egusphere-2025-5710, 2025.

Atkinson, J. D., Murray, B. J., Woodhouse, M. T., Whale, T. F., Baustian, K. J., Carslaw, K. S., Dobbie, S., O'Sullivan, D., and Malkin, T. L.: The importance of feldspar for ice nucleation by mineral dust in mixed-phase clouds, Nature, 498, 355–358, https://doi.org/10.1038/nature12278, 2013.

Barr, S. L., Wyld, B., McQuaid, J. B., Neely Iii, R. R., and Murray, B. J.: Southern Alaska as a source of atmospheric mineral dust and ice-nucleating particles, Sci. Adv., 9, eadg3708, https://doi.org/10.1126/sciadv.adg3708, 2023.

Barry, K. R., Hill, T. C. J., Jentzsch, C., Moffett, B. F., Stratmann, F., and DeMott, P. J.: Pragmatic protocols for working cleanly when measuring ice nucleating particles, Atmospheric Research, 250, 105419, https://doi.org/10.1016/j.atmosres.2020.105419, 2021.

Barry, K. R., Hill, T. C. J., Nieto-Caballero, M., Douglas, T. A., Kreidenweis, S. M., DeMott, P. J., and Creamean, J. M.: Active thermokarst regions contain rich sources of ice-nucleating particles, Atmospheric Chemistry and Physics, 23, 15783–15793, https://doi.org/10.5194/acp-23-15783-2023, 2023.

Barry, K. R., Hill, T. C. J., Kreidenweis, S. M., DeMott, P. J., Tobo, Y., and Creamean, J. M.: Bioaerosols as indicators of central Arctic ice nucleating particle sources, Atmospheric Chemistry and Physics, 25, 11919–11933, https://doi.org/10.5194/acp-25-11919-2025, 2025.

Beall, C. M., Stokes, M. D., Hill, T. C., DeMott, P. J., DeWald, J. T., and Prather, K. A.: Automation and heat transfer characterization of immersion mode spectroscopy for analysis of ice nucleating particles, Atmospheric Measurement Techniques, 10, 2613–2626, https://doi.org/10.5194/amt-10-2613-2017, 2017.

Beck, I., Moallemi, A., Heutte, B., Pernov, J. B., Bergner, N., Rolo, M., Quéléver, L. L. J., Laurila, T., Boyer, M., Jokinen, T., Angot, H., Hoppe, C. J. M., Müller, O., Creamean, J., Frey, M. M., Freitas, G., Zinke, J., Salter, M., Zieger, P., Mirrielees, J. A., Kempf, H. E., Ault, A. P., Pratt, K. A., Gysel-Beer, M., Henning, S., Tatzelt, C., and Schmale, J.: Characteristics and sources of fluorescent aerosols in the central Arctic Ocean, Elementa: Science of the Anthropocene, 12, 00125, https://doi.org/10.1525/elementa.2023.00125, 2024.

Böhmländer, A., Lacher, L., Höhler, K., Brus, D., Doulgeris, K.-M., Girdwood, J., Leisner, T., and Möhler, O.: Measurement of the ice-nucleating particle concentration using a mobile filter-based sampler on-board of a fixed-wing uncrewed aerial vehicle during the Pallas Cloud Experiment 2022, Earth System Science Data, 17, 6157–6164, https://doi.org/10.5194/essd-17-6157-2025, 2025.

Boose, Y., Welti, A., Atkinson, J., Ramelli, F., Danielczok, A., Bingemer, H. G., Plötze, M., Sierau, B., Kanji, Z. A., and Lohmann, U.: Heterogeneous ice nucleation on dust particles sourced from nine deserts worldwide – Part 1: Immersion freezing, Atmospheric Chemistry and Physics, 16, 15075–15095, https://doi.org/10.5194/acp-16-15075-2016, 2016.

Bradley, J. A., Arndt, S., Šabacká, M., Benning, L. G., Barker, G. L., Blacker, J. J., Yallop, M. L., Wright, K. E., Bellas, C. M., Telling, J., Tranter, M., and Anesio, A. M.: Microbial dynamics in a High Arctic glacier forefield: a combined field, laboratory, and modelling approach, Biogeosciences, 13, 5677–5696, https://doi.org/10.5194/bg-13-5677-2016, 2016.

Broadley, S. L., Murray, B. J., Herbert, R. J., Atkinson, J. D., Dobbie, S., Malkin, T. L., Condliffe, E., and Neve, L.: Immersion mode heterogeneous ice nucleation by an illite rich powder representative of atmospheric mineral dust, Atmospheric Chemistry and Physics, 12, 287–307, https://doi.org/10.5194/acp-12-287-2012, 2012.

Brown, L. D., Cai, T. T., and DasGupta, A.: Interval Estimation for a Binomial Proportion, Statist. Sci., 16, https://doi.org/10.1214/ss/1009213286, 2001.

Bullard, J. E. and Mockford, T.: Seasonal and decadal variability of dust observations in the Kangerlussuaq area, west Greenland, Arctic, Antarctic, and Alpine Research, 50, S100011, https://doi.org/10.1080/15230430.2017.1415854, 2018.

Bullard, J. E., Baddock, M., Bradwell, T., Crusius, J., Darlington, E., Gaiero, D., Gassó, S., Gisladottir, G., Hodgkins, R., McCulloch, R., McKenna-Neuman, C., Mockford, T., Stewart, H., and Thorsteinsson, T.: High-latitude dust in the Earth system, Reviews of Geophysics, 54, 447–485, https://doi.org/10.1002/2016RG000518, 2016.

Bullard, J. E., Prater, C., Baddock, M. C., and Anderson, N. J.: Diurnal and seasonal source-proximal dust concentrations in complex terrain, West Greenland, Earth Surface Processes and Landforms, 48, 2808–2827, https://doi.org/10.1002/esp.5661, 2023.

Carlson, D. F., Pavalko, W. J., Petersen, D., Olsen, M., and Hass, A. E.: Maker Buoy Variants for Water Level Monitoring and Tracking Drifting Objects in Remote Areas of Greenland, Sensors, 20, 1254, https://doi.org/10.3390/s20051254, 2020.

Carrivick, J. L. and Tweed, F. S.: A review of glacier outburst floods in Iceland and Greenland with a megafloods perspective, Earth-Science Reviews, 196, 102876, https://doi.org/10.1016/j.earscirev.2019.102876, 2019.

https://doi.org/10.5194/egusphere-2026-484
Preprint. Discussion started: 16 February 2026

Ceppi, P., Brient, F., Zelinka, M. D., and Hartmann, D. L.: Cloud feedback mechanisms and their representation in global climate models, WIREs Climate Change, 8, e465, https://doi.org/10.1002/wcc.465, 2017.

Chen, J., Wu, Z., Augustin-Bauditz, S., Grawe, S., Hartmann, M., Pei, X., Liu, Z., Ji, D., and Wex, H.: Ice-nucleating particle concentrations unaffected by urban air pollution in Beijing, China, Atmospheric Chemistry and Physics, 18, 3523–3539, https://doi.org/10.5194/acp-18-3523-2018, 2018.

Conen, F., Morris, C. E., Leifeld, J., Yakutin, M. V., and Alewell, C.: Biological residues define the ice nucleation properties of soil dust, Atmospheric Chemistry and Physics, 11, 9643–9648, https://doi.org/10.5194/acp-11-9643-2011, 2011.

Conen, F., Eckhardt, S., Gundersen, H., Stohl, A., and Yttri, K. E.: Rainfall drives atmospheric ice-nucleating particles in the coastal climate of southern Norway, Atmospheric Chemistry and Physics, 17, 11065–11073, https://doi.org/10.5194/acp-17-11065-2017, 2017.

Crusius, J., Schroth, A. W., Gasso, S., Moy, C. M., Levy, R. C., and Gatica, M.: Glacial flour dust storms in the Gulf of Alaska: hydrologic and meteorological controls and their importance as a source of bioavailable iron, Geophysical Research Letters, 38, https://doi.org/10.1029/2010GL046573, 2011.

Dagsson-Waldhauserova, P., Arnalds, O., and Olafsson, H.: Long-term frequency and characteristics of dust storm events in Northeast Iceland (1949–2011), Atmospheric Environment, 77, 117–127, https://doi.org/10.1016/j.atmosenv.2013.04.075, 2013.

Daily, M. I., Tarn, M. D., Whale, T. F., and Murray, B. J.: An evaluation of the heat test for the ice-nucleating ability of minerals and biological material, Atmospheric Measurement Techniques, 15, 2635–2665, https://doi.org/10.5194/amt-15-2635-2022, 2022.

David, R. O., Cascajo-Castresana, M., Brennan, K. P., Rösch, M., Els, N., Werz, J., Weichlinger, V., Boynton, L. S., Bogler, S., Borduas-Dedekind, N., Marcolli, C., and Kanji, Z. A.: Development of the DRoplet Ice Nuclei Counter Zurich (DRINCZ): validation and application to field-collected snow samples, Atmospheric Measurement Techniques, 12, 6865–6888, https://doi.org/10.5194/amt-12-6865-2019, 2019.

DeMott, P. J., Cziczo, D. J., Prenni, A. J., Murphy, D. M., Kreidenweis, S. M., Thomson, D. S., Borys, R., and Rogers, D. C.: Measurements of the concentration and composition of nuclei for cirrus formation, Proceedings of the National Academy of Sciences, 100, 14655–14660, https://doi.org/10.1073/pnas.2532677100, 2003.

DeMott, P. J., Prenni, A. J., Liu, X., Kreidenweis, S. M., Petters, M. D., Twohy, C. H., Richardson, M. S., Eidhammer, T., and Rogers, D. C.: Predicting global atmospheric ice nuclei distributions and their impacts on climate, Proceedings of the National Academy of Sciences, 107, 11217–11222, https://doi.org/10.1073/pnas.0910818107, 2010.

DeMott, P. J., Prenni, A. J., McMeeking, G. R., Sullivan, R. C., Petters, M. D., Tobo, Y., Niemand, M., Möhler, O., Snider, J. R., Wang, Z., and Kreidenweis, S. M.: Integrating laboratory and field data to quantify the immersion freezing ice nucleation activity of mineral dust particles, Atmospheric Chemistry and Physics, 15, 393–409, https://doi.org/10.5194/acp-15-393-2015, 2015.

DeMott, P. J., Hill, T. C. J., Petters, M. D., Bertram, A. K., Tobo, Y., Mason, R. H., Suski, K. J., McCluskey, C. S., Levin, E. J. T., Schill, G. P., Boose, Y., Rauker, A. M., Miller, A. J., Zaragoza, J., Rocci, K., Rothfuss, N. E., Taylor, H. P., Hader, J. D., Chou, C., Huffman, J. A., Pöschl, U., Prenni, A. J., and Kreidenweis, S. M.: Comparative measurements of ambient atmospheric concentrations of ice nucleating particles using multiple immersion freezing methods and a continuous flow diffusion chamber, Atmospheric Chemistry and Physics, 17, 11227–11245, https://doi.org/10.5194/acp-17-11227-2017, 2017.

https://doi.org/10.5194/egusphere-2026-484
Preprint. Discussion started: 16 February 2026

Donhauser, J. and Frey, B.: Alpine soil microbial ecology in a changing world, FEMS Microbiology Ecology, 94, https://doi.org/10.1093/femsec/fiy099, 2018.

Dreischmeier, K., Budke, C., Wiehemeier, L., Kottke, T., and Koop, T.: Boreal pollen contain ice-nucleating as well as ice-binding 'antifreeze' polysaccharides, Sci Rep, 7, 41890, https://doi.org/10.1038/srep41890, 2017.

Duan, P., Hu, W., Wu, Z., Bi, K., Zhu, J., and Fu, P.: Ice nucleation activity of airborne pollen: A short review of results from laboratory experiments, Atmospheric Research, 285, 106659, https://doi.org/10.1016/j.atmosres.2023.106659, 2023.

Failor, K. C., Schmale, D. G., III, Vinatzer, B. A., and Monteil, C. L.: Ice nucleation active bacteria in precipitation are genetically diverse and nucleate ice by employing different mechanisms, The ISME Journal, 11, 2740–2753, https://doi.org/10.1038/ismej.2017.124, 2017.

Fécan, F., Marticorena, B., and Bergametti, G.: Parametrization of the increase of the aeolian erosion threshold wind friction velocity due to soil moisture for arid and semi-arid areas, Annales Geophysicae, 17, 149–157, https://doi.org/10.1007/s00585-999-0149-7, 1999.

Field, P. R., Lawson, R. P., Brown, P. R. A., Lloyd, G., Westbrook, C., Moisseev, D., Miltenberger, A., Nenes, A., Blyth, A., Choularton, T., Connolly, P., Buehl, J., Crosier, J., Cui, Z., Dearden, C., DeMott, P., Flossmann, A., Heymsfield, A., Huang, Y., Kalesse, H., Kanji, Z. A., Korolev, A., Kirchgaessner, A., Lasher-Trapp, S., Leisner, T., McFarquhar, G., Phillips, V., Stith, J., and Sullivan, S.: Chapter 7. Secondary Ice Production - current state of the science and recommendations for the future, Meteorological Monographs, AMSMONOGRAPHS-D-16-0014.1, https://doi.org/10.1175/AMSMONOGRAPHS-D-16-0014.1, 2016.

Fröhlich-Nowoisky, J., Hill, T. C. J., Pummer, B. G., Yordanova, P., Franc, G. D., and Pöschl, U.: Ice nucleation activity in the widespread soil fungus *Mortierella alpina*, Biogeosciences, 12, 1057–1071, https://doi.org/10.5194/bg-12-1057-2015, 2015.

Frossard, A., Hammes, F., and Gessner, M. O.: Flow Cytometric Assessment of Bacterial Abundance in Soils, Sediments and Sludge, Front. Microbiol., 7, https://doi.org/10.3389/fmicb.2016.00903, 2016.

Górniak, D., Marszałek, H., Kwaśniak-Kominek, M., Rzepa, G., and Manecki, M.: Soil formation and initial microbiological activity on a foreland of an Arctic glacier (SW Svalbard), Applied Soil Ecology, 114, 34–44, https://doi.org/10.1016/j.apsoil.2017.02.017, 2017.

Gratzl, J., Böhmländer, A., Pätsi, S., Pogner, C.-E., Gorfer, M., Brus, D., Doulgeris, K. M., Wieland, F., Asmi, E., Saarto, A., Möhler, O., Stolzenburg, D., and Grothe, H.: Locally emitted fungal spores serve as high-temperature ice nucleating particles in the European sub-Arctic, Atmospheric Chemistry and Physics, 25, 12007–12035, https://doi.org/10.5194/acp-25-12007-2025, 2025.

Grimes, M., Carrivick, J. L., Smith, M. W., and Comber, A. J.: Land cover changes across Greenland dominated by a doubling of vegetation in three decades, Sci Rep, 14, 3120, https://doi.org/10.1038/s41598-024-52124-1, 2024.

Groot Zwaaftink, C. D., Grythe, H., Skov, H., and Stohl, A.: Substantial contribution of northern high-latitude sources to mineral dust in the Arctic, Journal of Geophysical Research: Atmospheres, 121, 13,678-13,697, https://doi.org/10.1002/2016JD025482, 2016.

Hamzehpour, N., Marcolli, C., Pashai, S., Klumpp, K., and Peter, T.: Measurement report: The Urmia playa as a source of airborne dust and ice-nucleating particles – Part 1: Correlation between soils and airborne samples, Atmospheric Chemistry and Physics, 22, 14905–14930, https://doi.org/10.5194/acp-22-14905-2022, 2022.

https://doi.org/10.5194/egusphere-2026-484
Preprint. Discussion started: 16 February 2026

Harrison, A. D., Whale, T. F., Rutledge, R., Lamb, S., Tarn, M. D., Porter, G. C. E., Adams, M. P., McQuaid, J. B., Morris, G. J., and Murray, B. J.: An instrument for quantifying heterogeneous ice nucleation in multiwell plates using infrared emissions to detect freezing, Atmospheric Measurement Techniques, 11, 5629–5641, https://doi.org/10.5194/amt-11-5629-2018, 2018.

Harrison, A. D., Lever, K., Sanchez-Marroquin, A., Holden, M. A., Whale, T. F., Tarn, M. D., McQuaid, J. B., and Murray, B. J.: The ice-nucleating ability of quartz immersed in water and its atmospheric importance compared to K-feldspar, Atmospheric Chemistry and Physics, 19, 11343–11361, https://doi.org/10.5194/acp-19-11343-2019, 2019.

Hill, T. C. J., DeMott, P. J., Tobo, Y., Fröhlich-Nowoisky, J., Moffett, B. F., Franc, G. D., and Kreidenweis, S. M.: Sources of organic ice nucleating particles in soils, Atmospheric Chemistry and Physics, 16, 7195–7211, https://doi.org/10.5194/acp-16-7195-2016, 2016.

Hiranuma, N., Augustin-Bauditz, S., Bingemer, H., Budke, C., Curtius, J., Danielczok, A., Diehl, K., Dreischmeier, K., Ebert, M., Frank, F., Hoffmann, N., Kandler, K., Kiselev, A., Koop, T., Leisner, T., Möhler, O., Nillius, B., Peckhaus, A., Rose, D., Weinbruch, S., Wex, H., Boose, Y., DeMott, P. J., Hader, J. D., Hill, T. C. J., Kanji, Z. A., Kulkarni, G., Levin, E. J. T., McCluskey, C. S., Murakami, M., Murray, B. J., Niedermeier, D., Petters, M. D., O'Sullivan, D., Saito, A., Schill, G. P., Tajiri, T., Tolbert, M. A., Welti, A., Whale, T. F., Wright, T. P., and Yamashita, K.: A comprehensive laboratory study on the immersion freezing behavior of illite NX particles: a comparison of 17 ice nucleation measurement techniques, Atmospheric Chemistry and Physics, 15, 2489–2518, https://doi.org/10.5194/acp-15-2489-2015, 2015.

Hoose, C. and Möhler, O.: Heterogeneous ice nucleation on atmospheric aerosols: a review of results from laboratory experiments, Atmospheric Chemistry and Physics, 12, 9817–9854, https://doi.org/10.5194/acp-12-9817-2012, 2012.

Huang, Z., Huang, J., Hayasaka, T., Wang, S., Zhou, T., and Jin, H.: Short-cut transport path for Asian dust directly to the Arctic: a case study, Environ. Res. Lett., 10, 114018, https://doi.org/10.1088/1748-9326/10/11/114018, 2015.

Huffman, J. A., Prenni, A. J., DeMott, P. J., Pöhlker, C., Mason, R. H., Robinson, N. H., Fröhlich-Nowoisky, J., Tobo, Y., Després, V. R., Garcia, E., Gochis, D. J., Harris, E., Müller-Germann, I., Ruzene, C., Schmer, B., Sinha, B., Day, D. A., Andreae, M. O., Jimenez, J. L., Gallagher, M., Kreidenweis, S. M., Bertram, A. K., and Pöschl, U.: High concentrations of biological aerosol particles and ice nuclei during and after rain, Atmospheric Chemistry and Physics, 13, 6151–6164, https://doi.org/10.5194/acp-13-6151-2013, 2013.

Jensen, L. Z., Simonsen, J. K., Pastor, A., Pearce, C., Nørnberg, P., Lund-Hansen, L. C., Finster, K., and Šantl-Temkiv, T.: Linking biogenic high-temperature ice nucleating particles in Arctic soils and streams to their microbial producers, Aerosol Research, 3, 81–100, https://doi.org/10.5194/ar-3-81-2025, 2025.

Joly, M., Attard, E., Sancelme, M., Deguillaume, L., Guilbaud, C., Morris, C. E., Amato, P., and Delort, A.-M.: Ice nucleation activity of bacteria isolated from cloud water, Atmospheric Environment, 70, 392–400, https://doi.org/10.1016/j.atmosenv.2013.01.027, 2013.

Kanji, Z. A., Ladino, L. A., Wex, H., Boose, Y., Burkert-Kohn, M., Cziczo, D. J., and Krämer, M.: Overview of Ice Nucleating Particles, Meteorological Monographs, 58, 1.1-1.33, https://doi.org/10.1175/AMSMONOGRAPHS-D-16-0006.1, 2017.

Kawai, K. and Matsui, H.: Contributions of Dust Source Regions to Ice Nucleating Particles in Mixed-Phase Clouds Simulated with a Global Climate–Aerosol Model, Journal of Climate, 38, 4925–4939, https://doi.org/10.1175/JCLI-D-24-0696.1, 2025.

Kawai, K., Matsui, H., and Tobo, Y.: Dominant Role of Arctic Dust With High Ice Nucleating Ability in the Arctic Lower Troposphere, Geophysical Research Letters, 50, e2022GL102470, https://doi.org/10.1029/2022GL102470, 2023.

https://doi.org/10.5194/egusphere-2026-484
Preprint. Discussion started: 16 February 2026

Korolev, A.: Limitations of the Wegener–Bergeron–Findeisen Mechanism in the Evolution of Mixed-Phase Clouds, Journal of the Atmospheric Sciences, 64, 3372–3375, https://doi.org/10.1175/JAS4035.1, 2007.

Korolev, A. and Leisner, T.: Review of experimental studies of secondary ice production, Atmospheric Chemistry and Physics, 20, 11767–11797, https://doi.org/10.5194/acp-20-11767-2020, 2020.

Marsh, G., Bourquin, M., Leale, A., Schmale, J., Bröder, L., and Altshuler, I.: Soil microbial diversity, dispersal limited community assembly and greenhouse gas cycling across a Greenlandic glacial chronosequence, FEMS Microbiology Ecology, in preparation.

Mason, R. H., Si, M., Li, J., Chou, C., Dickie, R., Toom-Sauntry, D., Pöhlker, C., Yakobi-Hancock, J. D., Ladino, L. A., Jones, K., Leaitch, W. R., Schiller, C. L., Abbatt, J. P. D., Huffman, J. A., and Bertram, A. K.: Ice nucleating particles at a coastal marine boundary layer site: correlations with aerosol type and meteorological conditions, Atmospheric Chemistry and Physics, 15, 12547–12566, https://doi.org/10.5194/acp-15-12547-2015, 2015.

Matsui, H., Kawai, K., Tobo, Y., Iizuka, Y., and Matoba, S.: Increasing Arctic dust suppresses the reduction of ice nucleation in the Arctic lower troposphere by warming, npj Clim Atmos Sci, 7, 1–9, https://doi.org/10.1038/s41612-024-00811-1, 2024.

McCluskey, C. S., Ovadnevaite, J., Rinaldi, M., Atkinson, J., Belosi, F., Ceburnis, D., Marullo, S., Hill, T. C. J., Lohmann, U., Kanji, Z. A., O'Dowd, C., Kreidenweis, S. M., and DeMott, P. J.: Marine and Terrestrial Organic Ice-Nucleating Particles in Pristine Marine to Continentally Influenced Northeast Atlantic Air Masses, Journal of Geophysical Research: Atmospheres, 123, 6196–6212, https://doi.org/10.1029/2017JD028033, 2018a.

McCluskey, C. S., Hill, T. C. J., Humphries, R. S., Rauker, A. M., Moreau, S., Strutton, P. G., Chambers, S. D., Williams, A. G., McRobert, I., Ward, J., Keywood, M. D., Harnwell, J., Ponsonby, W., Loh, Z. M., Krummel, P. B., Protat, A., Kreidenweis, S. M., and DeMott, P. J.: Observations of Ice Nucleating Particles Over Southern Ocean Waters, Geophysical Research Letters, 45, 11,989-11,997, https://doi.org/10.1029/2018GL079981, 2018b.

Meinander, O., Dagsson-Waldhauserova, P., Amosov, P., Aseyeva, E., Atkins, C., Baklanov, A., Baldo, C., Barr, S. L., Barzycka, B., Benning, L. G., Cvetkovic, B., Enchilik, P., Frolov, D., Gassó, S., Kandler, K., Kasimov, N., Kavan, J., King, J., Koroleva, T., Krupskaya, V., Kulmala, M., Kusiak, M., Lappalainen, H. K., Laska, M., Lasne, J., Lewandowski, M., Luks, B., McQuaid, J. B., Moroni, B., Murray, B., Möhler, O., Nawrot, A., Nickovic, S., O'Neill, N. T., Pejanovic, G., Popovicheva, O., Ranjbar, K., Romanias, M., Samonova, O., Sanchez-Marroquin, A., Schepanski, K., Semenkov, I., Sharapova, A., Shevnina, E., Shi, Z., Sofiev, M., Thevenet, F., Thorsteinsson, T., Timofeev, M., Umo, N. S., Uppstu, A., Urupina, D., Varga, G., Werner, T., Arnalds, O., and Vukovic Vimic, A.: Newly identified climatically and environmentally significant high-latitude dust sources, Atmospheric Chemistry and Physics, 22, 11889–11930, https://doi.org/10.5194/acp-22-11889-2022, 2022.

Miller, A. J., Brennan, K. P., Mignani, C., Wieder, J., David, R. O., and Borduas-Dedekind, N.: Development of the drop Freezing Ice Nuclei Counter (FINC), intercomparison of droplet freezing techniques, and use of soluble lignin as an atmospheric ice nucleation standard, Atmos. Meas. Tech., 14, 3131–3151, https://doi.org/10.5194/amt-14-3131-2021, 2021.

Moon, T., Fisher, M., Stafford, T., and Harden, L.: QGreenland (3.0.0), https://doi.org/10.5281/ZENODO.12823307, 2023.

Morris, C. E., Sands, D. C., Glaux, C., Samsatly, J., Asaad, S., Moukahel, A. R., Gonçalves, F. L. T., and Bigg, E. K.: Urediospores of rust fungi are ice nucleation active at > −10 °C and harbor ice nucleation active bacteria, Atmospheric Chemistry and Physics, 13, 4223–4233, https://doi.org/10.5194/acp-13-4223-2013, 2013.

Morrison, H., de Boer, G., Feingold, G., Harrington, J., Shupe, M. D., and Sulia, K.: Resilience of persistent Arctic mixed-phase clouds, Nature Geosci, 5, 11–17, https://doi.org/10.1038/ngeo1332, 2012.

https://doi.org/10.5194/egusphere-2026-484
Preprint. Discussion started: 16 February 2026

Murray, B. J., O'Sullivan, D., Atkinson, J. D., and Webb, M. E.: Ice nucleation by particles immersed in supercooled cloud droplets, Chem. Soc. Rev., 41, 6519–6554, https://doi.org/10.1039/C2CS35200A, 2012.

Murray, B. J., Carslaw, K. S., and Field, P. R.: Opinion: Cloud-phase climate feedback and the importance of ice-nucleating particles, Atmospheric Chemistry and Physics, 21, 665–679, https://doi.org/10.5194/acp-21-665-2021, 2021.

Niemand, M., Möhler, O., Vogel, B., Vogel, H., Hoose, C., Connolly, P., Klein, H., Bingemer, H., DeMott, P., Skrotzki, J., and Leisner, T.: A Particle-Surface-Area-Based Parameterization of Immersion Freezing on Desert Dust Particles, Journal of the Atmospheric Sciences, 69, 3077–3092, https://doi.org/10.1175/JAS-D-11-0249.1, 2012.

O'Sullivan, D., Murray, B. J., Malkin, T. L., Whale, T. F., Umo, N. S., Atkinson, J. D., Price, H. C., Baustian, K. J., Browse, J., and Webb, M. E.: Ice nucleation by fertile soil dusts: relative importance of mineral and biogenic components, Atmos. Chem. Phys., 14, 1853–1867, https://doi.org/10.5194/acp-14-1853-2014, 2014.

O′Sullivan, D., Murray, B. J., Ross, J. F., Whale, T. F., Price, H. C., Atkinson, J. D., Umo, N. S., and Webb, M. E.: The relevance of nanoscale biological fragments for ice nucleation in clouds, Sci Rep, 5, 8082, https://doi.org/10.1038/srep08082, 2015.

Paramonov, M., David, R. O., Kretzschmar, R., and Kanji, Z. A.: A laboratory investigation of the ice nucleation efficiency of three types of mineral and soil dust, Atmospheric Chemistry and Physics, 18, 16515–16536, https://doi.org/10.5194/acp-18-16515-2018, 2018.

Pereira Freitas, G., Adachi, K., Conen, F., Heslin-Rees, D., Krejci, R., Tobo, Y., Yttri, K. E., and Zieger, P.: Regionally sourced bioaerosols drive high-temperature ice nucleating particles in the Arctic, Nat Commun, 14, 5997, https://doi.org/10.1038/s41467-023-41696-7, 2023.

Petters, M. D., Parsons, M. T., Prenni, A. J., DeMott, P. J., Kreidenweis, S. M., Carrico, C. M., Sullivan, A. P., McMeeking, G. R., Levin, E., Wold, C. E., Collett Jr., J. L., and Moosmüller, H.: Ice nuclei emissions from biomass burning, Journal of Geophysical Research: Atmospheres, 114, https://doi.org/10.1029/2008JD011532, 2009.

Pouleur, S., Richard, C., Martin, J.-G., and Antoun, H.: Ice Nucleation Activity in Fusarium acuminatum and Fusarium avenaceum, Applied and Environmental Microbiology, 58, 2960–2964, https://doi.org/10.1128/aem.58.9.2960-2964.1992, 1992.

Pratt, K., Murphy, S., DeMott, P., Kok, G., Campos, T., Rogers, D., Prenni, A., Heymsfield, A., Seinfeld, J., and Prather, K.: Flight-based chemical characterization of biomass burning aerosols within two prescribed burn smoke plumes, Atmospheric Chemistry and Physics, 11, 12549–12565, https://doi.org/10.5194/acp-11-12549-2011, 2011.

Prospero, J. M., Blades, E., Mathison, G., and Naidu, R.: Interhemispheric transport of viable fungi and bacteria from Africa to the Caribbean with soil dust, Aerobiologia, 21, 1–19, https://doi.org/10.1007/s10453-004-5872-7, 2005.

Pummer, B. G., Budke, C., Augustin-Bauditz, S., Niedermeier, D., Felgitsch, L., Kampf, C. J., Huber, R. G., Liedl, K. R., Loerting, T., Moschen, T., Schauperl, M., Tollinger, M., Morris, C. E., Wex, H., Grothe, H., Pöschl, U., Koop, T., and Fröhlich-Nowoisky, J.: Ice nucleation by water-soluble macromolecules, Atmospheric Chemistry and Physics, 15, 4077–4091, https://doi.org/10.5194/acp-15-4077-2015, 2015.

Sanchez-Marroquin, A., Arnalds, O., Baustian-Dorsi, K. J., Browse, J., Dagsson-Waldhauserova, P., Harrison, A. D., Maters, E. C., Pringle, K. J., Vergara-Temprado, J., Burke, I. T., McQuaid, J. B., Carslaw, K. S., and Murray, B. J.: Iceland is an episodic source of atmospheric ice-nucleating particles relevant for mixed-phase clouds, Science Advances, 6, eaba8137, https://doi.org/10.1126/sciadv.aba8137, 2020.

https://doi.org/10.5194/egusphere-2026-484
Preprint. Discussion started: 16 February 2026

Šantl-Temkiv, T., Sahyoun, M., Finster, K., Hartmann, S., Augustin-Bauditz, S., Stratmann, F., Wex, H., Clauss, T., Nielsen, N. W., Sørensen, J. H., Korsholm, U. S., Wick, L. Y., and Karlson, U. G.: Characterization of airborne ice-nucleation-active bacteria and bacterial fragments, Atmospheric Environment, 109, 105–117, https://doi.org/10.1016/j.atmosenv.2015.02.060, 2015.

Šantl-Temkiv, T., Lange, R., Beddows, D., Rauter, U., Pilgaard, S., Dall'Osto, M., Gunde-Cimerman, N., Massling, A., and Wex, H.: Biogenic Sources of Ice Nucleating Particles at the High Arctic Site Villum Research Station, Environ. Sci. Technol., 53, 10580–10590, https://doi.org/10.1021/acs.est.9b00991, 2019.

Sassen, K., DeMott, P. J., Prospero, J. M., and Poellot, M. R.: Saharan dust storms and indirect aerosol effects on clouds: CRYSTAL-FACE results, Geophysical Research Letters, 30, 2003GL017371, https://doi.org/10.1029/2003GL017371, 2003.

Schneider, J., Höhler, K., Heikkilä, P., Keskinen, J., Bertozzi, B., Bogert, P., Schorr, T., Umo, N. S., Vogel, F., Brasseur, Z., Wu, Y., Hakala, S., Duplissy, J., Moisseev, D., Kulmala, M., Adams, M. P., Murray, B. J., Korhonen, K., Hao, L., Thomson, E. S., Castarède, D., Leisner, T., Petäjä, T., and Möhler, O.: The seasonal cycle of ice-nucleating particles linked to the abundance of biogenic aerosol in boreal forests, Atmospheric Chemistry and Physics, 21, 3899–3918, https://doi.org/10.5194/acp-21-3899-2021, 2021.

Shi, Y., Liu, X., Wu, M., Zhao, X., Ke, Z., and Brown, H.: Relative importance of high-latitude local and long-range-transported dust for Arctic ice-nucleating particles and impacts on Arctic mixed-phase clouds, Atmospheric Chemistry and Physics, 22, 2909–2935, https://doi.org/10.5194/acp-22-2909-2022, 2022.

Sprenger, M. and Wernli, H.: The LAGRANTO Lagrangian analysis tool – version 2.0, Geoscientific Model Development, 8, 2569–2586, https://doi.org/10.5194/gmd-8-2569-2015, 2015.

Stopelli, E., Conen, F., Guilbaud, C., Zopfi, J., Alewell, C., and Morris, C. E.: Ice nucleators, bacterial cells and *Pseudomonas syringae* in precipitation at Jungfraujoch, Biogeosciences, 14, 1189–1196, https://doi.org/10.5194/bg-14-1189-2017, 2017.

Storelvmo, T.: Aerosol Effects on Climate via Mixed-Phase and Ice Clouds, Annual Review of Earth and Planetary Sciences, 45, 199–222, https://doi.org/10.1146/annurev-earth-060115-012240, 2017.

Storelvmo, T., Tan, I., and Korolev, A. V.: Cloud Phase Changes Induced by CO2 Warming—a Powerful yet Poorly Constrained Cloud-Climate Feedback, Curr Clim Change Rep, 1, 288–296, https://doi.org/10.1007/s40641-015-0026-2, 2015.

Sze, K. C. H., Wex, H., Hartmann, M., Skov, H., Massling, A., Villanueva, D., and Stratmann, F.: Ice-nucleating particles in northern Greenland: annual cycles, biological contribution and parameterizations, Atmospheric Chemistry and Physics, 23, 4741–4761, https://doi.org/10.5194/acp-23-4741-2023, 2023.

Tan, I., Storelvmo, T., and Zelinka, M. D.: Observational constraints on mixed-phase clouds imply higher climate sensitivity, Science, 352, 224–227, https://doi.org/10.1126/science.aad5300, 2016.

Tobo, Y., Adachi, K., DeMott, P. J., Hill, T. C. J., Hamilton, D. S., Mahowald, N. M., Nagatsuka, N., Ohata, S., Uetake, J., Kondo, Y., and Koike, M.: Glacially sourced dust as a potentially significant source of ice nucleating particles, Nat. Geosci., 12, 253–258, https://doi.org/10.1038/s41561-019-0314-x, 2019.

Twohy, C. H., DeMott, P. J., Pratt, K. A., Subramanian, R., Kok, G. L., Murphy, S. M., Lersch, T., Heymsfield, A. J., Wang, Z., Prather, K. A., and Seinfeld, J. H.: Relationships of Biomass-Burning Aerosols to Ice in Orographic Wave Clouds, Journal of the Atmospheric Sciences, 67, 2437–2450, https://doi.org/10.1175/2010JAS3310.1, 2010.

https://doi.org/10.5194/egusphere-2026-484
Preprint. Discussion started: 16 February 2026

Ullrich, R., Hoose, C., Möhler, O., Niemand, M., Wagner, R., Höhler, K., Hiranuma, N., Saathoff, H., and Leisner, T.: A New Ice Nucleation Active Site Parameterization for Desert Dust and Soot, Journal of the Atmospheric Sciences, 74, 699–717, https://doi.org/10.1175/JAS-D-16-0074.1, 2017.

Vali, G.: Quantitative Evaluation of Experimental Results and the Heterogeneous Freezing Nucleation of Supercooled Liquids, Journal of the Atmospheric Sciences, 28, 402–409, https://doi.org/10.1175/1520-0469(1971)028%253C0402:QEOERA%253E2.0.CO;2, 1971.

Vergara-Temprado, J., Miltenberger, A. K., Furtado, K., Grosvenor, D. P., Shipway, B. J., Hill, A. A., Wilkinson, J. M., Field, P. R., Murray, B. J., and Carslaw, K. S.: Strong control of Southern Ocean cloud reflectivity by ice-nucleating particles, Proceedings of the National Academy of Sciences, 115, 2687–2692, https://doi.org/10.1073/pnas.1721627115, 2018.

Welti, A., Bigg, E. K., DeMott, P. J., Gong, X., Hartmann, M., Harvey, M., Henning, S., Herenz, P., Hill, T. C. J., Hornblow, B., Leck, C., Löffler, M., McCluskey, C. S., Rauker, A. M., Schmale, J., Tatzelt, C., van Pinxteren, M., and Stratmann, F.: Ship-based measurements of ice nuclei concentrations over the Arctic, Atlantic, Pacific and Southern oceans, Atmospheric Chemistry and Physics, 20, 15191–15206, https://doi.org/10.5194/acp-20-15191-2020, 2020.

Wex, H., Huang, L., Zhang, W., Hung, H., Traversi, R., Becagli, S., Sheesley, R. J., Moffett, C. E., Barrett, T. E., Bossi, R., Skov, H., Hünerbein, A., Lubitz, J., Löffler, M., Linke, O., Hartmann, M., Herenz, P., and Stratmann, F.: Annual variability of ice-nucleating particle concentrations at different Arctic locations, Atmospheric Chemistry and Physics, 19, 5293–5311, https://doi.org/10.5194/acp-19-5293-2019, 2019.

Wieber, C., Jensen, L. Z., Vergeynst, L., Meire, L., Juul-Pedersen, T., Finster, K., and Šantl-Temkiv, T.: Terrestrial runoff is an important source of biological ice-nucleating particles in Arctic marine systems, Atmospheric Chemistry and Physics, 25, 3327–3346, https://doi.org/10.5194/acp-25-3327-2025, 2025.

Xi, Y., Xu, C., Downey, A., Stevens, R., O. Bachelder, J., King, J., L. Hayes, P., and K. Bertram, A.: Ice nucleating properties of airborne dust from an actively retreating glacier in Yukon, Canada, Environmental Science: Atmospheres, 2, 714–726, https://doi.org/10.1039/D1EA00101A, 2022.